

**DEEP LEARNING FOR BRAIN TUMOR
DETECTION AND CLASSIFICATION
USING MRI IMAGES**

Thesis Submitted for the Award of the Degree of

DOCTOR OF PHILOSOPHY

In

Electronics and Communication Engineering

By

BHUKYA RAMU

Registration Number: 42000065

Supervised By

Dr. Sandeep Bansal (15732)

Associate Professor

School of Electronics and Electrical Engineering



LOVELY PROFESSIONAL UNIVERSITY, PUNJAB

2024

DECLARATION

I, hereby declare that the presented work in the thesis entitled “**DEEP LEARNING FOR BRAIN TUMOR DETECTION AND CLASSIFICATION USING MRI IMAGES**” in fulfilment of degree of **Doctor of Philosophy (Ph.D) in Electronics & Communication Engineering** is outcome of research work carried out by me under the supervision of **Dr Sandeep Bansal**, working as **Associate Professor**, in the **School of Electronics and Electrical Engineering** of Lovely Professional University, Punjab. In keeping with general practice of reporting scientific observations, due acknowledgements have been made whenever work described here has been based on findings of other investigator(s). This work has not been submitted in part or full to any other University or Institute for the award of any degree.

(Signature of Scholar)

Name of the scholar: **Bhukya Ramu**
Registration No.: **42000065**
School of Electronics and Electrical Engineering
Lovely Professional University, Punjab, India.

CERTIFICATE

This is to certify that the work reported in the Ph. D. thesis entitled “**DEEP LEARNING FOR BRAIN TUMOR DETECTION AND CLASSIFICATION USING MRI IMAGES**” submitted in fulfilment of the requirement for the reward of a degree of **Doctor of Philosophy (Ph. D) in Electronics & Communication Engineering** in the School of **Electronics and Electrical Engineering**, is a research work carried out by **Bhukya Ramu (42000065)** is a bonafide record of his original work carried out under my supervision and that no part of the thesis has been submitted for any other degree, diploma or equivalent course.

(Signature of Supervisor)

Name of supervisor: **Dr. Sandeep Bansal**

Designation: **Associate Professor**

School: **School of Electronics & Electrical Engineering**

University: **Lovely Professional University**

ABSTRACT

According to the World Health Organization (WHO) records in USA in the year 2015, approximately 166039 humans are faced and living with a brain tumor, in United Kingdom (UK), brain and other Central Nervous System (CNS) tumors were the ninth most common cancer in 2013, with approximately 10,608 people diagnosed. In 2012, it was the eighth leading cause of cancer-related deaths, with around 5,200 fatalities. In 2019, it was estimated that over 28,000 people under the age of 20 in the United States were diagnosed with a brain tumor. According to statistics from the National Cancer Institute (NCIS), the death rate from brain tumors in the USA averages 34 per day, 245 per week, 1,063 per month, and 12,674 per year.

Brain tumors are a critical health concern, with early detection playing a pivotal role in improving patient outcomes. Magnetic Resonance Imaging (MRI) is a widely used medical imaging modality for diagnosing brain tumors due to its non-invasive nature and high-resolution imaging capabilities. In recent years, deep learning techniques have revolutionized medical image analysis, offering enhanced accuracy and efficiency in the detection of various diseases, including brain tumors. This abstract presents an overview of a deep learning-based approach for the detection of brain tumors in MRI images. Our proposed methodology leverages Convolutional Neural Networks (CNNs) and advanced neural network architectures to automatically detect and classify brain tumors in MRI scans. The process begins with pre-processing techniques to enhance image quality and reduce noise, followed by region-of-interest extraction to focus on the relevant brain regions. Subsequently, the extracted regions are fed into a deep learning model, which learns intricate patterns and features within the images to distinguish between tumor and non-tumor regions.

Computer-vision image-based brain disease detection has gained a lot of attention in the past few years and has proved to be a highly successful tool in this field. As an emerging technology for recognizing and categorizing various diseases, Digital Image Processing successfully tackles the limitations encountered during manual inspection. Thanks to AI, particularly for Deep Learning, uses Convolutional Neural Networks to learn features directly from the raw data for image recognition and classification problems. The main aim of this research is to design an optimized deep convolutional neural network for categorizing brain tumor in MRI. The dataset used for training and

evaluation comprises a diverse collection of MRI images, including scans from different modalities, orientations, and tumor types. We employ data augmentation techniques to expand the dataset and improve the model's ability to generalize to unseen cases. The performance of our deep learning model is assessed in terms of sensitivity, specificity, accuracy. Our results demonstrate the potential of deep learning techniques for brain tumor detection in MRI images, showcasing high accuracy and sensitivity. The proposed approach exhibits promise for assisting radiologists in their clinical decision-making process by providing reliable and timely tumor detection, ultimately contributing to improved patient care and outcomes.

This research contributes to the field of medical image analysis by providing a comprehensive overview of deep learning applications in brain tumor detection and presenting a practical and accurate framework for clinical implementation. The proposed framework has the potential to revolutionize the way brain tumors are diagnosed and assist medical professionals in making more informed decisions for timely and precise treatment

ACKNOWLEDGEMENT

First and foremost, I would like to thank **God Almighty** for giving me the wisdom, strength, knowledge, ability, and opportunity to undertake this project. It gives me a great delight to express my gratitude to many people, without their support and inspiration; this thesis work would not have been possible.

I would like to express my sincere gratitude to my supervisor **Dr. Sandeep Bansal**, Associate Professor, SEEE, Lovely Professional University for the continuous support of my Ph.D. study and related research, for their patience, motivation, and immense knowledge. His guidance helped me in all the time of research and writing of this thesis. It was a great pleasure for me to have a chance to work with him. I have really learned the basics of research from during this tenure.

I would like to thank all the **faculty and staff members** of the School of Electronics and Electrical Engineering, Lovely Professional University, Punjab, India for their help and support. I am deeply thankful to **Chancellor, Vice Chancellor Lovely Professional University, Registrar, Dean (Academic), Dean (School of Engineering & Electrical Engineering), DRP and RDC members** for their moral support and for providing me with all the necessary facilities during my candidature.

I also express my deep sense of gratitude to all faculty and staff members of Electronics and Communication Engineering Department of Geethanjali College of Engineering and Technology for their constant moral support and inspiration.

I owe to my family members for all types of support. Without their affection, there would have been nothing to write an acknowledgement. In particular, I thank my parents, **Mr. Bhukya Surya and Mrs. Rangamma** and my grandparents, **Mr. K V Rao & Vimala**, for their wishes, affection, love, inspiration, and never-ending support that helped me in the difficult stages of my work. Very special thanks to my loving and caring wife **Sindhu**, for her love, affection, continuous support and encouragement. I also thank all my family members for their moral support, well wishes, and love.

Last but not the least, I express my gratitude to those who helped me directly and indirectly with the successful completion of the research work.

Thank you all for encouraging me and inspiring me to achieve my dreams.

Bhukya Ramu

42000065

Department of Electronics and Communication Engineering

Lovely Professional University

CONTENT

Name of the Content		Page No
Title		
Declaration		i
Certificate		ii
Abstract		iii
Acknowledgement		v
Table of Contents		vii
List of Figures		xiii
List of Tables		xvi
Acronyms		xvii
CHAPTER 1: INTRODUCTION		
	1.1 Introduction	1
	1.1.1 Digital Image Processing Categories	2
	1.1.2 Digital Image Processing Purposes	2
	1.1.3 Applications of Digital Image Processing	3
	1.1.4 Medical Imaging Applications	4
	1.1.5 Types of Brain Tumor	6
	1.1.6 Views of Brain Tumor Images	8
	1.1.7 Types of MRI Techniques	10
	1.1.8 Views of Noisy and De-Noisy Images	11
	1.1.9 Brain Tumor Detection	12
	1.1.10 Segmentation of Brain Tumor	13
	1.1.11 ML Based Brain Tumor Detection	15

	1.1.12 Deep Learning Based Brain Tumor Detection	16
	1.1.13 Brain Image Classification	18
	1.1.14 Diagnosis of Brain Tumor	18
	1.1.15 Biopsy of Brain Tumor	19
	1.1.16 Problem Identification	20
	1.1.17 Motivation	22
	1.1.18 Research Issues and Objectives	24
	1.1.19 Research Methodology	25
	1.1.20 Contribution of Thesis	26
	1.1.21 Thesis Structure	26
	CHAPTER 2 LITERATURE SURVEY	
	2.1 Introduction	30
	2.1.1 Biomedical Image Analysis	31
	2.1.2 Brain Digital Image Processing for MR Images	33
	2.1.3 MRI and Other Imaging Modalities	35
	2.1.4 Tumor Characterization	36
	2.2 Classification and Description of Survey	38
	2.2.1 Analysis Based on DL Techniques	38
	2.2.2 Analysis Based on Optimization	42
	2.2.3 Analysis Based on DL Techniques with Optimization	46
	2.2.4 Analysis Based on ML Techniques	49
	2.2.5 Research Papers Related to DL	53
	2.3 Research Gaps and Challenges	62

	2.4 Summary	63
	CHAPTER 3 DEEP LEARNING	
	3.1 Introduction to Deep Learning	65
	3.2 Basics of Neural Network	76
	3.3 The Artificial Neuron	77
	3.4 Deep Neural Networks	78
	3.5 Deep Network Architectures	81
	3.6 Recurrent Neural Networks	84
	3.7 Convolutional Neural Networks	85
	3.8 Max-Pooling	88
	3.9 Understanding Transfer Learning	88
	3.10 Transfer Learning for Deep Learning	89
	3.11 Shelf Pre-trained Models as Feature Extractors	89
	3.12 Pre-Trained Models	90
	CHAPTER 4 TUMOR REGION SEGMENTATION	
	4.1 Introduction	91
	4.2 Proposed Methodology	94
	4.2.1 About UNET	94
	4.3 Proposed Tumor Region Segmentation from MRI Images	94
	4.4 Block Diagram	96
	4.5 Improved Adaptive Gamma Correction	98
	4.6 Convolutional Neural Network UNET	101
	4.7 Training	102
	4.8 Result and Discussion	105

	4.9 Dataset	105
	4.10 Result Analysis	108
	4.10.1 Accuracy	108
	4.10.2 Sensitivity	108
	4.10.3 Specificity	109
	4.10.4 Precision	109
	4.10.5 F1 Score	109
	4.11 Conclusion	118
	CHAPTER 5 BRAIN TUMOR DETECTION	
	5.1 Introduction	119
	5.2 Materials and Methods	122
	5.2.1 Block Diagram	122
	5.2.2. Preprocessing	123
	5.2.3. Image smoothing	123
	5.2.4. Adaptive Histogram Equalization	124
	5.2.5. UNET	124
	5.3 Statistical Feature Extraction	126
	5.3.1 Energy	126
	5.3.2 Entropy (EN)	126
	5.3.3 Inertia (IN)	127
	5.3.4 Correlation (CO)	127
	5.3.5 Inverse Difference Moment (IDM)	127
	5.3.6 Difference Entropy (DE)	127

	5.3.7 Local Binary Patterns (LBP)	127
	5.3.8 Shape Feature	128
	5.3.9 Extreme Learning Machine (ELM)	128
	5.4 Result and Discussion	129
	5.4.1 Dataset	129
	5.4.2 Performance Matrices	130
	5.5 Conclusion	133
	CHAPTER 6 TUMOR CLASSIFICATION	
	6.1 Introduction	134
	6.2 Proposed Method	136
	6.2.1 Block diagram	136
	6.2.2 Normalization	137
	6.2.3 Image smoothing	139
	6.2.4 Contrast Enhancement	139
	6.2.5 Edge Sharpening	139
	6.2.6 Gray Level Co-occurrence Matrix (GLCM)	140
	6.2.7 Features of GLCM	140
	6.2.8 Statistical Feature Extraction	142
	6.2.9 Google Net	145
	6.3 Extreme Learning Machine (ELM)	147
	6.4 Results And Discussions	149
	6.3.1 Dataset	149
	6.3.2 Performance Metrics	149

	6.5 Results Analysis	150
	6.6 Conclusions	154
	CHAPTER 7 CONCLUSION AND FUTURE DIRECTIONS	
	7.1 Conclusion	155
	7.2 Future Directions	156
	List of Publications	157
	References	158

LIST OF FIGURES

	Name of the Figure	Page No
Figure 1.1	Brain Tumor Images	6
Figure 1.2	Primary Brain Tumors	7
Figure 1.3	Brain MRI Viewed From Three Directions	9
Figure 1.4	MRI of the Brain	10
Figure 1.5	Types of MRI Technique	11
Figure 1.6	Example of Noisy Image and De-noisy Image	12
Figure 1.7	Different Types Of Image Classification Techniques	18
Figure 1.8	Biopsy of Brain	19
Figure 1.9	Block Schematic of the Proposed Research	25
Figure 1.10	Chapter-Wise Thesis Organization	27
Figure: 2.1	Digital Image Processing Implementation	31
Figure: 2.2	Cutaway MRI Scanner	35
Figure: 3.1	Deep Learning is Shown as a Venn diagram	67
Figure: 3.2	The Artificial Neuron	70
Figure: 3.3	An Example Of a Non-Linear, Separable Problem	72

Figure: 3.4	Shallow ANN With no Hidden Layer	76
Figure: 3.5	Structure of a DNN With Three Hidden Layers	79
Figure: 3.6	Deep Neural Network with Two Hidden Layers	80
Figure 3.7	Types of Machine Learning Models, Neural Networks, and Their Properties	81
Figure 3.8	Deep Neural Network Architectures	83
Figure 3.9	Stacked Autoencoder	83
Figure 3.10	Recurrent Neural Network	83
Figure 3.11	Feature Map Through a Convolution Layer	85
Figure 3.12	The Operation Of Local Contrast Normalization	86
Figure 3.13	The Max-Pooling Operation	86
Figure 3.14	Transfer Learning	89
Figure 3.15	Representation Of Deep Neural Networks Learn Hierarchal FeatureRepresentations	90
Figure 4.1	Proposed Brain Tumor Segmentation Using Parallel UNET	96
Figure 4.2	Block diagram for Improved Adaptive Gamma Correction	100
Figure 4.3	UNET Architecture used for MRI segmentation	104
Figure 4.4	Sample Images from the Dataset Input image and Mask	106
Figure 4.5	Improved Image Using Enhanced Adaptive Gamma Correction Technique	107
Figure 4.6	(a) Input images from the dataset (b) Segmented Enhancing Tumor Region, (c) Non enhancing Tumor, (d) Edema image	110
Figure 4.7	Shows the Comparison of the Proposed Technique with Previous Works	114
Figure 4.8	Shows the Validation and Training Loss Regarding the Quantity of Iterations	114
Figure 4.9	Depicts Validation and Training Accuracy Regarding the Quantity of Iterations	115
Figure 4.10	Indicates Training and Validation Loss for Non-Enhancing Tumor UNET Training Process	115

Figure 4.11	Indicates the Training and Validation Loss for Enhancing Tumor UNET Training Process	116
Figure 4.12	Indicates the Training and Validation Loss for Edema UNET Training Process	116
Figure 5.1	Proposed Method Block Diagram	123
Figure 5.2	Sample Input And Segmented Image (a) Input image (b) Segmented image	131
Figure 5.3	Comparative Accuracy Of Proposed Method	132
Figure 5.4	Comparative Precision Of Proposed Method	132
Figure 6.1	Block Diagram Of The Proposed Method Of Brain Tumor Classification And Segmentation Techniques	138
Figure 6.2	Architecture of Google Net	147
Figure 6.3	Architecture of ELM	147
Figure 6.4	Sample Images From The Dataset	149
Figure 6.5	Parallel And Vertical Histogram	151
Figure 6.6	Comparative Performance Of Accuracy With Existing Methods	152
Figure 6.7	Comparative Performance Of Specificity With Existing Methods	153
Figure 6.8	Comparative Performance Of Precision With Existing Methods	153
Figure 6.9	Confusion Matrix For The Proposed Method	154

LIST OF TABLES

	Name of the Table	Page No
Table 4.1	Assessment Of The Proposed Approach's Performance Through Iteration	111
Table 4.2	Evaluating The Proposed Method's Performance Across Epochs	111
Table 4.3	Assessing The Performance of The Proposed Method Using Testing-to-Training Ratio	112
Table 4.4	Performance of Proposed Method Concerning Conventional Techniques	113
Table 4.5	UNET Specifications	117
Table 4.6	Confusion Matrix	117
Table 5.1	Training Parameters of UNET	126
Table 5.2	Training Parameters of ELM	129
Table 5.3	Description of Dataset	130
Table 5.4	Performance Evaluation of the Proposed Method	132
Table 6.1	Performance Of Proposed Method With Existing Methods	151
Table 6.2	Performance Of Proposed Method With Existing Methods	151

ACRONYMS

ANPR	Automatic Number Plate Recognition
OCR	Optical Character Recognition
MRI	Magnetic Resonance Imaging
CT	Computed Tomography
CNS	Central Nervous System
WHO	World Health Organization
GBM	Glioblastoma Multiforme
ANN	Artificial Neural Network
SVM	Support Vector Machine
KNN	K-Nearest Neighbor
CSF	Cerebrospinal Fluid
FLAIR	Fluid-Attenuated Inversion Recovery
CAD	Computer-Aided Detection
WM	White Matter
GM	Gray Matter
MRF	Markov Random Field
ROI	Region of Interest
SOM	Self-Organizing Maps
AI	Artificial Intelligence
ML	Machine Learning

DL	Deep Learning
CNN	Convolutional Neural Networks
LSVRC	Large Scale Visual Recognition Challenge
ELM	Extreme Learning Machine
DCNN	Deep Convolutional Neural Network
GLCM	Gray Level Co-occurrence Matrix
RGB	Red Green Blue
SIFT	Scale Invariant Feature Transform
LBP	Local Binary Pattern
GRNN	Generalized Regression Neural Network
BPNN	Back Propagation Neural Networks
PCA	Principal Component Analysis
DWT	Discrete Wavelet Transform
DCT	Discrete Cosine Transform
RNN	Recurrent Neural Network
MLP	Multi-Layer Perceptron
R-FCN	Region-based Fully Convolutional Network
SGD	Stochastic Gradient Descent
ReLU	Rectified Linear Unit
GPU	Graphics Processing Units
RBM	Restricted Boltzmann Machines

DBN	Deep Belief Networks
LSTM	Long Short-Term Memory
GRU	Gated Recurrent Unit
LCN	Local Contrast Normalization
BRATS	Brain Tumor Segmentation Challenge
IAGC	Improved Adaptive Gamma Correction
AGC	Adaptive Gamma Correction
CDF	Cumulative Distribution Function
FLAIR	Recovery after Fluid-Attenuated Inversion
ELM	Extreme Learning Machine
AHE	Adaptive Histogram Equalization

CHAPTER 1

INTRODUCTION

1.1 Introduction

Digital Image Processing involves the transformation of an image into a digital representation. It encompasses a variety of procedures aimed at improving the image and extracting valuable data. The primary goal of this technique is to restore and sharpen the image to improve its visualization. It also facilitates pattern measurement and enables efficient image retrieval in addition; Digital Image Processing is of great significance in a variety of domains including computer science, business, and engineering. It belongs to the realm of signal processing, where an input image, whether it is a photograph or a video frame, undergoes precise operations to generate an output image with specific desired attributes.

The process of Digital Image Processing commonly revolves around working with 2D signals and employing established signal processing techniques to manipulate and analyze the images effectively. The chapter provides a historical overview of the system for segmenting brain tumors using Digital Image Processing techniques. The subsequent section explores the common challenges encountered in Brain Tumor Detection. Later in this chapter, the research motivation is discussed, along with specific research problems and objectives. A diagram is used to visually represent the stages of the research methodology employed. Lastly, the contributions of the thesis, as well as the publications and organization of the thesis, are illustrated using a flow chart.

The process of Digital Image Processing encompasses three sequential steps, which are as follows:

- Acquire the image by means of digital photography or through an optical scanner.
- Perform manipulation and analysis on the image to achieve tasks such as image enhancement, pattern recognition, and data compression.
- Lastly, the results are reported, or the modified image is generated based on the analysis of the image.

1.1.1 Digital Image Processing Categories

- Digital Image Processing
- Analog Image Processing

The analog technique, also referred to as the visual technique, is utilized handling physical copies, such as prints and photographs, in Digital Image Processing. With visualization methods, image analysts store information in several formats. The application of Digital Image Processing techniques is not restricted to a specific domain but should be studied considering the expertise of the analyst. Moreover, association plays a crucial role in Digital Image Processing using analog methods, where analysts harness a blend of supplementary data and their own expertise. Furthermore, digital image techniques enable the manipulation of digital images by leveraging raw data from imaging sensors. These techniques typically involve three phases: information extraction to obtain the original information, enhancement and display of the image, and pre-processing tasks.

1.1.2 Digital Image Processing Purposes

Digital Image Processing serves various purposes across different domains. Some of the key purposes of Digital Image Processing are:

Image Enhancement: Digital Image Processing techniques are employed to improve the quality of images by enhancing their visual appearance. This includes adjusting brightness, contrast, sharpness, and reducing noise or artifacts present in the image.

Image Restoration: Image restoration techniques are used to recover or restore images that have been degraded or corrupted due to various factors such as noise, blur, or compression. These techniques aim to reconstruct the original image as accurately as possible.

Image Compression: Digital Image Processing techniques enable the compression of images to reduce their file size while preserving important visual information. Compression algorithms remove redundant or irrelevant data to achieve efficient storage and transmission of images.

Image Segmentation: Digital Image Processing algorithms are utilized for segmenting or partitioning an image into meaningful regions or objects. This aids in object recognition, analysis, and understanding of the image content.

Object Detection and Recognition: Digital Image Processing plays a crucial role in detecting and recognizing objects within images. This includes tasks such as face detection, object tracking, and pattern recognition, which have applications in various fields like surveillance, autonomous vehicles, and augmented reality.

Image Analysis and Measurement: Digital Image Processing techniques are employed to extract quantitative information from images, such as measuring distances, angles, areas, or counting objects. This enables automated analysis and measurements for scientific, medical, and industrial applications.

Medical Imaging: Digital Image Processing finds extensive application in medical imaging for purposes such as improving image quality, segmenting structures of interest, and facilitating visualization. It plays a pivotal role in aiding medical professionals in tasks such as diagnosis, treatment strategy formulation, and the continuous monitoring of a wide range of medical conditions.

These are just a few examples of the purposes and applications of Digital Image Processing, which continue to evolve and find new applications in diverse fields.

1.1.3 Applications of Digital Image Processing

Remote sensing: is a field that utilizes sensors to capture images of the Earth's surface. These images can be obtained through multi-spectral scanners or remote sensing satellites mounted on aircraft. The captured images are then processed during transmission to ground stations. This approach involves interpreting the regions and objects depicted in the images, and it finds applications in various areas such as resource mobilization, agricultural production monitoring, city planning, and flood control. Remote sensing enables the collection of valuable data and information about the Earth's surface from a distance, providing insights and supporting decision-making processes in various fields.

Biomedical Imaging techniques: In this modality, various imaging tools such as MRI (Magnetic Resonance Imaging), Ultrasound, CT (Computed Tomography), and X-ray are utilized. These imaging techniques serve different purposes and have distinct principles of operation:

Magnetic Resonance Imaging (MRI): MRI, or Magnetic Resonance Imaging, relies on the utilization of powerful radio waves and magnetic fields can be used to create

incredibly detailed images of inside body systems. This technology proves especially valuable when it comes to capturing intricate visuals of soft tissues, including organs, muscles, and the brain, offering a level of precision that is often indispensable in medical diagnostics and research. MRI is commonly employed for diagnosing conditions such as tumors, joint injuries, and neurological disorders.

Ultrasound: Ultrasound imaging makes use of high-frequency sound waves to generate images of internal body structure. It is commonly used in prenatal care to monitor fetal development and detect any abnormalities. Additionally, ultrasound is used for imaging organs, blood vessels, and soft tissues, and can assist in guiding minimally invasive procedures.

Computed Tomography (CT): CT scans, also known as Computed Tomography scans, employ a sequence of X-ray images captured from various angles to produce cross-sectional images of the human body. This technique provides detailed information about bones, blood vessels, and organs. CT scans are valuable for diagnosing conditions like fractures, tumors, and internal bleeding.

X-ray: X-ray imaging involves using to create images of the bones and tissues, a small quantity of ionizing radiation is used. X-rays are frequently used to identify lung problems, infections, and fractures. They are widely available, relatively inexpensive, and provide quick results. Each of these imaging tools has its strengths and limitations, and they are chosen based on the specific requirements of the medical situation. By utilizing a combination of these imaging modalities, healthcare professionals can obtain a comprehensive understanding of the internal structures and conditions of the human body.

1.1.4 Medical Imaging Applications

- The biomedical imaging applications are given below:

Identification of lung disease: This inherent contrast in X-ray images between air-filled spaces and solid tissues provides valuable information for diagnosing various conditions and abnormalities within the body. Radiologists and healthcare professionals interpret these differences in density to identify fractures, tumors, infections, and other abnormalities that may be present.

Digital mammograms: Mammography is a frequently employed imaging method for

the purpose of detection and diagnosis of breast tumors and other breast abnormalities. In the process of analyzing mammograms, various Digital Image Processing techniques are employed to enhance the interpretation and extraction of relevant information.

Identification of heart disease: In the field of diagnosing heart diseases, it is crucial to analyze and identify specific features such as the shape and size of the heart. These diagnostic features play a significant role in categorizing different heart conditions and guiding appropriate treatments. To achieve this, image analysis approaches are employed to enhance the interpretation and diagnosis of heart-related diseases using radiographic images.

Medical imaging is a powerful technology utilized to obtain valuable insights into medical abnormalities. It involves generating visual representations of the body tissues or internal organs, which are then used for clinical diagnosis. Digital Image Processing is an integral part of the medical system and applications, playing a crucial role in the field of medicine from diagnosis to therapy. It exerts a notable influence on the operational processes in digital medical diagnostics. Early detection is crucial for improving the prognosis and survival rates of brain tumor patients. Identifying tumors at an early stage increases the chances of successful treatment and significantly improves overall patient outcomes. It enables medical professionals to initiate appropriate interventions promptly and develop personalized treatment plans based on the specific characteristics of the tumor.

Advancements in medical imaging technologies, such as MRI and CT scans, have greatly enhanced the detection of brain tumors. These imaging techniques provide detailed images of the brain, allowing for the identification of tumors at earlier stages, which is crucial for effective treatment and better patient outcomes. These imaging modalities allow for non-invasive visualization and detailed examination of the brain, helping to identify the presence, location, and characteristics of tumors. Early detection of tumors enables the timely implementation of appropriate treatment strategies, offering a chance to intervene before the disease advances or spreads to other parts of the body this can lead to better disease management and improved patient outcomes. In summary, the diagnosis of tumors in the early stages is crucial for improving survival possibilities and treatment outcomes.

Brain tumors occur as the accumulation or abnormal expansion of biological the cells in the human brain. These tumors can arise from the division of abnormal cells, which separate from the normal brain cells. Over time, these abnormal cells continue to develop and increase in size within the rigid skull that surrounds the brain. The growth of the tumor mass within the confined space of the skull exerts pressure on the brain cells, leading to a range of complex issues and severe pain. As the tumor grows, it can interfere with the normal functioning of the brain, disrupting various neurological processes. The increased pressure on surrounding brain tissue can cause symptoms such as headaches, seizures, cognitive impairments, motor deficits, and changes in behavior or personality. The specific symptoms experienced can differ based on the position and size of the brain tumor.

1.1.5 Types of Brain Tumor

There are typically four types of brain tumors: primary tumors, secondary tumors (also known as metastatic tumors), benign tumors, and malignant tumors. The growth of any of these tumor types can have severe implications for a patient's life as it occurs within the confines of the skull.

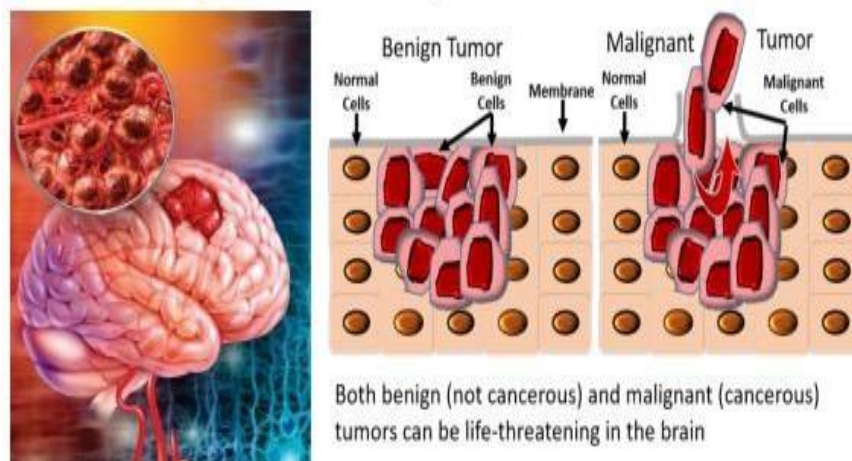


Figure 1.1 Brain tumor images [SMane, Mansa et al. (2014)].

Primary Tumor: A primary brain tumor originates within the brain itself. These tumors can develop from different types of brain cells and are categorized based on the specific. The type of cell and its location within the brain are determining factors. Primary brain tumors can manifest as either benign or malignant growths.

Secondary Tumor (Metastatic Tumor): A secondary brain tumor, often referred to as a metastatic tumor, develops when cancer cells from a different region of the body

migrate and establish themselves in the brain. These tumors are considered secondary because they have originated from cancer that started elsewhere in the body. Metastatic brain tumors are always malignant.

Benign Tumor: A benign brain tumor is a development that is usually slow-growing and not malignant, And does not invade nearby tissues. Despite being non-cancerous, benign tumors can lead to complications and health concerns depending on their size and their specific location within the brain.

Malignant Tumor: Malignant brain tumor is a cancerous growth that can rapidly invade nearby healthy tissues and potentially the potential for spread to other areas of the brain or central nervous system exists. Malignant tumors are generally more aggressive and pose a greater threat to a patient's health and well-being. Growth of any type of brain tumor can have detrimental effects on a patient's life due to the confined space within the skull. Figure 1.2 is referenced as illustrating primary brain images, which likely depicts visual representations or scans of primary brain tumors for diagnostic or research purposes.

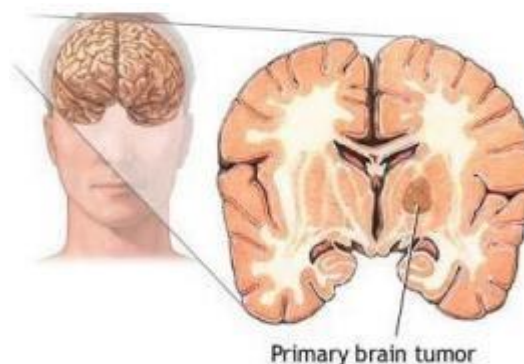


Figure 1.2 Primary brain tumors [Kieran MW, Chi SN, Manley PE, et al. (2015)]
Proper diagnosis, accurate classification, and timely treatment are crucial in managing brain tumors to mitigate their harmful effects and improve patient outcomes. Treatment options can encompass surgery, radiation therapy, chemotherapy, targeted therapies, or a combination of these strategies, depending on the type, location, and stage of the tumor.

GBM (Glioblastoma) stands out as the most aggressive and prevalent form of glioma, constituting approximately 54% of all glioma cases. Gliomas, including GBM, are characterized by their fast infiltrative growth within the brain. Unfortunately, after

diagnosis, the prognosis for GBM is generally poor, with an average survival time of around 1 year. Among all malignant brain tumors, Gliomas make up roughly 30% of both brain tumors and CNS tumors. Gliomas are further categorized into four distinct grades according to the World Health Organization (WHO) classification.

Grade I: Grade I tumors are considered benign tumors with cells that closely resemble normal glial cells. They typically have a slow growth rate and are less aggressive compared to higher-grade gliomas. **Grade II:** Grade II tumors show slightly abnormal cell characteristics compared to normal glial cells. They are considered low-grade gliomas and have a relatively slow growth rate. **Grade III:** Grade III tumors are classified as malignant gliomas. They exhibit more pronounced cellular abnormalities and have a faster growth rate compared to lower-grade gliomas. **Grade IV:** Grade IV gliomas are the most severe and aggressive stage of glioma. The most common grade IV glioma is Glioblastoma Multiforme (GBM). Grade IV tumors exhibit pronounced tissue abnormalities that are observable without the need for microscopic examination.

1.1.6 Views of Brain Tumor Images

In standard clinical procedures, the evaluation of acquired images is typically carried out manually, relying on quantitative measures or criteria such as the primary visible diameter in an axial slice. There is so a substantial possibility for an automated and highly accurate method to analyze brain tumor scan images, offering immense potential for therapy planning and diagnosis. The manual annotation process is performed by experienced raters, revealing variations in the areas due to obscured or smoothed intensity gradients between surrounding tissues and tumor structures these discrepancies can often be attributed to partial volume effects or bias field artifacts. Furthermore, the detection of brain tumor lesions hinges exclusively on disparities in relative intensity, their specific location, size, and shape for each individual patient. As the number of patients has increased, there has been a corresponding increase in the amount of data collected. Figure 1.3 provides a visual representation of the Brain MRI as viewed from three different perspectives.

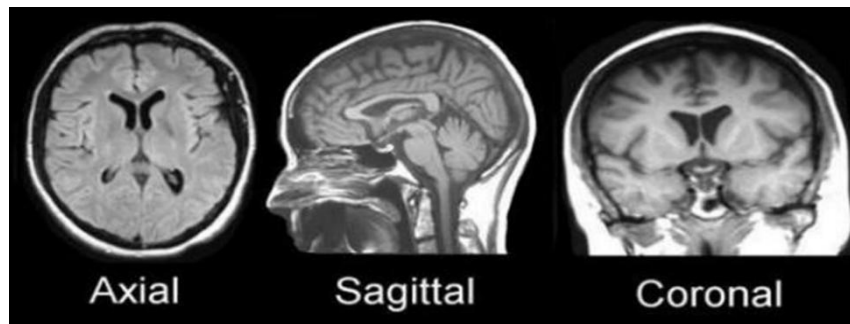


Figure 1.3 Brain MRI viewed from three directions [Ullah, Zahid & Lee, et al. (2020)]

MR sequences: MRI techniques are widely employed for exploration and analysis of brain tumors. Each technique is utilized for different imaging processes, encompassing a range of MR sequences. Currently, multiple MR sequences are often combined to attain more precise and valuable results. MRI plays a crucial role in advanced research endeavors focused on studying the human brain. The image in question offers valuable insights into the soft tissue structures. Furthermore, MR images greatly enhance our understanding of brain pathology and enable accurate identification of abnormalities. However, the volume of data involved makes manual interpretation challenging, thus necessitating the adoption of advanced image analysis tools. The demand for such tools has significantly increased as a result.

MR imaging methods are frequently employed for imaging brain tumor growth and accurately identifying their location due to their high resolution. MR images offer greater flexibility compared to X-ray and CT scan images. One significant advantage of MR images is that they are radiation-free, which is beneficial for the well-being of the human body as radiation can be harmful. Various techniques such as atlas methods, knowledge-oriented systems, fuzzy schemes, shape-based techniques, neural networks, and variation segmentation are utilized for categorizing MRI scans; MRI classification commonly involves two existing schemes: unsupervised and supervised processes. In the supervised model, Artificial Neural Networks (ANN), Support Vector Machines (SVM), and K-Nearest Neighbors (KNN) are frequently utilized. On the other hand, the unsupervised approach encompasses techniques such as Self-Organization Maps and Fuzzy C-means clustering. Researchers often employ both unsupervised and supervised processes to classify MRI scans as either abnormal or

normal; MR images play a crucial role in identifying tumor regions by employing various contrast agents to highlight specific features. However, medical imaging research encounters challenges when it comes to accurately identifying brain tumors in MR images. Tumor tissues exhibit notable differences compared to normal tissues in many patients. MR images offer precise visualization of the anatomical tissue structure, and the data derived from these images are immensely valuable for detecting brain tumors. To identify brain tumors, MR images are accurately segmented using computer-assisted clinical tools. This necessitates brain image segmentation, which is considered one of the most challenging tasks. Manual segmentation of brain MRI is known for being a time-consuming and non-reproducible procedure that often leads to non-uniform segmentation results, varying among different specialists. In such cases, computer-assisted tools provide valuable support. Figure 1.4 provides a visual representation of a brain MRI.

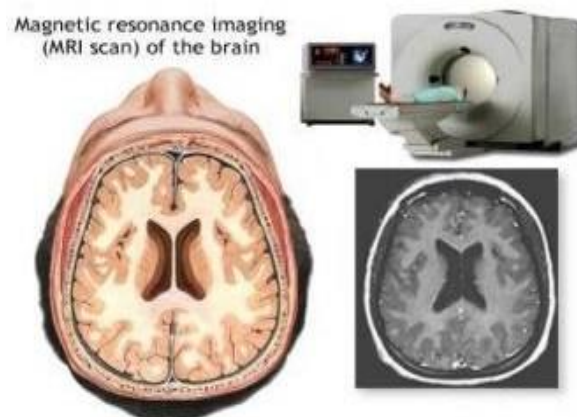


Figure 1.4 MRI of the brain [V. Vijaya Kishore and V. Kalpana et.al. (2019)]

1.1.7 Types of MRI Techniques

T1 Weighted Image: In the realm of MRI, T1 refers to the duration it takes for the protons within a tissue revert to their original magnetization state within the static magnetic field. A T1-weighted image, compared to other T2-weighted images, offers high anatomical detail. However, it may not provide as much relevant information when examining brain tumors. T1-weighted images, when enhanced with a contrast agent, can effectively highlight the flow of blood. This can result in hyper-intense appearances of vessels and the active part of a tumor, making them easily

distinguishable from surrounding tissues. Active tumors are commonly examined using these enhanced T1-weighted images, especially in the investigation of malignant tumors. Additionally, these images are commonly referred to as "contrast-enhanced T1-weighted images."

T2 Weighted Image: T2 is the time reference, required for protons to lose coherence after being disturbed by coherent oscillations from the radio frequency pulse. T2-weighted images are more sensitive to water content compared to T1 images. As a result, (CSF) appears hyper-intense, making it easier to detect pathologies in T2-weighted images.

FLAIR Image: Fluid-Attenuated Inversion Recovery (FLAIR) is a dedicated MRI sequence crafted to attenuate or suppress the signal from fluids in the image, thereby enhancing the visibility of other structures and CSF during brain imaging. This technique effectively distinguishes lesions from CSF by causing the CSF to appear hypo-intense in T2-weighted images. FLAIR is commonly used in brain tumor imaging. Figure 1.5 provides a visual depiction of different types of MRI techniques, including FLAIR.

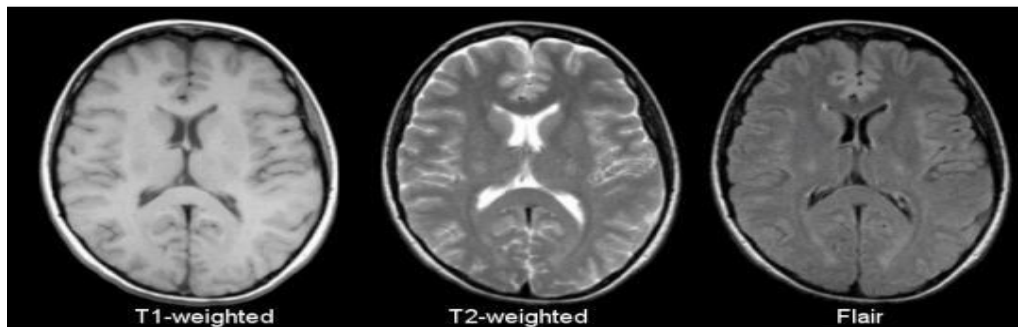


Figure 1.5 Types of MRI Technique [Filippi, M., Rocca et.al. (2011)]

1.1.8 Views of Noisy and De-Noisy Images

In Digital Image Processing, image de-noising and filtration serve as essential preprocessing steps. De-noising involves employing specific restoration techniques to remove noise that may be introduced during image transmission, compression, or acquisition. This process aims to maximize and enhance the quality of the image, leading to more accurate and improved results. Figure 1.6 provides an example

illustrating the difference between a noisy image and a de-noised image.

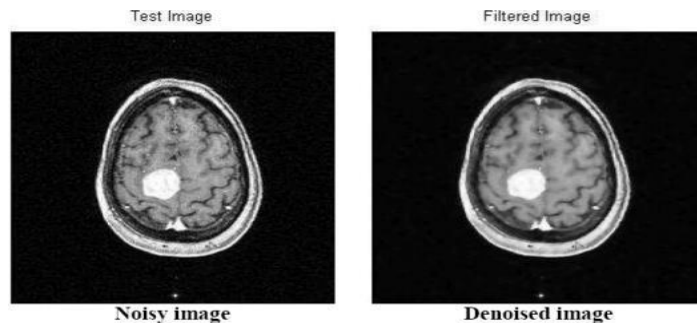


Figure 1.6 Example of noisy image and de-noisy image [Gomathi, P et.al. (2020)]

1.1.9 Brain Tumor Detection

Tumor detection represents a pivotal facet of biomedical image analysis and has evolved as a substantial advancement in clinical investigations undertaken by healthcare professionals. Imaging techniques are initially employed to identify tumors and document medical images. To differentiate the suspicious tumor area from the surrounding healthy tissue, software-oriented algorithms are applied to process the obtained images. These types of algorithms have a crucial function in segregating and outlining tumor areas, thereby contributing to precise tumor detection and diagnosis. Segmentation is an essential undertaking within the realm of medical imaging that is performed by specialists to achieve higher accuracy. However, it is a time-consuming operation that poses challenges. To address these challenges, radiologists have increasingly adopted semi-automatic segmentation techniques. This strategy has the ability to mitigate the drawbacks of fully computerized segmentation models by involving the radiologist in the segmentation process. By combining the expertise of radiologists with automated segmentation methods, Enhancing the efficiency and precision of segmentation in medical imaging is achievable.

Image segmentation represents a pivotal stage in which the affected area is isolated from the remainder of the image. Accurate segmentation techniques play a critical part in defining the tumor's size and placement, thereby aiding in treatment planning. Expert physicians are responsible for defining the initial settings and training data used in the segmentation process. Numerous research studies are conducted to extract

visual data and identify various types of tumors. These investigations aim to improve the understanding and characterization of different tumor types using visual information extracted from medical images.

Timely identification of any disease is essential for successful treatment and improving the likelihood of patient survival, particularly in the case of brain tumors. Timely identification not only lowers the risk to the patient's life but also enhances the chances of effective treatment, with cure rates reaching as high as 90%. However, achieving tumor detection requires the expertise of specialized medical professionals who can assess the patient's condition and interpret diagnostic results accurately. Their involvement is necessary to ensure accurate and timely detection, leading to appropriate treatment interventions. Due to the challenges of handling brain tumor detection for all individuals, the significance of computer-aided detection (CAD) becomes even more pronounced. CAD serves as the initial stage of tumor detection and is performed automatically by specialized software. While MRI produces brain images, the software is responsible for detecting various areas or sections indicative of a brain tumor. CAD assists human experts in generating preliminary reports regarding tumor possibilities. In the detection of brain tumors, computer-based detection plays a vital and influential role, enhancing the efficiency and accuracy of the diagnostic process. Currently, CADe (Computer-Aided Detection) systems are commonly utilized for the explicit and efficient identification of anomalies in the brain. CADe, also referred to as CADx (Computer-Aided Diagnosis) systems, assist doctors in interpreting medical images. These systems provide an interdisciplinary tool that integrates computer vision, AI, and Digital Image Processing techniques from pathology and radiology. The abnormal growth of brain tumor tissue or its impact on the central nervous system can significantly interfere with proper brain function.

1.1.10 Segmentation of Brain Tumor

Brain tumors are divided into segments it is crucial in the processing of medical images. There are three main categories of brain tumor segmentation models: interactive methods, automated and semi-automatic techniques. Semi-automatic

approaches involve User interactions are frequently seen as classification approaches. The purpose of brain tumor segmentation in the medical imaging field is to accurately separate tumor tissues, includes edema and necrosis, in white matter (WM), gray matter (GM), and cerebrospinal fluid (CSF), normal brain tissues. This classification process allows for precise localization and analysis of tumor-related structures within the brain. The segmentation process plays a crucial role in identifying tumor tissues using medical imaging techniques, and assessments are frequently carried out on improved images. The accuracy achieved through segmentation is of great importance in the medical field, as it aids in early disease detection. Accurate segmentation results are particularly significant for treatment planning and surgical interventions, where precision is a critical factor in determining appropriate treatments for patients. However, the current approach may be inefficient and time-consuming, as it lacks consideration of automatic classifications and decision-making processes.

There are various difficulties in analyzing MRI brain tumor image. that motivate the need for more in-depth analysis. Brain tumor segmentation and auto classification techniques hold the potential to improve the accuracy of diagnosis for various medical images. Segmentation is essential for classifying image pixels based on different anatomical regions such as blood vessels, muscles, and bones. It is also used to identify and classify pathological regions, including multiple sclerosis lesions, tissue deformities, and cancerous areas. Furthermore, obtaining good image segmentation involves considering certain aspects to ensure accurate delineation and identification of regions of interest within the image.

1. Significant difference in the segmented image was obtained in the adjacent regions.
2. Regions of the segmented image are similar.
3. The segmented region boundary is not coarse and smooth.
4. Regions in the internal area must be clear with no small holes.

The use of an automated classification system for brain tumors is a useful tool that aids medical professionals in providing patients with effective care. These systems utilize MRI images, which are commonly employed by radiologists for brain

diagnosis. In recent times, researchers have developed various automated systems that utilize MR images to classify and detect brain tumors. Additionally, in brain tumor segmentation, hybrid approaches combining cellular automata and FCM (Fuzzy C-means) algorithms have been proposed. The challenges associated with seed growing segmentation methods have been addressed by introducing a novel similarity function incorporating 'Gray-Level Co-occurrence Matrix' (GLCM), and the performance of these approaches has been evaluated using the BraTS2020 dataset. A proposed automated method for brain tumor detection utilizes tumor extraction and image segmentation techniques. The method involves extracting the tumor area and capturing circularity features from the segmented brain images. The segmented images are compared against ground truth images to see how accurate the segmentation was to measure the average similarity. Additionally, a method for segmenting MR brain images that is semi-automatic has been created. This method uses active contour methodology with an initialized region of interest (ROI) to perform segmentation of the required area and incorporates human participation to create a feature map from MR images.

The brain is segmented using the Markov Random Field (MRF) model. Brain tumors are found using an automated detection method in 3D images. The process involves histogram matching and bias field correction to segment the region of interest (ROI) from the background of the image. The performance and accuracy of the segmentation are evaluated using the BRATS2020 dataset. In recent times, numerous research studies have focused on the development of automatic tumor detection methods for various types of tumors. In the field of MR images, researchers are actively exploring novel approaches to enhance the efficiency of segmentation and automatic tumor detection. Artificial Neural Networks (ANNs) have made significant contributions in medical imaging and Digital Image Processing. They serve as a prominent framework for disease diagnosis and medical image analysis. ANNs excel in handling complex tasks that require brain-like performance. Their efficient structure has positioned them as a crucial tool in various medical fields.

1.1.11 ML Based Brain Tumor Detection

Machine Learning (ML) refers to statistical models and algorithms used to perform

specific tasks without explicit programming or instructions. ML algorithms are a crucial component of the discipline of medical imaging makes substantial use of artificial intelligence (AI). ML can be categorized into two major types: unsupervised learning and supervised learning. In supervised learning, algorithms are trained to identify the mapping function between input variables and their corresponding output labels. This enables the algorithm to make predictions for new subjects based on related output labels. Using methods like ANN, SVM, and KNN, supervised learning aims to discover innate patterns within the training data. Self-Organizing Maps (SOM) and Fuzzy C-Means (FCM) are frequently employed to examine input variables in unsupervised learning. In order to extract features, training images often utilize statistical, grayscale, and texture features. However, in certain cases, tumor segmentation is required prior to the feature extraction stage. These features are referred to as handcrafted features, as they require domain expertise to identify the relevant and important features. Handcrafted feature extraction is prone to error and can be time-consuming, especially when dealing with large amounts of data

1.1.12 Deep Learning Based Brain Tumor Detection

A branch of machine learning known as Deep Learning (DL) focuses on data representation and learning hierarchical features. DL algorithms utilize layered arrangements of nonlinear processing units for the purpose of feature extraction. The result of each layer serves as the input for the next layer, enabling a deep network to abstract and process data at various degrees of abstraction. Convolutional Neural Networks (CNNs) are a popular class of DL algorithms commonly used for visual imagery analysis. They are designed to minimize the need for extensive preprocessing and are inspired by biological processes in the human brain. CNNs are particularly effective in handling data arranged in multiple arrays or dimensions. The use of deep CNNs dates back to the late Lecun's introduction of the deep neural network in the 20th century called "LeNet" for document recognition applications. However, the popularity of deep CNNs surged in later years, particularly after the introduction of AlexNet, which achieved remarkable performance in image classification, specifically in the ImageNet Large Scale Visual Recognition Challenge (LSVRC) in 2010. AlexNet's success paved the way for subsequent advancements in CNN architectures

within the field of Deep Learning.

CNNs offer several advantages over traditional ML and feature learning approaches. One of their key benefits is the potential for achieving higher accuracy and robustness. Vanilla neural networks, which have increased training samples, can greatly improve accuracy. In CNNs, convolutional filters act as feature extractors, capturing more complex features such as structural and spatial information. This is accomplished by convolving small filters across input patterns, selecting important features, and subsequently training the classification network. The combination of feature extraction and classification training in CNNs contributes to their superior performance and ability to handle complex tasks.

When assessing the effectiveness of deep learning approaches for brain tumor classification dataset comprising images from various patients is typically used. A subset of these images is employed to test and train the classification model. While deep learning has shown promising results in brain tumor classification, it requires a large number of training samples, high computational resources, and lengthy training times; In contrast, Extreme Learning Machine (ELM) is a regression and classification method that has gained attention due to its ability to overcome some of the limitations associated with back propagation approaches. ELM exhibits lower complexity and faster training speeds, making it advantageous over other classifiers. The efficiency and speed of training are notable merits of ELM.

1.1.13 Brain Image Classification

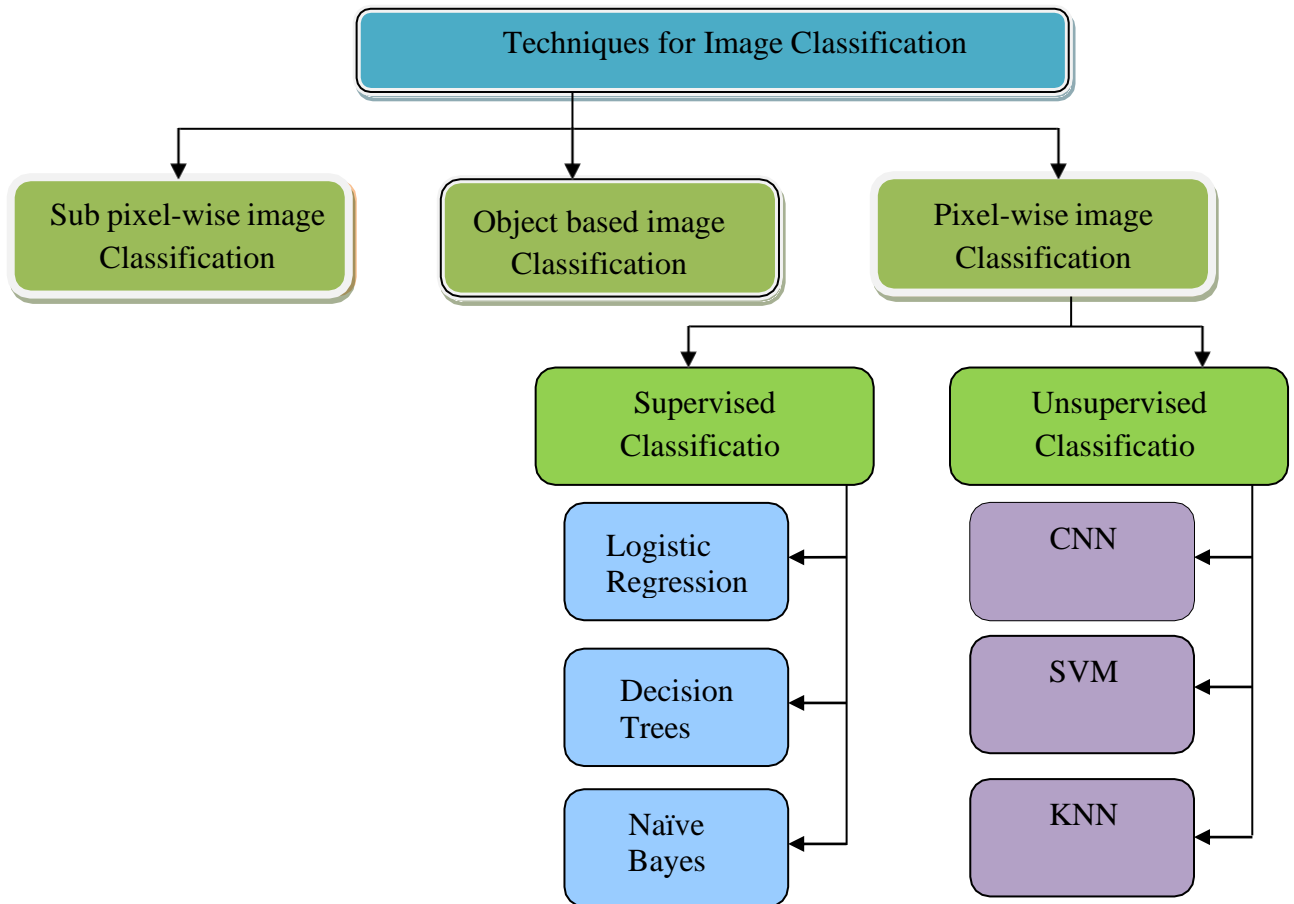


Figure 1.7 Different types of image classification techniques [Jalalian, Afsaneh et.al. (2017)]

Three main types of image classification methods are commonly used: object-based classification, pixel-based classification, and sub-pixel-based classification. Using object-based classification, pixels are categorized into useful items. and assigning class labels to those objects. Pixel-based classification assigns class labels to individual pixels based on their spectral properties. Sub-pixel-based classification goes a step further by considering the fractional contribution of different classes within each pixel. Figure 1.7 provides a visual representation of the different types of image classification techniques

1.1.14 Diagnosis of Brain Tumor

Doctors utilize various tests to identify and diagnose brain tumors. These tests may

also find out if the tumor has spread to other bodily regions, a condition known as metastasis, which is rare in primary brain tumors. Multiple tests are conducted by doctors to gather essential information for determining the most suitable treatment approach. During a biopsy, a sample of the tumor is taken to determine the specific type of tumor. This can be done either by removing the entire tumor through surgery or by taking a small tissue sample for analysis. The extracted tissue sample is then sent to a laboratory for further testing, such as histological examination or molecular analysis, to obtain a more accurate diagnosis. In light of the biopsy's findings, the doctor may recommend additional tests or procedures if further information is needed to establish a precise diagnosis or guide treatment decisions.

1.1.15 Biopsy of Brain Tumor

It is indeed a procedure that involves drilling a hole in the skull to access the brain and remove a sample of the tumor or surrounding tissue to be looked at under a microscope. That process is considered invasive and carries certain risks, given the delicate nature of the brain. The precise location of the tumor and guidance during the biopsy procedure are often aided by imaging techniques such as MRI or CT scans. Figure 1.8 provides a visual representation of the biopsy of the brain, illustrating the process involved in obtaining a tissue sample for diagnostic purposes.

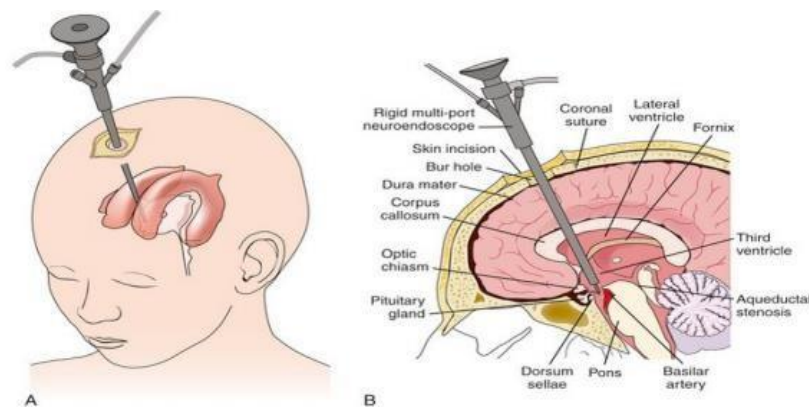


Figure 1.8 Biopsy of Brain [Muhammad Naeem Tahir et.al. (2018)]

Imaging tests play a crucial role in helping doctors differentiate between a primary brain tumor and a tumor that has spread to the brain from another part of the body. These tests provide detailed images of the internal structures and aid in the diagnostic process. When selecting a diagnostic test, doctors take several factors into consideration, including

Signs and symptoms

General health and Age

Type of tumor

Outcomes of earlier medical tests

The diagnosis of brain tumors is typically carried out by a team of medical professionals, including neurologists and internists. Specialists in the diagnosis and treatment of brain, spinal cord, and other neurological conditions include neurologists and CNS. They have expertise in identifying and evaluating various neurological problems, including brain tumors. Internists, on the other hand, are physicians who specialize in the care of adult patients and are skilled in diagnosing and managing a diverse array of medical conditions. In the context of brain tumor diagnosis, both neurologists and internists play important roles in evaluating patients, conducting necessary tests, and determining appropriate treatment approaches.

1.1.16 Problem Identification

Accuracy and Reliability: Attaining precise and dependable results poses a significant hurdle in segmentation and detection of brain tumors. The diverse characteristics of tumors, such as their varying sizes, shapes, and locations within the brain, make it challenging to accurately identify and segment them from brain images. Therefore, it is imperative to develop a resilient and trustworthy algorithm capable of accurately detecting tumors of different types and sizes. This is essential for ensuring effective diagnosis and planning appropriate treatment strategies.

Computational Efficiency: Another obstacle is to achieve computational efficiency in the process of segmentation and detection. Brain images are typically extensive and intricate, demanding substantial computational resources and time for processing. It is crucial to develop efficient algorithms that can handle these computational demands while preserving accuracy. This is particularly important in clinical settings where prompt decision-making is critical. By enabling real-time or near-real-time analysis, efficient algorithms can facilitate timely diagnoses and enhance the overall workflow.

Variability and Heterogeneity: The presence of considerable variability and heterogeneity in the appearance, texture, and characteristics of brain tumors presents a formidable challenge for segmentation and detection algorithms. These algorithms

must be adaptable and capable of accounting for different tumor types and subtypes. It is crucial to develop robust algorithms that can effectively handle this variability and accurately detect tumors across diverse patients and imaging modalities. By addressing this challenge, we can enhance the reliability and generalizability of the algorithms, leading to improved tumor detection and diagnosis in clinical practice

Handling Image Artifacts: Brain images frequently encounter artifacts, including noise, partial volume effect, and imaging distortions, which can adversely impact the accuracy of tumor segmentation and detection. It is crucial to develop techniques that can effectively handle and mitigate these artifacts to ensure reliable and accurate results. This may involve implementing pre-processing steps, such as denoising and normalization, to improve the quality of the images. Additionally, incorporating artifact-aware algorithms that are specifically designed to handle these challenges can further enhance the accuracy of tumor segmentation and detection. By addressing these artifacts, we can minimize their impact on the analysis and improve the overall robustness of the algorithms.

Limited Training Data: Obtaining labeled training data for brain tumor segmentation and detection can be challenging due to the need for expert annotations and the rarity of certain tumor types. Limited training data can hinder the performance and generalizability of machine learning algorithms. To address this challenge, it is crucial to develop techniques that can augment the available data. One approach is data augmentation, which involves generating synthetic samples to expand the training dataset. Another strategy is to leverage transfer learning, where pre-trained models from related tasks or datasets are used to kick start the training process. Additionally, unsupervised learning approaches can be employed to extract valuable information from unlabeled data, thereby increasing the available training resources. By incorporating these techniques, the limitations imposed by a scarcity of labeled data can be overcome, leading to improved performance and adaptability of the algorithms for brain tumor segmentation and detection.

Clinical Validation and Adoption: In Clinical practice needs to successfully include brain tumor segmentation and detection technologies, it is crucial to conduct thorough clinical validation studies. These studies should be designed to provide robust evidence of the algorithms' effectiveness, reliability, and safety when applied in real-

world clinical scenarios. To ensure widespread acceptance and utilization of these technologies, it is necessary to overcome various barriers to adoption. This includes obtaining regulatory approval, seamlessly integrating the algorithms with existing healthcare systems, and addressing concerns related to liability and trust. By addressing these challenges and demonstrating the clinical validity of the algorithms, they can be successfully implemented in clinical settings, ultimately leading to improved patient care and outcomes.

Addressing these challenges requires collaboration between researchers, clinicians, and technologists to develop robust and accurate algorithms that can enhance the efficiency and effectiveness of brain tumor segmentation and detection, ultimately improving patient outcomes.

1.1.17 Motivation

Advance detection and diagnosis are vital because brain tumors can profoundly impact an individual's health and overall quality of life. The utilization of segmentation and detection algorithms can play a pivotal role in identifying brain tumors at an early stage, facilitating prompt medical intervention and leading to improved patient outcomes. By enabling early detection, these algorithms contribute to a higher likelihood of successful treatment and enhanced quality of life for individuals affected by brain tumors

Treatment Planning and Monitoring: Effective treatment planning depends on how to correctly segment and diagnose brain tumors. Precisely delineating the boundaries of the tumor is essential in assisting surgeons in determining the most suitable surgical approach while ensuring the preservation of healthy brain tissue. Moreover, segmentation algorithms provide valuable assistance in monitoring the progression or regression of tumors during and after treatment. This information is vital for making informed decisions regarding therapy adjustments and evaluating the efficacy of the treatment. By facilitating precise tumor delineation and providing valuable insights throughout the treatment process, these algorithms significantly contribute to optimizing treatment outcomes and improving patient care.

Improved Patient Care: Brain tumor segmentation and detection algorithms have the potential to enhance patient care by providing quantitative measurements and

objective data. These algorithms offer clinicians valuable information that can assist in making informed decisions, such as selecting appropriate treatment strategies and assessing treatment response. By providing accurate and reliable tumor detection, these algorithms can reduce the risk of misdiagnosis or overlooking smaller tumors, ultimately improving patient management and personalized care. The objective and quantitative nature of the data provided by these algorithms contribute to a more precise understanding of the tumor's characteristics and progression, enabling clinicians to tailor treatment plans to individual patients.

Time and Cost Efficiency: Automating the process of brain tumor segmentation and detection brings significant benefits by reducing the time and effort required for manual analysis. Clinicians can save valuable time by minimizing tedious and repetitive tasks, allowing them to dedicate more attention to interpreting the results and delivering personalized care to their patients. In addition, automated algorithms have the potential to reduce healthcare costs associated with image interpretation. By providing a more efficient and consistent approach to tumor segmentation and detection, these algorithms contribute to streamlined workflows and standardized analysis. This not only improves the overall efficiency of healthcare services but also ensures a more consistent and reliable interpretation of brain images. Ultimately, automation in this domain leads to enhanced patient care, reduced healthcare costs, and improved clinical outcomes

Research and Development: The utilization of brain tumor segmentation and detection algorithms it plays a pivotal role in advancing medical research and development. These algorithms make it easier to analyze brain imaging data in large-scale studies and clinical trials, enabling researchers to effectively investigate tumor characteristics, treatment outcomes, and correlations with patient demographics. This deeper understanding of brain tumors facilitates the development of targeted treatment approaches, leading to improved patient outcomes and a more comprehensive knowledge of this complex medical condition.

Accessibility and Outreach: The development of precise and efficient the creation of algorithms for the Brain tumor segmentation and detection have the potential to improve patient access to medical care, especially in underserved areas where specialized medical expertise is limited. Automated algorithms enable telemedicine

and remote diagnosis, allowing healthcare professionals to analyze brain images and provide initial assessments from a distance. This technology helps bridge healthcare disparities, ensuring that patients receive timely and appropriate care regardless of their location. The primary motivation behind brain tumor segmentation and detection is its ability to enhance early detection, improve treatment planning and monitoring, provide superior patient care, increase efficiency, advance medical research, and improve accessibility to healthcare services. These advantages ultimately contribute to better patient outcomes, reduced healthcare costs, and advancements in the field of neuro-oncology Top of Form.

1.1.18 Research Issues and Objectives

The primary goals of this study are to tackle the challenges associated with real-time brain tumor detection through efficient preprocessing algorithms and feature extraction methods. The aim is to identify brain tumors in real-time and provide a cost-effective solution to society by comparing it with existing systems and techniques. The major components targeted in the present study include:

- **Pre-processing Algorithm:** It is responsible for the accurate extraction of brain tumor .
- **Segmentation:** It is responsible for dividing an image or a digital representation of an object into multiple distinct regions or segments based on specific criteria or characteristics.
- **Feature Extraction:** It is responsible for various exact features of the tumor that can act as a base for exact classification.
- **Classification:** It is responsible for the exact identification and related tumor location.

To work on the above-mentioned significant components, first, there is a need to identify the platform that is capable enough to perform the challenging task. This helps to implement the system with greater accuracy and lesser time and how to verify the system's effectiveness. After the selection of the platform, Datasets selection needs to identify carefully.

- How to select an efficient dataset.
- How to train the selected dataset.

- Which deep-network should be used to increase the efficiency and deploy the pre-trained Network?
- Which edge device is compatible with a selected platform?

By taking into consideration all the above-discussed points, the researcher summarizes the following objectives.

- **RO1:** To extract the tumor region in MRI brain images.
- **RO2:** To develop a pre-processing algorithm to enhance the quality of MRI images.
- **RO3:** To develop deep learning based novel algorithm to classify brain tumors into three classes, normal (no tumor), benign and malignant).
- **RO4:** Performance verification of the projected method by comparing it with already existing techniques.

1.1.19 Research Methodology

Below is a generalized block schematic of the proposed research work

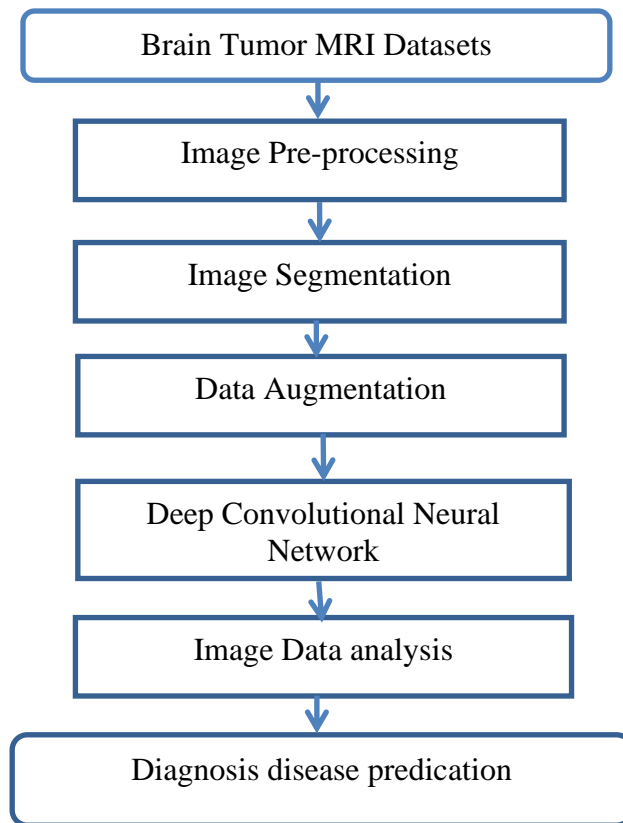


Figure 1.9 Block Schematic of the Proposed Research

1.1.20 Contribution of Thesis

The ongoing search focuses on the specific research inquiries and aims to provide the following contributions mentioned in the thesis. A thorough literature review of all preprocessing, segmentation, and classification methods is conducted.

1. A thorough research has been conducted to examine various preprocessing, segmentation, and classification techniques.
2. The backdrop must be removed and the algorithm must be implemented through the merger of preprocessing techniques.
3. To comprehend the diverse Brain tumor datasets available for research, a thorough investigation has been conducted.
4. Based on the classes, resolution, and number of samples available in each class, training datasets have been chosen.

A platform has been chosen in order to create a system with special features for brain tumor detection.

1.1.21 Thesis Structure

The flow chart in Figure 1.10 shows the thesis' overall structure as well as its chapter-by-chapter layout. Chapter 1 primarily deals with introduction the literature review of all the practices currently in use is covered in Chapter 2 of Preprocessing, Feature Extraction, and Classification. Chapter 3 is about Deep learning concepts and various architectures. Chapter 4 explains the detailed methodology and developed algorithms to create a pre-processing algorithm to improve the quality of MRI images and to extract the tumor location in MRI brain images. Chapters 5 to develop deep learning based novel algorithm to classify brain tumors into three classes. Chapter 6 performance verification of the projected method by comparing it with already existing techniques. And Chapter 7 explains the Conclusion and future scope.

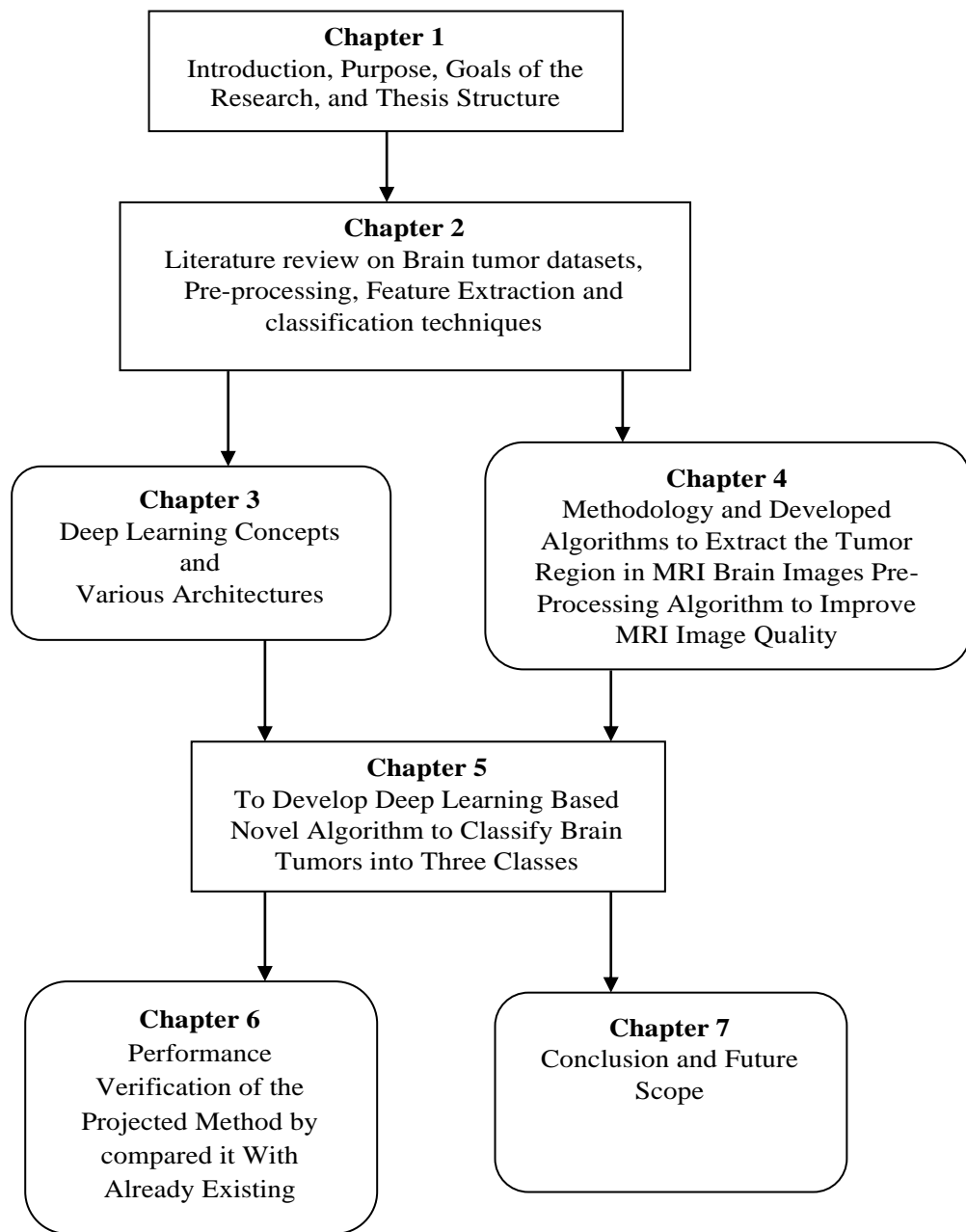


Figure 1.10 Chapter-Wise Thesis Organization

This thesis is structured into seven chapters, each covering different phases of the research development process. The organization of the thesis and a brief summary of each chapter are as follows:

- **Chapter 1:** This chapter provides an extensive overview of the research conducted in this study. Additionally, it presents a concise introduction to the diagnosis of brain tumors based on clinical backgrounds using MRI scans, which encompasses the crucial task of identifying both abnormal and normal brain conditions. Furthermore, it highlights the research's underlying motivation and outlines its objectives.
- **Chapter 2:** This chapter presents a comprehensive review of previous studies focusing on the segmentation, Brain tumor classification and automatic MRI image detection. It extensively discusses the various methods and techniques employed in this particular research.
- **Chapter 3:** This chapter offers an elaborate overview of the classification and segmentation of brain tumors using deep learning concepts and various architectures.
- **Chapter 4:** This chapter presents a methodology and developed algorithms aimed at extracting the tumor region in MRI brain images. Additionally, a pre-processing a new algorithm to improve the quality of MRI images is introduced. The focus lies on the contribution of a proposed technique for brain tumor segmentation utilizing the cascaded UNET architecture. Furthermore, an enhanced adaptive gamma correction is applied to the input images for improve quality of individual pixels.
- **Chapter 5:** This chapter provides a thorough explanation of the creation of a revolutionary Deep Learning (DL) algorithm for classification of the brain tumors. Into three distinct classes. The algorithm encompasses four essential phases: (I) Pre-processing (II) Segmentation (III) Brain Feature Extraction, and (IV) Brain Tumor Classification. The proposed approach incorporates an ensemble technique that combines Google Net and ELM (Extreme Learning

Machine) for enhanced performance.

- **Chapter 6:** In this chapter, we go over the research's results. and give the findings to you. We analyze and interpret the outcomes of our study, highlighting the key findings and their significance.
- **Chapter 7:** In this chapter, we provide a comprehensive conclusion based on the findings and outcomes of our research, we summarize the main contributions, insights, and implications of the study Furthermore, and we outline the future scope and potential avenues for further research in the field, identifying areas that can benefit from additional investigation and development.

CHAPTER 2

LITERATURE SURVEY

2.1 INTRODUCTION

Digital Image Processing is a methodology that involves converting an image into a digital format. It utilizes various techniques to enhance and extract important information from the image. In Digital Image Processing, the input is typically an image, and the output can be either another image or specific characteristics of the input image. When processing images using computer applications, they are typically treated as 2D signals, similar to how the human visual system perceives them. Initially, images are commonly in analog form, but for the purpose of storage, manipulation, and transmission through computer systems, they are transformed into a digital format. A, DI can be described as a two-dimensional array composed of pixels. It is an important form of information that is perceived, processed, and interpreted by the human brain. The brain dedicates a significant portion of its capacity to process visual information. Digital Image Processing (DIP) is a field of computer-based intelligence that involves automated enhancement, analysis, and interpretation of visual information. It aims to clarify and provide guidance in understanding the acquired visual data. The Digital Image Processing is plays important role it has used for different application in various fields.

Like as:

1. Space Digital Image Processing Telescopic and Planetary Exploration Images-(Space Digital Image Processing).
2. in the field of Medical Image Processing (MIP) (CT-scan, X-ray and blood/vascular/cellular microscopic images).
3. Automatic and pattern recognition (zip code, license board, and biometrics recognition)

In general DIP encompasses it has major areas as given in Figure 2.1: image formation, Image Enhancement, Image Management, Image visualization, and analysis.

1. Image formation: comprises the steps from image capturing till it forms into a digital image matrix.

2. Image enhancement: Collection of methods that are used to upgrade the pictorial appearance of an image without any distortions.
3. Image visualization: refers to all types of manipulation of this matrix (like shading illumination, display) resulting in an optimized output of the image.
4. Image management: process sums up all techniques that provide the efficient storage, communication, transmission, archiving, and access (retrieval) of image data. Thus, the methods of telemedicine are also a part of the image management.
5. Image analysis: includes all the steps to obtain the quantitative measurements along with theoretical evaluation of images.

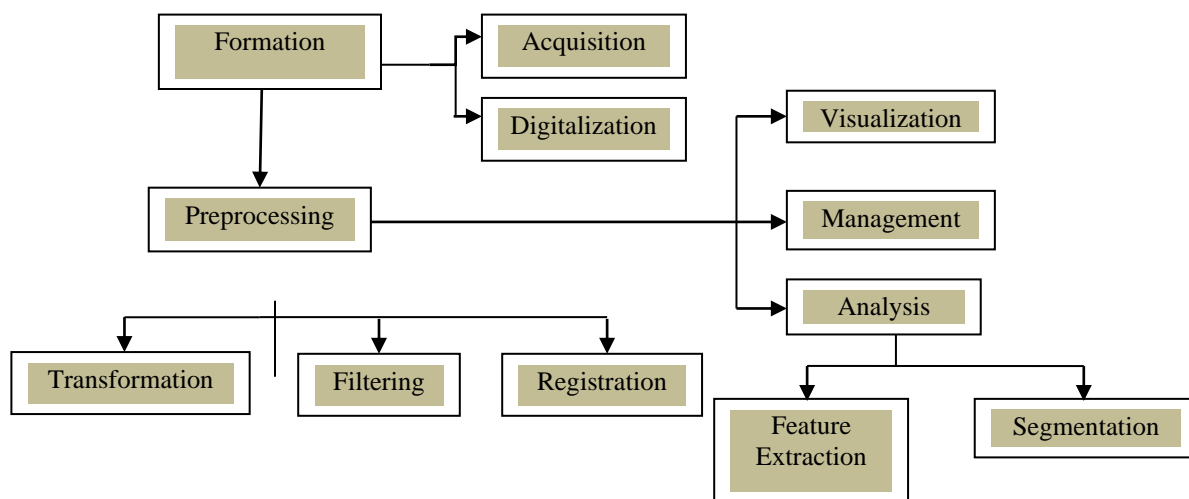


Figure: 2.1. Digital Image Processing Implementation [Kumar, Y., Gupta, N., Chhabra, A. et al. (2017)]

2.1.1 Biomedical Image Analysis

The field of Biomedical Image Analysis (BIA) primarily focuses on utilizing computational methods to extract insights from images of biological tissues. This encompasses a wide range of applications, including medical diagnostics aimed at establishing correlations between imaging data and various conditions, as well as studying the structure and function of organs in the human body. BIA involves

constructing computational models using several sorts of data, including image data and supplementary information ranging from demographic records to genetic markers in clinical studies. The primary objective of the analysis, measurements, and data processing is to derive meaningful conclusions about populations, whether they consist of healthy individuals or cases affected by specific conditions, based on representative samples. Since biomedical imaging systems can generate large volumes of images, a comprehensive analysis is required. Typically, experts perform meticulous evaluation procedures on medical images, leading to time-consuming processes and requiring significant effort to form opinions. Experts in the field rely on their professional experience to analyze (Magnetic Resonance) MR images both qualitatively and quantitatively. However, this analysis is inherently constrained by the limitations of the human visual system, which can only perceive fragments of the overall image. Furthermore, the image acquisition process itself introduces noise, such as swab and pepper noise, which can degrade the quality of the images. Additionally, during MRI examinations, auditory noise can arise from patient discomfort, resulting in communication difficulties and potential hearing impairments. To address these biases and obtain clearer images, measures can be taken to mitigate the effects of noise.

Reducing patient movements and minimizing temporary discomfort can be achieved by avoiding verbal exchanges during the checkup. The use of headphones during MRI examinations can significantly reduce robotic arm and leg movements, leading to improved image quality. By reducing auditory noise, it becomes easier to discern fine details in the images, facilitating the diagnosis process for medical experts. Furthermore, image denoising plays a crucial role in various fields, including astrophysics and criminology, as it allows researchers to extract meaningful data. Denoising techniques are employed to eliminate noise from the images without compromising the integrity of the original features, making it a vital step in BIA. The primary objective of biomedical Digital Image Processing methods is to accurately identify the objects of interest visually. Medical images are utilized to depict the distribution of physical attributes and aid healthcare professionals in measuring, diagnosing, treating, and understanding various medical conditions. They offer a non-invasive way to see the body's interior structures.

Without the need for surgical intervention. However, challenges arise due to the presence of overlapping objects in an image and the close proximity of pixel values in medical images, making the interpretation process quite challenging. To effectively address these issues, it is preferable to apply a preprocessing step to the image before further analysis. The purpose of preprocessing is to enhance the image's features by reducing unwanted artifacts or enhancing the structures relevant to subsequent analysis. Segmentation aims to divide an image into distinct regions that are semantically meaningful, homogeneous, and non-overlapping based on their original properties such as depth, color, texture, or shape. The results of segmentation can be categorized as either complete or partial. In the complete form, the segmented regions align closely with the objects present in the input image, resulting in a set of disjoint regions that correspond to the image objects. On the other hand, in the partial form, the segmented regions may not directly correspond to specific objects in the input image. In medical imaging, various anatomical structures of the human body, including bones, blood vessels, spine, knees, tissues, and pathological conditions like tumors, multiple sclerosis lesions, and Alzheimer's disease, are analyzed. Analyzing brain scans aids in identifying significant data that assists in making quantifiable assessments of a patient's condition for improved treatment outcomes. Image analysis involves identifying abnormalities or characteristics at specific points or regions. Segmentation plays a vital role in BIA. In the context of medical image segmentation of the brain, it refers to the process of labeling each pixel or voxel to identify the corresponding anatomical structure or tissue. These segmented regions have diverse applications in studying and analyzing medical conditions. A procedure called segmentation divides an image into homogenous, non-overlapping areas based on several characteristics like intensity, depth, color, or texture. In order to improve the interpretation and analysis of medical Images, segmentation tries to deliver more exact and detailed information.

2.1.2 Brain Digital Image Processing for MR Images

Currently, MRI systems have the capability to produce high-resolution images of organs with exceptional detail, reaching up to 535 Argentinean situations (presumably referring to the maximum resolution or quality). However, the information obtained from an MRI

scan cannot be fully analyzed by the human eye alone, given its limitations. This has led to the utilization of Computer-Aided Diagnosis (CAD), which allows for in-depth analysis of both high and low-resolution MRI images. CAD assists radiologists in examining abnormal regions more clearly and accurately. The indispensability of medical Digital Image Processing has become evident as it plays a crucial role in saving millions of lives through early and precise diagnosis. MRI is considered one of the most important and a versatile tool available to radiologists and researchers today and there has been significant advancement in technology and clinical applications. The efficiency, quality, and time required for MRI procedures have significantly improved as a result.

- Robust high- field attraction schemes,
- High- position functioning of grade systems,
- Wide range of technical Radio- frequencies (RF) coils,
- Development of computer technologies.

The advancements in technology and software have led to the production of highly detailed images of the human body, focusing on all organs. These developments enable user-friendly progress and processing capabilities, enhancing the diagnostic capabilities of radiologists. MRI is widely used in various diagnostic examinations, providing clinicians with enhanced information. It helps reduce the risks associated with radiation exposure and invasive procedures, while also improving diagnostic strategies to save time and resources. The advancements in computer processing and acquisition techniques, such as compressed sensing, have enabled the generation of fast and highly detailed images. The use of 3 Tesla (3T) magnetic field strengths and advanced magnetic field configurations provide enhanced visualization of both anatomical and functional aspects. Moreover, the progress in MRI scanner technology includes improvements in ease of installation and patient comfort. The cutaway view of an MRI scanner reveals the presence of RF (radiofrequency) and gradient coils, which are essential components of the system.

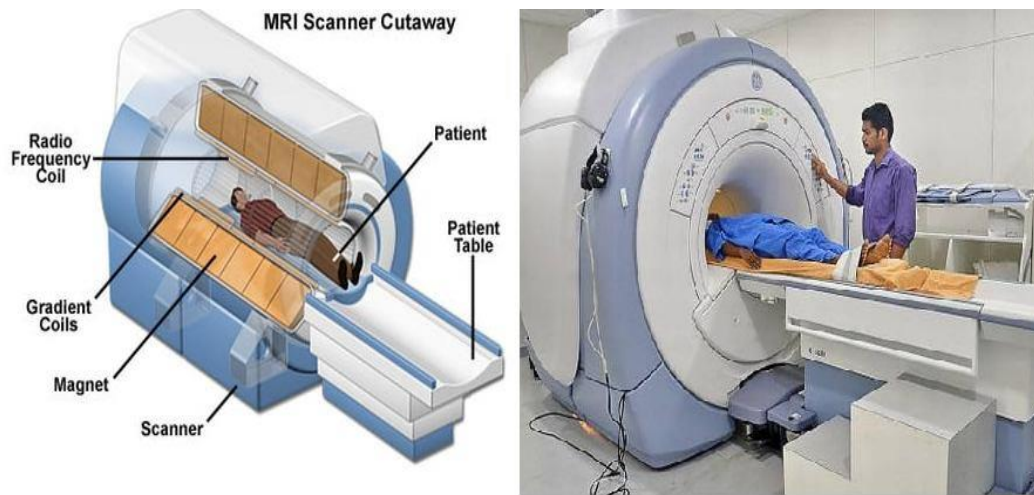


Figure: 2.2. Cutaway MRI Scanner [Al-Tamimi, M. S. H., & Sulong, G. et.al. (2014)]

2.1.3 MRI and Other Imaging Modalities

X-ray imaging, also known as radiography, is a primary imaging modality used to visualize the human body. As they travel through the body, X-rays, a type of electromagnetic radiation, interact with tissues and ionize them. The speed of X-ray imaging is well recognized, cost-effectiveness, and portability. There are various types of specialized X-ray techniques: 2D mammography is commonly used for breast imaging and is considered the gold standard in detecting bone abnormalities. 3D mammography, also known as tomosynthesis, is gaining popularity as an alternative method for breast cancer diagnosis. Each of these X-ray techniques utilizes the different ways in which tissues interact with X-rays to provide diagnostic information. Other imaging modalities have emerged over the years to address the limitations of X-ray imaging and showcase technological advancements. Tomographic Images, Such As Those Produced by Single Photon Emission Computed Tomography (SPECT), Nuclear Magnetic Resonance (NMR), CT, and Positron Emission Tomography (PET), and Ultrasound, are widely used by clinicians and radiologists to provide additional diagnostic information and fill the gaps left by X-ray imaging.

CT: X-ray imaging and MRI are often compared as both modalities produce images that depict anatomical structures with varying shades of gray to represent different intensity details. However, the underlying principles for image formation and the detailed visualization of tissues in each modality are not the same. In the case of CT (Computed

Tomography), like other imaging modalities, it involves directing energy into the body and assessing how that energy is absorbed or altered as it passes through the tissues, but in the form of X-ray beams.

Nuclear Medicine: Nuclear medicine and Single Photon Emission Computed Tomography (SPECT) utilize radioactive substances to introduce radioactive energy into the body and capture the decay of these substances to form images of radioactive volumes and their distribution. Contrast agents containing radioactive isotopes emit gamma rays as they decay, similar to X-rays but with higher energy. These gamma rays are detected by a gamma camera, which generates the final image.

PET: Positron Emission Tomography relies on the use of a radioactive tracer and detectors to measure its distribution based on radioactive decay. In PET, the radioactive decay produces small the imaging system picks up positrons, which are subatomic particles. Despite having poorer resolution than MRI, PET scans are nevertheless useful for learning about how different organs work. Areas of increased metabolic activity are directly correlated with anatomical location, making PET particularly useful in detecting tumors and assessing their activity.

2.1.4 Tumor Characterization

CT: The degree of tissue attenuation and contrast in X-ray images is determined by the absorption of X-ray energy at each point in the image. As a result, bones, being denser structures in the body, absorb more X-rays and appear brighter in the image. On the other hand, tissues such as blood, cerebrospinal fluid (CSF), and other soft tissues have lower density and absorb fewer X-rays, resulting in a darker appearance in the image. This contrast in X-ray attenuation allows for differentiation between different tissues and structures in the body.

MRI: The interpretation and contrast in MRI images are based on entirely different principles compared to CT. The interactions between tissues and radio waves in a magnetic field are what cause the brightness changes in MRI images. Different tissues exhibit different signal intensities, resulting in areas appearing bright, dark, or various shades of gray. The radio waves and magnetic fields used in MRI can be manipulated in various ways to modify the appearance of specific tissues, allowing for greater versatility

in image interpretation.

In T1-weighted MRI brain images, fluids tend to appear dark, while in T2-weighted MRI images, fluids appear bright. MRI acquisitions can also be tailored to highlight changes in blood flow, fat content, and tissue relaxation characteristics. This enables the detection of various illnesses and offers helpful data for making a diagnosis and developing a therapy plan.

Despite its limitations, MRI is currently considered among the most popular available and frequently used imaging modalities for assessing tumors and pathologies in the body. It offers unparalleled versatility compared to CT and other imaging techniques, allowing for a wide range of applications in medical practice. Various Digital Image Processing techniques are applied to MR brain images to facilitate interpretation and analysis. Advancements in MRI technology have led to improvements in image quality and acquisition speed. MRI uses the property of nuclear magnetic resonance (NMR) to capture signals from within the body and visualize its internal structures. By applying a powerful magnetic field and radiofrequency (RF) pulses, MRI can manipulate the magnetization of protons in the body to generate detailed images. The analysis of MR images often involves a pre-processing step to enhance image quality. This may include techniques such as image denoising and skull stripping using morphological Digital Image Processing methods. Tumor detection and segmentation can be performed manually or automatically. In manual processes, tumor regions are identified by human observers on consecutive image slices, which can be time-consuming and subjective.

The segmentation of the brain is a crucial step in BIA, where the boundaries of different brain regions are identified and marked. MRI is particularly effective in capturing detailed images of various brain structures and is highly regarded for analyzing and correlating abnormal findings. It provides greater contrast and resolution compared to modalities like X-ray, CT, PET, and SPECT. X-ray imaging is commonly used for evaluating internal body structures, especially related to bone fractures. CT is valuable for the assessment of multiple trauma cases. PET utilizes radioactive tracers to detect and analyze the functional activity of organs and tumors. SPECT, another nuclear medical imaging modality, uses radioactive substances to produce 3D images that depict the

functioning of internal organs in the body.

2.2 Classification and Description of Survey

In this section, an examination of various studies was conducted, focusing on the classification of brain tumors. The reviewed literature encompassed diverse models, which were classified into five distinct types as outlined below.

- Analysis utilizing deep learning (DL) techniques.
- Analysis centered on optimization methods.
- Analysis combining DL techniques with optimization approaches.
- Analysis employing machine learning (ML) techniques.
- Others

2.2.1 Analysis Based on DL Techniques

A method for automatic segmentation using CNN that makes use of 3x3 kernels was proposed by Pereira et al. in 2016. By using smaller kernels, the deep architecture of the network was able to benefit from a reduced number of weights, which helps to mitigate over fitting. The use of intensity normalization in the pre-processing was also explored in the study. Phase, a factor that was not commonly explored in CNN-based segmentation approaches. Data augmentation techniques were found as more prominent in segmenting brain tumors in MRI images. The proposed method had been evaluated on the BRATS 2013 database, where it achieved the first position in completing and improving the regions of the Challenge dataset based on the Dice Similarity Coefficient metric. Furthermore, the proposed approach secured the top overall position in the online evaluation platform for the BRATS 2013 Challenge. In the subsequent BRATS 2015 Challenge, the same approach participated and obtained obtaining Similarity of dice Coefficient ratings for the complete, core, and upgraded areas were 0.78, 0.65, and 0.75, respectively, put them in second place.

Mohsen et al. (2018) introduced a Deep Learning (DL) framework called the DNN classifier for categorizing MRI brain image into four classes: metastatic bronchogenic carcinoma, normal, sarcoma, and glioblastoma tumors. The proposed model utilized an efficient methodology that combined the discrete wavelet transform (DWT) with the

DNN for accurate classification of brain MRIs. Additionally principal component analysis (PCA) and DWT as integrated feature extraction technologies were used in the investigation, into the analysis and classifier. The executed results of the said model demonstrated superior performance regarding the reduced time consumption and hardware requirements compared to existing approaches.

Hemanth et al. (2019) proposed a novel Multi-Directional Convolutional Neural Network (MDCNN) for MR brain image classification in patients with brain cancers. The primary objective of this research was to reduce the computational complexity associated with traditional DCNNs. The training algorithm of the MDCNN introduced certain modifications to minimize the number of parameter adjustments. Notably, the weight adjustment approach in the convolutional layer was eliminated in this adopted method. Instead, the weights of the fully connected layer were obtained through simple assignment process. Experimental results of the proposed model demonstrated promising outcomes, surpassing the performance of existing models in the field.

Sultan et al. (2019) conducted a study where they implemented DL model based on CNN for the classification of different types of brain tumors using two publically accessible data sets. The standard model successfully categorized cancers into several categories, including pituitary tumors, gliomas, and meningiomas. Furthermore, gliomas were differentiated into three grades: II, III, and IV grades, respectively. The dataset used in the proposed method included between 73 and 233 patients, and a significant portion of the images were T1-weighted contrast enhanced images. Compared to other existing models, the adopted approach significantly improved sensitivity, specificity, and overall accuracy.

Kumar et al. (2019) developed a Deep Neural Network (DNN) that achieved superior performance in both segmentation and classification tasks. The approach involved using Dynamic Wavelet Allocation (DWA) for image compression, which combined the feature reduction property of autoencoders with the image decomposition properties of wavelet transform. Additionally, an optimization algorithm was employed to extract and learn the principal components from large data distributions. The combination of these components in the adopted model had a remarkable effect on reducing feature

dimensionality and improving classification tasks through DNN. The DWA-DNN classifier outperformed traditional classifiers such as DNN or Autoencoder-DNN, yielding better outcomes in terms of accuracy and performance.

Nawab et al. (2019) developed a DL framework utilizing deep Convolutional Neural Networks (CNNs) to address challenges in image classification tasks. DL demonstrated its strength in feature representation by capturing both high-level and low-level information, effectively integrating classification and feature extraction through self-learning. However, DL models typically require large training datasets, which may be scarce in certain medical imaging scenarios. To overcome this limitation, the authors employed a block-wise fine-tuning approach with Transfer Learning (TL) and pre-trained deep CNN models. The proposed model was evaluated on a benchmark dataset of T1-weighted Contrast-Enhanced MRI images. It exhibited a generic nature by requiring minimal preprocessing, avoiding the need for handcrafted features, and achieving competitive accuracy through 5-fold cross-validation. Comparative analysis with existing (Machine Learning) ML and DL models demonstrated the superior performance of the suggested strategy. The simulation results on the Contrast-Enhanced MRI dataset showcased higher accuracy compared to traditional schemes.

Navid et al. (2019), Introduced to novel DL model for classifying brain tumors for MR images. The model was pre-trained using a deep neural network (NN) with on multiple MR image datasets, a Generative Adversarial Network (GAN) discriminator. Through convolutional layers, the model was able to learn the MR images framework during the pre-training process and extract reliable features. Subsequently, the entire deep network was replaced, and the fully connected layer was to distinguish between the three groups of cancers, it was trained as a classifier. The deep NN classifier consisted of six layers and 1.7 million weight parameters. To prevent overtraining of the network on a small dataset, the pre-training as the GAN discriminator was combined with different approaches, such as data augmentations (e.g., mirroring, dropout, and image rotation).

Huang et al. (2020) proposed a novel approach for the classification of brain tumors in medical imaging using complex network-based CNN. The adopted model aimed to enhance the effectiveness and practicality of medical image analysis. They introduced a

CNN with complex networks, called CNNBCN, along with a modified activation function specifically designed for MRI-based brain tumor classification. Unlike manual optimization, the network framework was generated randomly using graph algorithms. These graphs were then mapped onto the accessible neural network through a network generator. The modified CNNBCN approach achieved an impressive accuracy of approximately 95.49%, surpassing other models for brain tumor classification. Furthermore, the experimentation showed that the modified CNNBCN approach had lower loss compared to DenseNet, MobileNet, and ResNet approaches. Although the adopted CNNBCN approach did not yield satisfactory outcomes in classifying brain tumor images, it contributed to enriching the neural network methodology in this context. M. I. Sharif et al. (2021) suggest a deep learning strategy for classifying brain tumor diseases. They utilize the BraTS2018 and BraTS2019 datasets for their study. They use a transfer learning to hone the Densenet201 model and extract features. In addition, they use the Modified Genetic Algorithm (MGA) and the entropy-kurtosis-based high feature value (EKbHFV) to choose the best features. A technique based on nonredundant serial data is used to produce fusion, and the resulting features are classified using the cubic SVM. Remarkably, the approach achieves an accuracy exceeding 95%. Additionally, the authors compare the results of different deep learning models regarding their capacity to analyze brain tumors, including VGG16, AlexNet, GoogLeNet, and ResNet50. The rating criteria include processing speed and accuracy. Notably, AlexNet has the fastest processing time at around 1.2 seconds, which is slashed to 8.3 milliseconds with the use of a GPU. ResNet50, on the other hand, has the highest accuracy at about 95.8%.

A brain tumor detection technique that combines edge detection and the U-NET model was put forth by Maqsood et al. (2021). The framework for tumor segmentation integrates fuzzy logic edge detection and improves images contrast. The U-NET architecture is used for classification, and features are retrieved from decaying sub band images. This method successfully recognizes meningioma in brain imaging.

An approach proposed by Usman Zahid et al. (2022) introduces an effective solution for brain tumor detection and classification through optimal deep learning feature fusion. Manual removal of tumors detection and classification takes a lot of time, expensive, and

laborious. In this research, a fully automated architecture based on deep feature fusion is proposed to address these challenges. A comprehensive database of MRI images, encompassing four distinct tumor categories, is prepared for evaluation purposes. The proposed approach delivers a remarkable level of accuracy of approximately 96.7%, surpassing existing techniques. However, the study reveals the presence of redundant and irrelevant features, emphasizing the importance of selecting optimal features. Furthermore, it demonstrates that the fusion of these optimal features not only improves accuracy but also significantly reduces prediction time, aligning with the primary objective of the research. Nonetheless, it is worth noting that the fusion process increases computational time during testing. To overcome this limitation, future endeavors will explore lightweight deep learning frameworks and leverage optimized feature fusion approaches for tumor classification and detection.

A. Sekhar et al. (2022) present a brain tumor classification approach that combines both ML and DL techniques. The authors focus on three distinct brain tumor classes: glioma, meningioma, and pituitary. To extract deep features, they employ transfer learning to fine-tune the GoogLeNet model. These extracted features are subsequently classified using the SVM, KNN, and softmax algorithms.

A. Gumaiei et al. (2022) present an algorithm aimed at early identification and types of brain tumors, which is crucial for effective patient treatment. With advancements in technology, automated healthcare systems enable experts to provide better treatment to patients. The researchers propose the use of ML and DL algorithms to address medical image diagnosis challenges. Among the DL models, CNNs have gained significant popularity and a number of domains, including Digital Image Processing; have produced ground-breaking achievements. Systems based on CNN prove to be efficient in diagnosing aiding medical professionals in selecting a course of treatment for brain tumors. Notably, 190 of the more than 200 DL-based investigations on medical images that were carried out in 2016 used CNNs. Prominent CNN models such as AlexNet, VGG, and GoogLeNet are currently utilized in medical image classification tasks.

2.2.2 Analysis Based on Optimization

When considering optimization techniques for brain tumors, various approaches can be

utilized to improve diagnosis, treatment planning, and surgical interventions. These techniques aim to enhance the accuracy of tumor segmentation from medical imaging data, optimize radiation therapy treatment planning, aid in surgical planning, and optimize treatment parameters based on genetic profiles. Additionally, machine learning algorithms, such as deep learning, can be leveraged to improve brain tumor diagnosis, classification, and treatment response prediction. Multi-objective optimization techniques are also employed to address the conflicting objectives involved in brain tumor management. It is crucial to emphasize that these optimization techniques should be implemented by qualified medical professionals in accordance with established clinical guidelines, as they are just one component of the comprehensive treatment strategy for brain tumors.

Dmour et al. (2018) introduced a fusion-based clustering technique for MRI tissue segmentation. Their approach involved calculating the pixel intensity of each pixel as part of the clustering process. During the training phase, they experimented with K-means, Fuzzy C-Means, and Self-Organizing Maps (SOM) clustering algorithms. In the ensemble model segmentation procedure, they utilized multiple Artificial Neural Networks (ANNs) and selected the one that yielded the highest majority vote result. In a different study, Hasan, Khan et al. (2018) proposed a model for segmenting cancer cells based on their behavior in brain cancer. To identify the cell behavior in genes, they employed SVM, random forest, and Naive Bayes classifiers.

In order to quickly pick an ideal feature subset with good discriminatory capacity from a set of available features, Saini et al. (2018) developed a unique feature selection approach for classifying brain tumor MR images. The Fisher criteria and the PFree Bat optimization technique were combined to create the model. The traditional Bat algorithm had limitations in the exploration phase, so modifications were made to guide the Bat using local best positions, global best positions, and pulse frequency. The enhanced version of the Bat algorithm, called the PFree Bat algorithm, directly updated the Bat position and rejected the velocity equation. The proposed approach utilized the Fisher criteria to choose the ideal combination of features for classifying brain tumors. After that, an LS SVM classifier was used to classify the area of interest as either low grade or

high grade using these chosen features. The adopted model achieved a 100% recognition rate within a significantly shorter time compared to other hybrid models. Additionally, an integrated index was implemented to determine the best performing algorithm based on metrics such as computational time, accuracy, and number of features.

Sharif et al. (2018) a novel strategy for treating brain tumors classification and segmentation, incorporating a best feature selection method and improved saliency segmentation. The approach consisted of four pipeline measures: tumor segmentation, feature extraction, classification, and tumor preprocessing. The preprocessing stage involved manual skull stripping to extract the Region of Interest (ROI) and reduce noise using a Gaussian filter. Tumor segmentation was performed using an enhanced thresholding approach based on binomial standard deviation and mean variance. Texture and geometric features were extracted, and a serial-based model was used to fuse these features. The Genetic Algorithm (GA) was utilized to pick the aspects that are most pertinent. Finally, a SVM was used to classify the selected characteristics. with a linear kernel function. The proposed scheme was tested on both Private and Harvard datasets. The Private Dataset was collected from Nishtar Hospital Multan in Pakistan. The adopted approach achieved improved classification accuracy, demonstrating its effectiveness across different datasets and validating its authenticity.

Anitha et al. (2019) proposed a novel image classification method for identifying abnormal brain tumors in MR images using a modified GA. The method involved extracting texture features using the Gray Level Dependence Matrix (GLDM) from the images. The modified GA was utilized to extract the most relevant features from the images. The proposed model incorporated various binary operations for generating offspring during the mutation and crossover processes. These binary operations were designed with objectives that differed from traditional binary operations in GA. The optimal features obtained were then classified using a Backpropagation Neural Network (BPN). The effectiveness of the suggested method was assessed by contrasting its sensitivity, positive predictive value (PPV), accuracy, and specificity to those of other methods.

Narmatha et al. (2020) proposed a novel algorithm called FBSO (Fuzzy Brain-Storm

Optimization) that combines the Brain-Storm Optimization (BSO) algorithm with a fuzzy model for brain tumor classification and segmentation. The Brain-Storm Optimization approach prioritized maximum attention to cluster centers, but it could sometimes lead to local optima similar to other swarm algorithms. To address this while the BSO algorithm helped to improve the results of the investigation, the fuzzy technique repeatedly iterated network frameworks. When examined using the BRATs 2018 dataset, the adopted model displayed robustness, improved precision, high accuracy, and a better F1 score.

Alhassan et al. (2020) proposed an automated segmentation model for MRI images of brain tumors, aiming to increase effectiveness of classification and segmentation processes. The adopted model consisted of segmentation and preprocessing processes to identify tumor or malignant and benign tissues using various clustering and data processing techniques. The proposed work utilized modern learning-based models to process multimodal MRI images and performs automated segmentation to detect brain tumors. The BAFCOM clustering algorithm was recommended for tumor segmentation, and the Bat Algorithm was employed to determine the distance and initial centroids within the pixels of the tumor. The distance between non-tumor and tumor regions of interest (RoI) was calculated to aid in the segmentation process. The MRI image was then evaluated using the ECN approach to classify it as either brain tumor or normal. The performance of the adopted model was assessed using the ECN algorithm, which differentiated between the two types of tumors present in the MRI images. The ECN classifier was evaluated based on measurement factors such as F1-score, accuracy, recall, and precision. Additionally, the Genetic Algorithm (GA) was applied to the automatic tumor stage classification, resulting in improved classification accuracy.

In the study conducted by Murmu et al. (2021), a deep learning (DL) model was explored for segmenting a medical disease using MRI and CT image datasets. The researchers employed the 2D-U-Net and 3D-U-Net methods for segmenting medical data. Within the 2D-U-Net model, the package nibabel was utilized for reading and visualizing the data. The 3D-U-Net model, on the other hand, was employed for segmentation and classification tasks using MRI and CT images. To evaluate the system, the researchers utilized the Medical Segmentation Decathlon (MSD) datasets specifically for Brain,

Heart, and Spleen segmentation. Performance evaluation was conducted based on metrics such as F1-score, Intersection over Union (IOU) and Dice similarity coefficient for the Brain, Heart, and Spleen datasets. The results demonstrated that this method outperformed previous network models across various aspects.

Qiu et al. (2021) developed a DL based U-Net model for segmenting 3D liver tumor images. This U-Net model incorporates a dynamic convolution model and attention mechanism to effectively enhance feature extraction capabilities. Additionally, a transfer learning (TL) model is employed during the training process, utilizing learned data transfer techniques specific to liver tumor segmentation. As a result, the TL-based U-Net method improves the model's fitting capability. The performance evaluation of the model yielded a Dice coefficient value of 94.9%. When compared to various traditional segmentation models, the U-Net model demonstrated a performance improvement of 4.4%.

Wang et al. (2022) investigated a context-aware neural network (NN) approach for segmenting lung infections. The authors specifically focused on two modules: autofocus and panorama, which aimed to extract intricate details and semantic information while capturing long-range contextual dependencies at both companion level and cross-level. Additionally, they proposed an original construction consistency correction to align the foreground and background by describing the fundamental connection between them. The success of their strategy was demonstrated by experimental findings on COVID-19 CT images of both single-class and multiclass structures. Notably, their method outperformed three benchmark datasets for COVID-19 disease segmentation in terms of mean Intersection over Union (mIoU) score.

2.2.3 Analysis Based on DL Techniques with Optimization

Amin et al. (2018) implemented a novel model that combined Genetic Algorithm (GA) and CNNs for non-invasive classification of various Glioma grades using MRI. The architecture of the CNN was determined using GA, which allowed for the exploration of different architectures compared to traditional methods that rely on trial and error or predefined frameworks. The ensemble algorithm, specifically bagging, was utilized to further improve the prediction accuracy by reducing the variance of the prediction errors.

The results demonstrated 90.9% accuracy in classifying the 3 Glioma grades. Additionally, the model achieved better accuracy in classifying Pituitary tumor, Meningioma, and Glioma types. The outcomes of the study highlighted the efficacy of the suggested model in classifying brain tumor MRI images.

Kaur et al. (2019) developed an automated detection approach for classifying tumor grades in MRI images. The approach involved delineating the Region of Interest (ROI) using edge and intensity magnitude-based multilevel thresholding algorithms. Texture attributes and intensity features were then extracted from the segmented ROIs. The optimal feature subset was derived using a combined model called PFreeBAT optimization. A new learning model, referred to as PFree BAT-based improved Fuzzy K-Nearest Neighbors (FKNN), was implemented using FKNN with PFree BAT optimization to classify MR images into two subdivisions: low-grade and high-grade. The model parameters, such as fuzzy strength and neighborhood size, were adaptively specified by the PFree BAT optimization model. The adopted model achieved an accuracy of 97.45% and 98% with feature selection when evaluated on the PD dataset.

Mishra et al. (2019) proposed a novel approach called MASCA (Modified ASCA) combined with Particle Swarm Optimization (PSO) based on the Local Learning-Based Radial Basis Function Neural Network (LLRBFNN) method for the automatic classification and identification of brain tumors. The traditional FCM Fuzzy C-Means (FCM) algorithm-based approach was ineffective in removing noise from MR images during the segmentation process. Therefore, the proposed model included an enhanced fast and robust FCM algorithm segmentation method to smoothen and reduce noise in brain tumor MR images. Features were extracted using the Gray-Level Co-occurrence Matrix (GLCM), and these features were used as inputs to the modified ASCA-PSO and LLRBFNN approach for classifying malignant and benign tumors. The weights of the LLRBFNN approach were optimized using the MASCA-PSO algorithm, which obtained a unique solution based on manual detection tasks performed by radiologists. The experimental results demonstrated higher classification accuracy for the MASCA-PSO based LLRBFNN approach compared to other LLRBFNN methods, such as the adaptive sine cosine optimization method, PSO, and the sine cosine optimization algorithm paired

with the LLRBFNN technique.

Sathish et al. (2020) introduced a clustering approach called Gaussian-based Hybrid Fuzzy C-Means (GHFC) and Fuzzy C-Means for segmentation by combining sparse FCM (Fuzzy C-Means) and FCM clustering techniques. The segmentation process utilized the Gaussian function. After segmentation, relevant features were extracted from the brain tumor images. These extracted features were then used as training data for the "exponential cuckoo-based Rough Boost Neural Network (RBNN) to find the training classes using a classifier. The proposed model's experimental findings showed increased accuracy and a low Mean Squared Error (MSE). The SIMBRATS and BRATS databases were used to conduct the experiment.

Sharan et al. (2020) proposed a DL model that was called Dolphin-SCA based deep CNN for brain tumor classification. The input MRI images underwent a pre-processing phase. The segmentation process utilized the Dolphin-SCA method in conjunction with the fuzzy deformable fusion strategy. Power LDP (Local Directional Pattern) and statistical characteristics were used to extract the features. The DCNN and Dolphin-SCA algorithms were used to classify brain tumors using these extracted features. Comparing the experimental findings of the chosen model to other traditional models for classifying brain tumors, they showed superior performance with the maximum accuracy.

Lee et al. (2021) introduced a boundary-aware sampling technique that focused on utilizing features from image patches located at the ground-truth boundary area. This approach was applied to perform lung segmentation in CT, liver segmentation in CT, chest radiographs, and segmentation of brain tumors and spinal cord gray matter in MRI images. The results indicated that this method enhanced the segmentation performance of popular deep learning (DL) models such as U-Net, U-Net++, and DeepLabV3+. The study further revealed that the robustness of domain shifts in segmentation tasks could be improved through the use of contrastive embedding. These findings highlight the potential of the boundary-aware sampling method in improving DL-based segmentation tasks across various medical imaging domains.

Geng et al. (2022) explored a medical image denoising pipeline method and implemented it as a generative adversarial network. The methods like as predictors, U-Net,

SRDenseNet, and DnCNN are investigated. The model's effectiveness has been verified using CT, PET, and MR imaging datasets. Regarding visual appeal and numerical measurements, the results demonstrate that this system performed a best-in-class denoising method, and the technique demonstrates a strong generalization potential. These predictions confirmed that this straightforward approach, while intriguing, demonstrates promising potential for clinical image denoising function that may be used to provide a clinical effect in the future.

Yu et al. (2022) examined the impacts of different k values, specifically 2, 4, 8, 16, 32, and 64, on the effectiveness of DL techniques like VGG-16, ResNet18, Inception V3, and VGG-19 for predicting corn diseases. The study found that using a k value of 32 yielded higher identification accuracy on samples and improved diagnostic recall for leaf spot, gray spot, rust, and diseases. The proposed method achieved an average diagnostic accuracy of 93% in corn disease prediction using DL methods. These promising results have significant implications for agricultural applications, providing effective disease protection measures in the field.

2.2.4 Analysis Based on ML Techniques

Whitney et al. (2017) used a guided ML approach to examine how race affected post-brain tumor surgery discharge disposition and length of stay (LOS). The study focused on a retrospective cohort of 41,222 individuals who underwent craniotomies for brain tumors between 2002 and 2011, using data from the Project National Inpatient Sample and Healthcare Cost. Using pre-hospitalization characteristics, 26 ML systems were trained to forecast LOS and non-home discharge. Ensemble models were developed by combining the most predictive algorithms. To look into how race affected the ensembles autonomously, partial dependence analysis was used. Better discrimination in predicting extended LOS and non-home disposition was shown by the guided ML strategy. The study also discovered that non-black race increased the chance of prolonged. It is important to note that the experimental outcomes of race were not obtained when analyzing the overall operative population or general inpatients. The findings contribute to understanding the influence of race on discharge and highlight the role of LOS in implementing interventions and recognizing race-related disparities.

Antony et al. (2018) conducted a study on predicting the grades of brain tumor types, specifically glioma and meningioma, using the Weighted Neighbour Distance approach. The researchers developed a Compound Hierarchy model that utilized the Morphology (wndchrm) tool and SVM classifiers. To enhance the SVM classifier's performance, an iterative technique was employed to determine the optimal boundary and kernel parameters. The streamlined features extracted from the Wndchrm tool were utilized in training the SVM classifier

Arokia et al. (2018) introduced a mixture approach based classification method using MRI images of meningioma brain tumors. The adopted scheme consisted of four stages. The initial stage involved processing the cells' boundaries to ensure the discrete region boundary for specific cells. Mathematical morphology was utilized to interpret the outcomes during this process. Accurate segmentation of cancer cell nuclei is crucial for automated cytological image analysis, with segmentation's key step being thresholding. The adaptive binarization approach, a crucial stage in medical Digital Image Processing, was used in the study. Additionally, a fresh hybrid Fuzzy SVM was implemented for meningioma brain tumor classification. The classification results were as follows: MM with RBF achieved 62.71%, MM with FSVM achieved 82.67%, feature extraction with SVM achieved 74.24%, and the proposed MM with Hybrid SVM achieved 91.64% accuracy, respectively.

Shree et al. (2018) conducted a study on enhancing the efficiency of noise removal and brain tumor segmentation using DWT. They employed the extraction of features based on GLCM. The statistical algorithm, PNN, and Bayesian network called Kernel Fisher discriminant analysis were used to acquire results. Furthermore, morphological filtering was implemented to eliminate noise after the segmentation process. The PNN classifier was employed for testing and training in tumor detection. Ultimately, the simulation results of their approach demonstrated high accuracy in distinguishing between normal and abnormal tissues.

Shrot et al. (2019) conducted a study on utilizing machine learning techniques with advanced and basic MR sequences to distinguish between several kinds of brain tumors. The research involved 141 patients, including 12 primary CNS lymphomas, 38

metastases, 41 glioblastomas, and 50 meningiomas. A computer-assisted classification approach was employed, combining perfusion MRI, DTI metrics, and morphologic MRI to classify the brain tumors. The adopted multistep scheme encompassed ROI definition, preprocessing, feature selection, classification, and feature extraction. SVMs were used for feature subset selection. The classification performance was evaluated through validation, without any human intervention, as the entire process was automated. The experimental results of the adopted model, employing binary SVM classification, demonstrated high sensitivity, accuracy, and specificity for metastases, glioblastomas, primary CNS lymphomas, and meningiomas, respectively.

Kalpana et al. (2019) developed a novel model for brain tumor (BT) segmentation called BT MLTS-HSO. The model involved feature extraction and classification using various classifiers such as DSVM, RBFN, NB, and KNN for MRBT images. The adopted approach consisted of three phases: (I) Classification Phase, (ii) Detection Phase, and (iii) Radiation Dosage Calculation Phase. Additionally, the HSO algorithm was employed using two MLT methods, Kapur and Otsu. Otsu thresholding was used to determine the threshold of the minimized weighted within-class variance. The proposed approach incorporated NN, ANFIS, and SVM, where a seed point was utilized to detect the tumor region, select it on a scale, and calculate radiation dosage and performance measures. Consequently, the adopted model demonstrated the ability to analyze the position and size of the tumor, and it achieved more accurate predictions compared to other models.

Krishna et al. (2020) introduced a novel method for efficiently classifying and segmenting using the MKSVM and rough K means method to create MRI images of brain tumors. When examining brain tumors, their suggested model produced precise and effective results by employing useful techniques. The images were first subjected to a preprocessing step, and then feature extraction was carried out using an upgraded GWT. Additionally, the standard GWT's mean of optimization method was adjusted. Utilizing the oppositional fruit fly approach, the optimization model's efficacy was verified and the feature values that resulted were then used to the segmentation process utilizing the clustering technique. Overall, the presented approach showcased superior sensitivity, classification accuracy, and specificity.

Rehman et al. (2020) introduced a machine learning model for localizing brain tumors in FLAIR MRI scans. The study utilized the BraTs 2012 dataset, which was co-registered and skull stripped. Trilateral filtering was used to reduce noise, and texton-map images were created using a bank of Gabor filters. First-order intensity statistical characteristics were used to extract low-level features after the image had been divided into superpixels. The texton-map with histogram level was computed for each superpixel. Instead of considering the contribution of low features, the model focused on combining features at the region level using texton-map images to localize brain tumors in the MR images. These features were fed into the classifier to predict three classes: non-tumor, tumor, and background region. The labels were used to calculate two different areas. The proposed model employed a LOOCV technique and achieved a score for the localization of the whole tumor area, which matched the confirmed score in the "MICCAI BraTS challenge." Additionally, the brain tumor localization model based on superpixel features using the texton-map image yielded similar results to other approaches. Recently, autonomous computer-based approaches in medical diagnosis have made significant progress in generating medical hypotheses for disease diagnosis.

Gokulalakshmi et al. (2020) devised an enhanced classification approach for diagnosing brain tumors from MRI images. The initial step involved using a filtering model to preprocess the acquired scan images. Feature extraction was performed using GLCM and DWT equations, resulting in more accurate outcomes. The K-means clustering model was employed for segmentation, where similar tissues were grouped together. Cells were also grouped using K-means clustering based on the extracted features, determining the number of groups and frames. Furthermore, the classification stage utilized the SVM technique for binary classification. The proposed approach was evaluated through simulation, and the results demonstrated superior precision, recall, and reduced processing time compared to traditional brain tumor detection methods.

Majib et al. (2021) presented a computer-assisted method for the detection of brain tumors. This study utilized hybrid ML models and extensively investigated the classification of brain tumor images without manual intervention. Additionally, To find the optimum transfer learning model for classifying brain tumors using a neural network,

16 alternative TL models were investigated. The researchers also offered a stacked classifier that surpassed all other established models by utilizing a number of enhancements. The VGG-SCNet (VGG Stacked Classifier Network) in particular achieved impressive precision, recall, and F1 scores of 99.2%, 99.1%, and 99.2% respectively. These results demonstrate the effectiveness of the proposed approach in accurately classifying brain tumors, providing a computer-assisted solution that minimizes manual effort.

2.2.5 Others Research Papers Related to Deep Learning

Ural et al. (2017) presented a brain tumor detection approach utilizing MRI images. The method's main goal was to identify and pinpoint the area of the brain tumor. using advanced Digital Image Processing techniques and PNN systems. Initially, a specialized clustering approach was applied to the MRI image. Subsequently, tumor areas were identified using level-set segmentation and thresholding methods. Furthermore, the PNN system was employed for automatic classification and analysis of the brain tumor based on the identified tumor areas. The study utilized 25 out-of-sample neuro images for optimizing and testing the proposed approach. The simulation results demonstrated improved classification accuracy for the neural network structures and Digital Image Processing techniques employed in the proposed model.

Ma et al. (2018) developed a multimodal volumetric MR image and the Random Forests and Multiscale Patch Driven Active Contour (RF-MPDAC) method; brain tumors may be automatically segmented. The proposed approach integrated random forests and the active contour model. Modality-specific random forests were utilized to incorporate local information from multimodal images, aiming to explore contextual and structural information of gliomas within the framework. Additionally, a multiscale patch-driven active contour approach was employed, leveraging sparse representation techniques to refine the gliomas framework. The experimental results demonstrated higher accuracy compared to other traditional approaches for brain tumor segmentation.

Rehman et al. (2019) developed an automated brain tissue classification approach using a regional classifier based on Random Forest (RF) for distinguishing between normal and abnormal tissues. The regional classification method employed in the study aimed to

accurately segment and detect tumors at the pixel level. Various region-based features, including fractal features, statistical measures, and texture histograms, were utilized in the proposed approach. To address class imbalance issues, the researchers employed RMD-SMOTE at the regional level. The study also compared the performance of standard supervised techniques such as RF, SVM, and AdaBoost classifiers, ultimately selecting the RF-based regional classifier due to its superior generalization performance. The proposed model achieved improved precision and specificity in the segmentation and detection of brain tumors.

Bal et al. (2018) presented an innovative model for automatic segmentation of brain tumors using RFCM (Rough Fuzzy C-Means) with shape-based topological properties. The rough-FCM approach effectively addressed the issue of overlapping partition problems through the utilization of fuzzy membership, upper and lower bounds of rough sets, which helped handle uncertainty in the dataset. The RFCM, combined with fuzzy boundary belonging and crisp lower approximation, demonstrated enhanced efficiency in brain tumor segmentation. Skull stripping was performed using a patch-based K-means approach. The proposed model was evaluated on standard benchmark datasets of MRI scans. The simulation results of the adopted model showcased superior performance with maximum accuracy.

Pinto et al. (2018) developed an automatic hierarchical brain tumor segmentation pipeline utilizing an innovative technique called ERT (Ensemble of Randomized Trees) that incorporated context-based features. The pipeline involved evaluating the location and shape of the tumor, followed by hierarchical two-stage classification to classify the tumor region into different types of tumor tissues. The model employed context-based features and higher randomized trees. Various features were calculated based on non-linear transformations of the MRI images. The experimental results of the proposed approach, evaluated on the BRATS 2013 dataset, demonstrated a better Dice Similarity Coefficient, indicating improved accuracy in tumor segmentation.

Gumaei et al. (2019) devised a brain tumor classification system using the RELM (Rational Extreme Learning Machine) with a hybrid feature extraction approach. The proposed model extracted features using a hybrid feature extraction process and

computed the features of the covariance matrix, which were then projected into a new feature set using Principal Component Analysis (PCA). The RELM algorithm was employed for the classification of brain tumor types. The presented model was evaluated on public datasets through a series of experiments using brain images. The experimental findings showed that the suggested model performed better than others, achieving high classification rates in the task of brain tumor classification.

Siva et al. (2020) proposed a hybrid approach that combines BFC-based segmentation with a DAE (Deep Autoencoder) system. A non-local mean filter was used for denoising during the preprocessing stage. The brain tumor was then divided up using the BFC model. Strong features were retrieved, including ST (Statistical Texture), WPTE (Weighted Phase Transport Entropy), and information theoretic measures. During the classification process, the hybrid model combined DAE with JOA (Joint Optimization Algorithm) and a softmax regression technique to categorize the regions of brain tumors. The experimental findings of the used model showed improved classification accuracy, demonstrating the efficacy of the suggested hybrid strategy for classifying brain tumors.

Imtiaz et al. (2020) proposed an innovative model for segmentation of brain tumors based on superpixel-level characteristics extracted from three 3D volumetric MR image planes (y-z, x-y, and z-x). To address the challenges of precise segmentation in homogeneous boundaries and to reduce pixel randomness, each image within a specific plane was divided into superpixels, which are irregular patches based on spatial and intensity similarity. Various textural and statistical features were extracted from each superpixel, with special emphasis on high labeling in tumor edges for all three planes. Feature selection was performed using histogram with local descriptor pattern analysis and consistency analysis to eliminate non-informative features and reduce feature dimension. The extremely Randomized Trees algorithm was employed for supervised classification of the superpixels into classes of tumors or non-tumors. According on the decisions made, pixel-level decisions were then made for each plane. When compared to conventional models, the suggested model's experimental findings showed superior tumor segmentation performance.

Bennai et al. (2020) developed a multi-agent model for the segmentation of 3D medical

images. The model was based on a group of interactive agents that worked together to segment a 3D image and modify the region growing algorithm. In the first association of agents, region seed placement and region growing were performed. The collaboration and interaction among the agents allowed for refinement of the segmentation by combining over-segmented regions in the second association. Initially, the group of agents partitioned the image voxels into non-edge and edge voxels based on the gradient magnitude between the voxels. Different groups of agents were employed for voxel partitioning and extraction, and homogeneous regions were detected. The simulation was conducted on MRI images of both pathological and healthy brains. The testing outcomes proved the usefulness of the chosen strategy, with superior performance over alternative approaches.

Neal et al. (2017) investigated the occurrence of recurrent thromboembolic events in patients with ischemic stroke who also have primary brain tumors. Recurrent thromboembolism and stroke mechanisms in people with primary brain tumors are still poorly understood. A retrospective cohort of patients having primary brain tumor diagnoses at Memorial Sloan Kettering Cancer Center between 2005 and 2015 with acute ischemic stroke verified by MRI was included in the study. Neurologists gathered information on therapies, patients' histories of cancer, stroke risk factors, and results. The primary outcomes of interest were recurrent thromboembolism (both venous and arterial) and recurrent ischemic stroke as a secondary outcome. Cumulative outcome rates were calculated using Kaplan-Meier statistics, and Cox hazards analysis was used to assess the association between outcomes and potential risk factors. The study identified 83 patients with primary brain tumors who experienced tumor-associated acute ischemic stroke. The findings revealed an increased risk of recurrent thromboembolism, including stroke from rare mechanisms, in patients with primary brain tumors.

Philipp et al. (2017) a study to find risk variables for neurocognitive deterioration in patients with common supratentorial brain tumors and modest neurological abnormalities. The study involves rigorous cognition testing and was carried out at a German academic institution, of patients diagnosed with pituitary adenoma, meningioma, cerebral metastasis, or glioblastoma multiforme, who were in better neurological condition. The

neurocognitive testing assessed various domains including short and long-term memory, depression, visual-spatial abilities, executive function, verbal fluency, anxiety, fluid intelligence, verbal working memory, and perceptual speed. The patients were compared to a group of healthy controls who were pair-matched based on sex, age, profession, and handedness. The study found that patients performed significantly poorer on neurocognitive tests compared to healthy controls. Risk factors such as frontal tumor location, left/dominant hemisphere involvement, and larger tumor volumes were associated with deficits in verbal fluency, executive functioning, and perceptual speed. Impairments in short- and long-term memory and visual-spatial abilities were more related to frontal tumor location. Patient self-awareness, clinical presentation, and tumor type did not show significant associations with specific neurocognitive impairments. The study highlighted that patients with new brain tumor diagnoses in good neurological condition can exhibit neurocognitive impairments in different domains, with left/dominant hemisphere involvement, larger tumor volumes, and frontal location being important predictors of such deficits.

Shah et al. (2017) conducted a study to evaluate a multi-modality and multiparametric imaging protocol in brain tumors and investigate the correlations among various imaging measures. The researchers focused on quantitatively imaging water content using a single multi-gradient echo (mGRE) acquisition. They employed a PCA-based approach for noise reduction in the multi-contrast data during the processing phase. The study utilized a hybrid MR-PET environment to apply the quantitative approach to brain tumor patients. The active tumor tissue was determined using FET-PET, while MRI contrasts were used for grey-matter, edema, and white matter segmentation. Although water content information itself was not directly relevant, its correlation with other quantitative measures provided insights into the microenvironment of water and tissue. The study found that oedema regions (79%) and active tumor tissue (84%) had higher water content compared to normal white matter (WM) (69%), which was similar to ordinary grey matter (GM) (83%). Furthermore, mean kurtosis was lower in oedema and tumor regions compared to normal GM and WM, while mean diffusivity was increased. Voxel-based associations among diffusion and water content indices were observed using diffusion

kurtosis tensor imaging, and correlations between FET-PET and quantitative MRI were reported for eight brain tumor patients. Overall efficient transverse relaxation times ($T2^*$) demonstrated stronger associations with FET-PET and other MR indices.

Elisee et al. (2017) proposed the LRACM (Local Region-Based Active Contour Model) for automatic selection in brain tumor segmentation applications based on image content. The architecture was designed to select one of the three LRACM methods: LACM-BIC (Local Active Contour Model with Bayesian Information Criterion), localized C-V (Chan-Vese) model, and LGDF (Local Gaussian Distribution Fitting) model. To make the appropriate selection, 12 visual features were extracted from the input image. The proposed approach utilized a supervised model. The simulation results demonstrated that the adopted approach successfully selected the most suitable LRACM for effectively handling the specific image requirements, particularly in the context of MRI images. The proposed architecture exhibited higher accuracy compared to using the three LRACM methods independently.

Markus et al. (2017) conducted a study to assess post-operative and pre-operative neurocognitive deficits in brain tumor patients using a screening test. The researchers utilized a computer-based neurocognitive assessment tool to screen data from brain tumor patients before and after surgery. A total of 196 patients who underwent tumor resections at their institution were tested using the NeuroCog Fx® software, two days before and three to four months after surgery. Patient-related information such as age, handedness, level of education, Karnofsky Performance Status (KPS), sex, post and pre-operative neurological status, histopathological diagnosis, and tumor location were recorded for testing purposes. The gathered outcomes were analyzed using a retrospective approach. The study found that a significant number of patients with meningiomas, metastases, and malignant gliomas exhibited notable deficits in various neurocognitive domains. However, there was no significant association between brain tumor location and neurocognitive deficits. The standardized neuropsychological assessment was deemed an essential part of patient care and management for individuals with brain tumors, providing a tailored and more personalized treatment approach.

Nidhi et al. (2017) proposed an adaptive and non-invasive method for tumor detection

using T2-weighted brain MR images. The approach involved preprocessing and segmenting the images through a customized multilevel Otsu's thresholding model. Shape and textural features were extracted from the segmented image, and the two most prominent features, identified using entropy measure, were selected. The SVM classifier was then applied to the MR images using these selected features. The study conducted simulations at NSCB Medical College, Jabalpur, MP, MRI & CT Scan Centre, and gathered a dataset from Research Centre Jabalpur & Charak Diagnostic. The results showed 98% accuracy at a 99% confidence interval and 100% sensitivity for both datasets. The proposed approach outperformed traditional models, demonstrating better efficacy in tumor detection.

Song et al. (2016) conducted a numerical investigation on the influence of brain tumor location during transcranial direct current stimulation (TDCS) in different electrode montages. They utilized a high-resolution realistic human-head model with brain tumors to examine the threshold area and density of peak current in the region of interest (RoI). The experimental results indicated that TDCS could be safely applied to patients with brain tumors to alleviate cancer-related pain associated with neuropsychiatric conditions. However, they observed significant changes in current distributions due to the presence of the brain tumor. The study provided clarification on the local and global effects of possible edema and tumor grade. These findings were valuable for clinical doctors and researchers in the treatment of brain tumor patients. Overall, the study showed advancements in the application of TDCS for brain tumor patients.

Sallemi et al. (2015) presented an innovative model for the modeling of tumor growth in brain glioblastomas. The tumor region was extracted using a distribution matching algorithm based on global pixel-wise information. The novel approach involved simulating tumor growth based on two key elements: the fast marching method and cellular automata (CFMM). This model calculated the evolution of the brain tumor over a specific time period. The researchers conducted experiments and carefully analyzed the outcomes using 20 selected cases of pathological MRI. The experimental results were compared to real tumor growth measurements, using the dice metric parameter as a ground truth reference. The simulation results showed good agreement with the adopted

algorithm in the proposed model. The primary goal of this model was to achieve advancements and progress that could assist radiologists in their diagnosis during clinical investigations. The use of advanced tools provided guidelines and clinical decisions that focused on enhancing objectivity and accuracy for clinicians.

Yang et al. (2015) introduced a DWT-based subspectral and whole-spectral analysis approach using single voxel MR Spectroscopy for improved brain tumor clustering. The model utilized the discrete wavelet transform (DWT) to analyze subspectral or whole-spectral information of key metabolites in the MR spectroscopy (MRS) signal. The separability of the extracted wavelet features was evaluated through unsupervised learning and clustering techniques. The study included 134 short echo time single voxel MRS data, covering low-grade and high-grade tumors as well as normal controls. By combining the DWT-based subspectral or whole-spectral analysis with unsupervised clustering, the approach achieved a balanced error rate of 7.8% and an overall clustering accuracy of 94.8% in clustering brain MRS data. The proposed method offered an alternative approach for feature extraction in brain tumor clustering, surpassing the traditional approaches of feature selection or dimensionality reduction through model fitting on single voxel MRS data.

Menze et al. (2015) reported the results and setup in connection with the MICCAI conferences in 2012 and 2013, the Multimodal Brain Tumor Segmentation Challenge (BRATS) was held. 65 multi-contrast MR scans were used in the evaluation of 20 conventional tumor segmentation techniques. Four raters personally marked these scans, and for comparison, 65 more scans were produced using tumor image modeling software. The study quantitatively evaluated the performance of the algorithms and found significant disagreement among the human raters in segmenting different tumor sub-regions, highlighting the complexity of the task. While various algorithms achieved performance comparable to human inter-rater variability for different sub-regions, no single algorithm consistently ranked at the top for all sub-regions. To address this, a hierarchical majority vote approach was used to fuse the segmentations from multiple algorithms, resulting in improved methodological performance. Additionally, the study found that individual algorithms consistently ranked well, indicating remaining

opportunities for further improvement. Overall, the availability of manual annotations and the BRATS image data provided valuable insights and contributed to better outcomes in brain tumor segmentation research.

Mendes et al. (2015) proposed an approach utilizing the Multimodal Imaging-based Connectome Analysis (MIBCA) toolbox to investigate the connectivity of brain tumor patients. Using a 3T MRI scanner with BrainPET, two patients with glioblastoma lesions in the left hemisphere had dynamic PET scans and simultaneous MRI. The collected data included dynamic ^{18}F -FET PET, T1-weighted MPRAGE, and diffusion tensor imaging (DTI). The MIBCA toolbox was employed to extract connectivity and imaging measures from the multimodal data and perform automatic preprocessing of MRI-PET data. Metrics such as cortical thickness from T1-weighted data, mean diffusivity (MD), node degree, fractional anisotropy (FA), pairwise region of interest (ROI) fiber tracking, and standardized uptake value (SUV) were computed and included in the study. Differences between the right and left hemispheres were assessed for all metrics using a 25% threshold. The data was visualized in connectograms, which displayed both metrics and structural connectivity in the areas close to the lesions, with a lower number of fibers connecting frontal regions with subcortical structures. These findings suggested that the presence of a tumor can affect both local and more distant structural connections. The study emphasized the need for further investigation with larger patient samples and the inclusion of a control group to validate these results.

Yu et al. (2016) conducted an analysis of brain tumor patients' brain anatomical networks using diffusion tensor imaging (DTI) to investigate the topological properties and connection densities. The study aimed to gain insights into the compensatory mechanisms and structural plasticity of the brain in tumor patients. The researchers constructed brain anatomical networks based on DTI data by tracking white matter fiber bundles and quantitatively describing the network's topological properties. A comparison was made between healthy controls and tumor patients using six DTI parameters: degree, regional efficiency, local efficiency, betweenness centrality, vulnerability, and clustering coefficient. A network-based statistic model was employed to localize changes in specific brain regions related to structural connectivity. The study found that the tumor patients

exhibited alterations in the low-world features of the cerebral structural network compared to the controls. The connection density in the tumor group was significantly increased, indicating the impact of tumors on the structural network. This suggests that the presence of brain tumors can lead to changes in the structural connectivity of the brain. Overall, the study provided novel insights into the compensatory mechanisms and structural plasticity in the brains of tumor patients using network analysis of DTI data.

Arakeri et al. (2015) developed a CAD model for accurate and automatic detection of brain tumors, aiming to minimize human errors in the detection process. The system utilized an ensemble classifier on magnetic resonance (MR) images to characterize brain tumors as malignant or benign. The first step of the system involved segmenting the brain tumor tissue from MR images using a segmentation technique. The shape, boundary, and texture features of the tumor were then extracted to characterize its properties. To identify the most relevant features, independent component analysis techniques and gain-based feature ranking were employed. Next, the extracted features were trained using an ensemble classifier comprising SVM, ANN, and KNN classifiers. This ensemble classifier allowed for improved accuracy and robustness in tumor characterization. The CAD system was evaluated on a dataset of 550 patients, consisting of T2-weighted MR images and T1-weighted post-contrast images. The system's performance was assessed using a leave-one-out approach, where each patient's data was used for testing while the remaining data was used for training. The simulation results demonstrated a high accuracy of 99.09% for the adopted segmentation approach, indicating its effectiveness in accurately identifying and characterizing brain tumors. The CAD system provided radiologists with a reliable tool to assist in the diagnosis of brain tumors, improving the accuracy and efficiency of the diagnostic process.

2.3 Research Gaps and Challenges

In stating that automatic classification of brain MRI has the potential to significantly impact clinical medicine by reducing the burden of manual labeling for physicians and providing more robust quantitative measurements to aid in disease diagnosis. Medical Digital Image Processing aims to automate tools that are currently used by the medical imaging community but still require expert assistance. One of the challenging tasks in

brain tumor detection is isolating abnormal tissues from the surrounding healthy brain tissues. The analysis of brain tumors often involves the use of MR images in medical Digital Image Processing, where core steps such as classification, segmentation, and feature extraction are automated to facilitate tumor detection. These automated processes help in accurately identifying and characterizing brain tumors, providing valuable information for diagnosis and treatment planning. By automating these steps, medical Digital Image Processing techniques can enhance the efficiency and accuracy of brain tumor analysis, enabling faster and more reliable diagnoses. It is important to continue developing and refining these automated methods to improve patient outcomes and assist healthcare professionals in their clinical decision-making.

The research in automatic brain tumor detection has been focused on the properties of non-invasive imaging, particularly MRI. The variability in areas, sizes, and shapes of tumors presents challenges in developing effective detection systems or CAD model. In past few decades, researchers in the fields of soft computing and medical Digital Image Processing have concentrated on the classification, segmentation, and combination of these techniques for automatic brain tumor detection. Numerous models and approaches have been developed and reviewed, considering the specific challenges and strengths associated with using MR images to detect different types of brain tumors. The current classification, detection, and segmentation techniques when it comes to medical imaging are discussed, highlighting the advantages and disadvantages of each modality. These discussions aim to provide insights into the performance and limitations of different approaches and assist in the selection of appropriate methods for specific applications. By considering the specific characteristics and challenges of brain tumor detection in MR images, researchers can develop more accurate and reliable models and techniques to aid in the diagnosis and treatment of brain tumors.

2.4 SUMMARY

In the reviewed papers on brain tumor classification, various methodologies were employed, and they were categorized into different groups for analysis. These categories included:

- Analysis based on DL techniques: Several papers utilized deep learning techniques, such as CNNs, to analyze brain tumor images and classify them into different categories. Automatic feature extraction and classification using DL approaches has produced encouraging results.
- Analysis based on optimization: Some papers focused on optimization algorithms and techniques to improve the performance of brain tumor classification. These optimization methods aimed to boost the classification models' precision and effectiveness.
- Analysis based on DL techniques with optimization: Certain studies combined deep learning techniques with optimization approaches to achieve better results in brain tumor classification. These hybrid models aimed to leverage the strengths of both DL and optimization methods.
- Analysis based on ML techniques: Other papers employed ML techniques, such as SVMs, decision trees, and random forests, for brain tumor classification. ML approaches have been widely used in medical image analysis and showed good performance in various studies.

Additionally, the reviewed papers identified several research gaps and challenges in brain tumor classification. These challenges included the need for larger and more diverse datasets, the lack of interpretability and explainability in deep learning models, the need for robust and generalizable models across different imaging modalities, and the importance of addressing class imbalance and data variability in tumor samples. By understanding these research gaps and challenges, future studies can focus on addressing these limitations and further advancing the field of brain tumor classification.

CHAPTER 3

DEEP LEARNING

3.1 Introduction to Deep Learning

The chapter centers on several fundamental principles concerning learning functions and the architecture of neural networks. It commences with an exploration of the core essence of learning functions, underlining their significance in the fields of artificial intelligence and machine learning. The chapter proceeds by introducing artificial neurons as the fundamental components that constitute neural networks. It elaborates on the fundamental structure of neural networks, highlighting the interconnected nature of artificial neurons and their capacity to process and transmit information. Moreover, the chapter delves into deep neural networks, which encompass multiple hidden layers. A comprehensive overview of the key ideas linked to deep neural networks is provided, along with a discussion of common architectures commonly employed in practical applications.

The concluding section of the chapter concentrates CNNs, offering a more comprehensive elucidation of this specific type of neural network. CNNs find extensive applications in Digital Image Processing and pattern recognition tasks. The chapter further explores the distinctive attributes of CNNs, such as the utilization of convolutional layers for extracting features and pooling layers for reducing dimensionality. In summary, the chapter serves as an introductory guide to learning functions, artificial neurons, neural network structures, deep neural networks, and convolutional neural networks. Its primary objective is to familiarize the reader with these fundamental concepts in the field of neural networks and lay the groundwork for further exploration of advanced topics.

“Deep learning methods are distinguished by their hierarchical organization, wherein each layer of the network acquires the ability to comprehend progressively intricate features or patterns. Human designers do not explicitly create these layers; instead, they are learned autonomously through a process called training, during which the network is exposed to vast amounts of data. Deep learning represents a subfield that falls within both artificial intelligence (AI) and machine learning. The overarching objective of AI is to develop models and algorithms that empower computers to solve intricate problems in an automatic, intuitive, and efficient manner. As a specific subset of AI, deep learning

centers on employing neural networks comprising multiple layers to learn and extract meaningful representations from the provided data.

Figure 3.1 presents a comprehensive illustration of the interrelationship between AI, machine learning, and deep learning, emphasizing the role of deep learning within the broader landscape of AI and machine learning. The figure demonstrates how deep learning methodologies play a crucial part in propelling the field of AI forward by empowering computers to autonomously learn and process intricate information.

In conclusion, deep learning methods utilize hierarchical representations learned from data to tackle intricate problems, and they belong to the subfields of both AI and machine learning. These techniques play a vital role in pushing the boundaries of AI capabilities and addressing challenges that traditional computational approaches find difficult. Indeed, the perception and comprehension of the content within images pose significant challenges for computers, but deep learning has demonstrated remarkable achievements in this domain. Specifically, CNNs have made significant strides in image recognition and understanding, showcasing the power of deep learning models in this area.

ANNs are machine learning algorithms inspired by the structure and functionality of the brain. They are composed of interconnected nodes, also known as artificial neurons, which process and transmit information. Deep learning is a specific subset of ANN algorithms that refers to neural networks with multiple layers. These deep neural networks have the capacity to learn hierarchical representations of data, enabling them to extract intricate patterns and features. In practice, the terms "deep learning" and "artificial neural networks" are often used interchangeably because deep learning is a prominent approach within the broader field of ANNs. Deep learning has garnered significant attention and popularity due to its ability to learn complex representations from vast amounts of data, leading to breakthroughs in various AI tasks including speech recognition, natural language processing, and picture recognition. While there are some technical distinctions between deep learning and ANN, they are closely related, and in many cases, the terms are used interchangeably to refer to the utilization of neural networks, especially deep neural networks, for machine learning tasks.

Deep learning has a long and evolving history that spans over sixty years, with various

names and incarnations based on research trends, available hardware and information systems, and prevailing methodologies from influential researchers. Throughout the rest of this chapter, we will delve into a brief yet insightful history of deep learning, tracing its journey as a powerful paradigm in the fields of machinery and computer vision learning, and how it has emerged as one of the most remarkable success stories in contemporary AI.

Figure 3.1: Deep Learning is shown as a Venn diagram [Chandankhede, Ankit, et.al (2023)]

The history of neural networks and deep learning is indeed rich and dates back to the 1940s. Over the years, the field has undergone various shifts and significant advancements. Some notable milestones include the emergence of cybernetics, which laid the foundation for understanding feedback mechanisms and control systems in both biological and artificial systems. The concept of connectivity, inspired by the organization of neurons in the brain, became a fundamental principle in developing neural network models. The popularization of ANNs gained traction during the 1980s and 1990s, where researchers explored their capabilities and limitations. However, due to certain challenges at the time, interest in neural networks declined briefly until the 2000s when breakthroughs in computing power, the availability of large datasets, and innovative algorithms led to the renaissance of deep learning.

This resurgence of interest and progress in deep learning has since led to remarkable advancements and breakthroughs in various fields, including computer vision, natural language processing, speech recognition, and more. The continuous evolution of neural

networks and deep learning has opened new frontiers in artificial intelligence and continues to shape the future of technology. While ANNs draw inspiration from the interactions of neurons in the human brain, they are not meant to be exact replicas or interactive representations of the brain's intricate workings. Instead, ANNs function as computational models that aim to mimic certain behaviors and processes observed in the brain. The design and architecture of ANNs are simplified abstractions of neural networks found in the brain, adapted to suit specific computational tasks. The neurons in ANNs process information using mathematical operations and activation functions, while the connections between neurons are governed by weights that are adjusted during the training process. This allows the ANN to learn and adapt to patterns and data it is exposed to, similar to how the brain learns from experiences and information.

While ANNs do not fully replicate the complexity of the human brain, they have proven to be highly effective in solving a wide range of problems and have become a cornerstone of the field of artificial intelligence and machine learning. Their ability to approximate and model complex relationships in data has led to significant advancements in various domains, making them indispensable tools in modern technological developments. The earliest foundations of neural networks can be attributed to the pioneering work of Warren McCulloch and Walter Pitts et al. in 1943. In their seminal paper, "A Logical Calculus of Ideas Immanent in Nervous Activity," they proposed a simple model of a neural network, specifically a binary classification system. This network aimed to distinguish between two distinct groups based on given input data.

McCulloch and Pitts' et al. model was built on binary thresholds, where the neurons would output either 0 or 1 based on the input signals. While this marked a significant step towards creating computational models inspired by the brain's neurons, the early network had its limitations. One major drawback was that the parameters of the network required manual calibration by a human operator. This manual tuning made the network less practical for tackling complex real-world problems. Despite its limitations, the McCulloch-Pitts model laid the groundwork for further research and the development of more sophisticated neural network architectures over the following decades. It set the

stage for the continuous exploration of neural networks, leading to the significant advancements and breakthroughs we witness in modern deep learning and artificial intelligence.

In the 1950s, Frank Rosenblatt et al. introduced the Perceptron, which was a notable advancement in neural network research. The Perceptron was a more sophisticated algorithm compared to the earlier McCulloch-Pitts model. One of the key contributions of the Perceptron was its ability to automatically learn the necessary weights for classifying inputs without requiring human intervention for manual calibration. The Perceptron became a milestone in the development of neural networks and marked a significant step towards creating more powerful and adaptable computational models. Its design and functioning played a crucial role in laying the foundation for further advancements in neural network research.

Figure 3.2 likely depicts the concept and design of the Perceptron, showcasing its architecture and how it automatically adjusts the weights to make classifications based on input data. The Perceptron's ability to learn and adapt from training data represented a major breakthrough, and it paved the way for the ongoing evolution and sophistication of neural networks in the years to come.

The development of Stochastic Gradient Descent (SGD) during that era was a significant contribution that revolutionized the training of neural networks and remains a fundamental optimization technique used in training deep neural networks to this day. SGD, introduced by Herbert Robbins and Sutton Monro et al. in the 1950s, enabled automatic weight adjustments in neural networks based on available data. This optimization method allowed the network to iteratively update its parameters to minimize the error between predicted outputs and actual targets during training. By iteratively making small updates to the weights, the network gradually improved its performance and learned to make better predictions on new data. The combination of the Perceptron and SGD provided a powerful and automated training approach for neural networks. This advancement garnered significant attention and marked the beginning of neural networks gaining importance in the area of pattern recognition and machine learning. The capability of automatic learning from data opened up new

possibilities and applications for neural networks, setting the stage for further research and development in the field of artificial intelligence and deep learning.

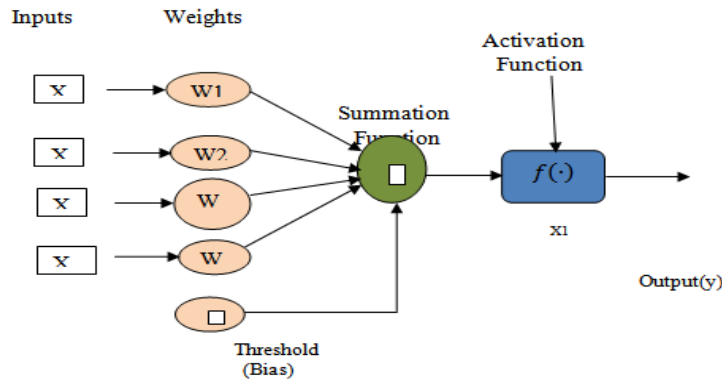


Figure 3.2: The Artificial Neuron [Liam G. Gannon et.al 2023]

The history of neural networks and deep learning is a fascinating journey filled with numerous milestones and transformative breakthroughs. Each advancement and shift in research focus has played a critical role in shaping the current state of deep learning, where complex neural network architectures and sophisticated learning algorithms are applied to tackle a vast array of tasks and challenges. As you progress through the chapter, you will gain a deeper understanding of the historical progression of neural networks. It will likely cover influential developments, such as the introduction of various neural network architectures, the resurgence of interest in deep learning due to advancements in hardware and data availability, and the remarkable successes achieved in fields like computer vision, natural language processing, and speech recognition.

The chapter will likely provide valuable insights into how the field of deep learning has evolved over time, leading to its current prominence in the world of artificial intelligence. It will showcase the ingenuity and dedication of researchers who have contributed to shaping this dynamic and ever-growing area of study. By exploring the historical context, you will gain a better appreciation for the profound impact of deep learning on technology, research, and society as a whole. The field of neural network research faced significant challenges during its early years. One crucial publication that had a notable impact on the progress of neural networks was the work by Marvin Minsky and Seymour Papert et al. in 1969. In their influential book, "Perceptrons," they

demonstrated the limitations of a single-layer neural network with a linear activation function (perceptron).

Minsky and Papert's et al. research showed that a perceptron without depth (i.e., a single-layer network) was unable to solve non-linear problems effectively. They specifically highlighted the inability of a perceptron to learn the XOR function, a classic example of a non-linear problem. The XOR dataset, as depicted in Figure 3.3, consists of two classes, represented by blue stars and red circles. These classes cannot be separated by a single straight line, making it challenging for a single-layer perceptron to correctly classify the data. Their findings had a negative impact on neural network research during that time. The limitations of computational resources at that era further exacerbated the challenges. As a result, interest in neural networks waned, and research in the field entered a period of stagnation, often referred to as the "AI winter." However, it's important to note that these challenges and setbacks were essential for the growth and eventual resurgence of neural networks. They prompted researchers to explore alternative architectures and training algorithms, leading to the development of multi-layer neural networks and more powerful learning methods.

Ultimately, as computational resources improved, and new algorithms such as backpropagation were introduced, neural network research experienced a renaissance, leading to the birth of modern deep learning and its tremendous success in solving complex tasks across various domains. Thus, the setbacks faced in the past were crucial for the evolution and maturation of the field, and they paved the way for the remarkable progress we witness in deep learning today. The backpropagation algorithm, introduced by Paul Werbos et al. in 1974, played a pivotal role in reviving and advancing neural network research. Backpropagation enabled the training of multi-layer feed-forward neural networks, overcoming one of the key limitations identified by Minsky and Papert et al. in 1969. One of the major breakthroughs achieved through backpropagation was the ability to incorporate nonlinear activation functions into neural networks. This critical advancement allowed researchers to explore and exploit the power of nonlinear features in data. Prior to backpropagation, linear activation functions severely limited the expressiveness and learning capacity of neural networks.

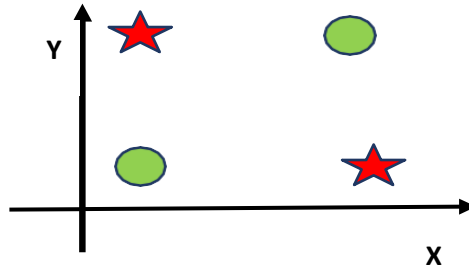


Figure 3.3: An example of a non-linear, separable problem [(Minsky et.al 1969)]

The work of Hornik, Stinchcombe, and White et al. in 1989 demonstrated that neural networks have the capacity to approximate continuous functions, providing valuable insights into their expressive power. This finding was a significant step forward in understanding the capabilities of neural networks to represent and learn complex relationships in data. However, it's crucial to recognize that the ability to approximate functions doesn't guarantee that a neural network will automatically learn the required parameters to accurately describe a given problem or feature. Effective training, appropriate network architecture, and careful tuning of hyper parameters are essential factors in achieving successful learning outcomes. The introduction of the back propagation algorithm, along with subsequent advancements in neural network research, indeed paved the way for exploring the nonlinear nature of data and addressing more complex problems. This progress allowed researchers to build deeper and more sophisticated neural network architectures that could learn hierarchical representations and extract intricate patterns from data.

The backpropagation method has been a fundamental cornerstone that revolutionized the training of neural networks. It allows for iterative learning from mistakes, adjusting the network's parameters to improve performance over time. With advancements in technology, faster and more sophisticated equipment, and the availability of vast amounts of training data, deep learning has emerged as the new iteration of neural networks. The term "deep" refers to the ability to create neural networks with many more hidden layers than previous incarnations. This depth enables the networks to learn hierarchical representations, where lower layers capture basic concepts and higher layers

learn more complex patterns. CNNs are a powerful application of deep learning, particularly in the field of object recognition. The seminal work by LeCun et al. in 1989 demonstrated the effectiveness of CNNs in automatically learning to recognize patterns, specifically in the context of handwriting character recognition.

Since then, CNNs have become a critical component in various computer vision tasks, including image classification, object detection, and segmentation. Their ability to automatically learn and extract features from raw pixel data has led to remarkable achievements in image recognition and understanding. The availability of large-scale datasets, powerful Graphics Processing Units (GPUs), and advancements in neural network architectures has contributed to the success and widespread adoption of deep learning and CNNs. These techniques have revolutionized numerous fields, including computer vision, natural language processing, speech recognition, and more. The progress in deep learning has opened up exciting possibilities for solving complex real-world problems and has reshaped the landscape of artificial intelligence research.

CNNs excel at learning hierarchical representations, where filters in earlier layers detect simple visual features like edges and corners, and higher layers differentiate between different groups of images, allowing them to recognize complex patterns and make accurate classifications. The learning process in deep neural networks can be broadly categorized into three types. Unsupervised learning: In unsupervised learning, the network learns from unlabeled data without any specific target outputs. The objective is to discover underlying patterns or structures within the data. Common techniques used in unsupervised learning include clustering, autoencoders, and generative models. Supervised learning: In supervised learning, the network is provided with both input data and corresponding target outputs.

The goal is for the network to learn the mapping between the inputs and the desired outputs. It is commonly used for tasks like image classification, object detection, and language translation, where the network learns to predict specific labels or values given input data. Semi-supervised learning: Semi-supervised learning is a combination of both supervised and unsupervised learning. A smaller collection of labeled data and a bigger set of unlabeled data are combined in this process. In order to perform better, the

network learns from both labeled and unlabeled input. on the task at hand. This approach is often used when acquiring labeled data is expensive or time-consuming. By employing these different learning techniques, deep neural networks can leverage both labeled and unlabeled data to enhance their learning capabilities and achieve remarkable performance on a wide range of tasks. The flexibility and adaptability of these learning methods have contributed to the success and widespread application of deep learning in various domains.

In supervised learning, the algorithm acts like a student taking a test under the guidance of a teacher (the provided dataset). The algorithm is presented with input data (questions) and their corresponding desired outputs (correct answers). The goal is for the algorithm to learn from these examples and automatically map the input data to the correct output, just as a student strives to provide correct answers based on previous experiences and the teacher's guidance. If the algorithm makes mistakes during training, the teacher (the dataset) provides feedback in the form of correct answers, guiding the algorithm to make more accurate predictions in the future. The algorithm iteratively adjusts its parameters to minimize the difference between its predictions and the provided correct outputs, gradually improving its performance.

CNNs and other deep learning techniques have indeed revolutionized the field of pattern recognition. They have demonstrated remarkable performance across a wide range of tasks, including image classification, object detection, speech recognition, natural language processing, and more. The ability of deep learning models to automatically learn hierarchical representations from data has been a game-changer, enabling them to capture complex patterns and features that were challenging for traditional machine learning approaches. The success of deep learning can be attributed to the availability of large-scale datasets, the development of powerful GPUs, and advancements in neural network architectures and training algorithms. As a result, deep learning has become the go-to approach in many real-world applications, pushing the boundaries of artificial intelligence and transforming various industries.

In a chaotic situation, algorithms may struggle to discover meaningful and discriminatory features due to the randomness of the data. Similarly, in the analogy of a

student, the student might attempt to answer and ask questions randomly, even if they do not know the correct answers. This kind of learning, known as unsupervised learning, can be more challenging than supervised learning, where clear labels and guidance are provided for the learning process. In the context of image classification, unsupervised learning algorithms would attempt to identify patterns in the data without explicit knowledge of the correct labels. This can be more difficult because the algorithm needs to find structure and meaning in the data without any specific guidance on what to look for. On the other hand, in supervised learning, where labeled datasets are used to evaluate models, the algorithm has a clear purpose in distinguishing patterns and connecting input data to the corresponding correct outputs (labels). This guidance allows the model to learn specific features that are relevant to the task at hand, such as recognizing objects in images. In the past, traditional image classification approaches used hand-crafted features to quantify image quality and extract relevant information. These features were carefully designed by domain experts to represent specific characteristics of the data. However, with the rise of deep learning and convolutional neural networks, the need for hand-crafted features has diminished. Deep learning models can automatically learn hierarchical representations and extract relevant features from raw pixel intensities without explicit feature engineering. This has proven to be highly effective in image classification tasks, as the models can discover and leverage intricate patterns that might not have been apparent to human designers. Overall, the power of deep learning lies in its ability to learn from large-scale data directly, extracting complex patterns and features without the need for hand-crafted features. This has led to remarkable progress in various areas of artificial intelligence, including image classification and other computer vision tasks.

3.2 Basics of Neural Network

Neural biological systems primarily consist of interconnected neurons, which are the basic building blocks responsible for processing and transmitting signals. These neurons are connected through axon terminals, forming a network that facilitates the flow of signals in a continuous path. The connectivity between neurons enables information processing and communication within the neural network. In the context of ANNs, these

models are inspired by the structure and functionality of neural biological systems. Figure 3.4 illustrates a shallow ANN, which refers to a neural network with no hidden layer. In this case, the input layer directly connects to the output layer, and there are no intermediate layers for additional computations.

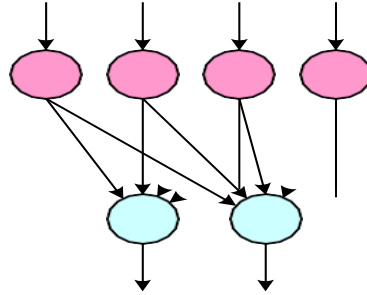


Figure 3.4: Shallow ANN with no hidden layer [Breen, Vivian et.al 2014]

In shallow ANNs, the input data is fed into the network, and the output is generated without any intermediate transformations or representations. Shallow ANNs can be useful for simple tasks that do not require complex feature extraction or hierarchical representations. However, for more intricate tasks that involve capturing complex patterns and representations, deep neural networks (DNNs) with multiple hidden layers are commonly used. Deep learning, as the name suggests, involves training deep neural networks that can learn hierarchical features from data and solve more complex problems effectively. Deep learning models with multiple hidden layers have shown remarkable performance in various tasks, including image recognition, natural language processing, and speech recognition. By leveraging the power of deep neural networks, researchers and practitioners have achieved breakthroughs and advancements in the field of artificial intelligence, contributing to the rapid progress in machine learning and its practical applications.

3.3 The Artificial Neuron

As for Figure 3.2, the output of such an artificial neuron represented as:

$$y = f\left(\sum_{n=0}^N W_n x_n + \theta\right) \quad (3.1)$$

Where X_n refers to the n th neuron input, W_n refers to the weight analogous to that input, θ refers to the neuron bias/threshold parameter, and N refers to the number of

neuron inputs. Besides, $f(\bullet)$ refers to the neuron's activation or transfer role, as set out in the section below.

Each neuron in a network is interconnected with every subsequent neuron to which it has connections. This interconnection allows a neuron to receive feedback from others, and the signal is then amplified by the related weight. The resulting output is combined with outputs from other adjacent neurons in the previous layer through the process of induction, leading to the activation of the current neuron. Activation functions play a crucial role in neural networks by introducing nonlinearity to the network's behavior. Since the sum of linear functions remains linear, using only linear activation functions in a single-layer network without weight sharing would limit the network's representational capacity. Therefore, the use of nonlinear activation functions is necessary to take advantage of the expressiveness offered by multiple layers in a network.

Rectifier functions, such as the Rectified Linear Unit (ReLU), are a popular choice for nonlinear activation mechanisms, offering an excellent alternative to traditional activation functions like the Hyperbolic Tangent Sigmoid. The main advantages of using ReLU as an activation function, as highlighted in the work by Glorot, Bordes, and Bengio et al. in 2011, include:

Simplicity: ReLU is a simple function to compute, involving only element-wise operations, which makes it computationally efficient.

Avoiding vanishing gradient problem: ReLU does not saturate for positive inputs, avoiding the vanishing gradient problem that can hinder learning in deeper networks.

Sparse activations: ReLU induces sparsity in the network as it turns off neurons with negative outputs, leading to more efficient memory usage and faster computations.

Overall, the use of nonlinear activation functions like ReLU is essential for enabling the expressive power of DNN and contributing to the success of DL in various tasks.

3.4 Deep Neural Networks (DNN)

A specific kind of neural network called a DNN classification comprises of multiple

hidden layers between the input and output layers. The quantity of covert layers in a deep neural network is not strictly defined, and the term "deep" refers to the fact that it has multiple hidden layers, making it deeper than traditional single-hidden-layer networks. Figure 3.5 represents a Deep Neural Network with three hidden layers. These hidden layers allow the network to learn hierarchical representations of the data, capturing complex patterns and features as information passes through each layer. One of the significant advantages of using multiple hidden layers is that it enables the network to act as a universal approximator, as demonstrated by Leshno, Lin, Pinkus, and Schocken et al. in 1993. The addition of hidden neuron layers allows deep neural networks to approximate a wide range of complex functions, provided that the network has a sufficient number of parameters and appropriate activation functions.

The depth of the network is crucial because it allows for the transformation of the input data through multiple nonlinear layers. Each hidden layer tests and enhances the nonlinear alterations made by the previous layers, contributing to the network's ability to represent complex relationships in the data. As the network becomes more extensive, with more hidden layers and neurons, its capacity to capture intricate patterns and generalize to different data increases. This enables deep neural networks to tackle complex tasks, such as image recognition, natural language understanding, and speech recognition, with impressive performance. The concept of deep learning, with its multi-layered architectures and powerful learning algorithms, has revolutionized the field of artificial intelligence and machine learning, leading to breakthroughs and advancements across various domains. The depth and representational power of deep neural networks are key factors behind their remarkable success in solving challenging real-world problems.

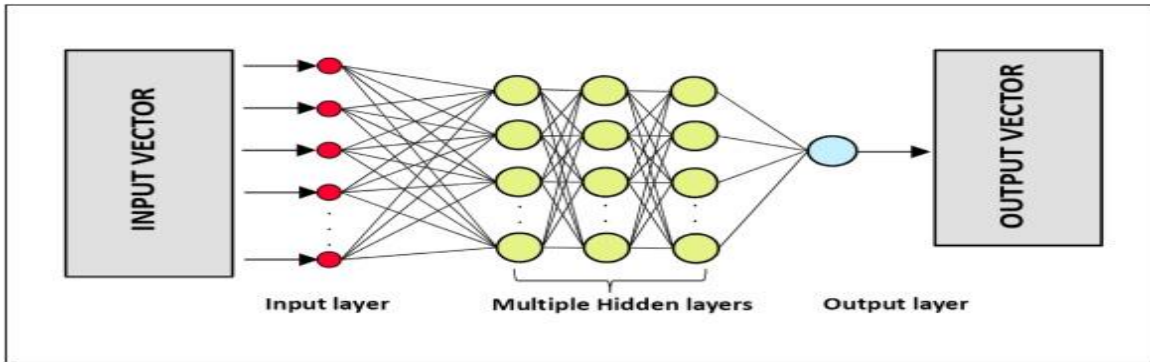


Figure 3.5. Structure of a DNN with three hidden layers [Adil Masood, Kafeel Ahmad,et.al. (2021)]

As stated by Bengio and LeCun et al. in 2007, a deep neural network with an exponentially higher number of neurons ($O(2^n)$) can be more powerful and expressive than a shallow network with only $O(\log n)$ layers. This property allows deep networks to efficiently capture complex relationships and features in data, making them capable of solving more challenging problems compared to shallow networks. Figure 3.5 demonstrates a classic example of a nonlinear, separable problem known as the XOR (Exclusive OR) dataset. The Perceptron, being a shallow linear classifier, is unable to solve this problem. Drawing a single line to separate the red stars from the green circles in the XOR dataset is impossible due to its nonlinear nature. The data points are not linearly separable, and therefore, a simple linear decision boundary is insufficient to correctly classify the data.

This limitation of the Perceptron and other shallow linear classifiers was one of the key motivations for the development of deeper neural networks with nonlinear activation functions. By introducing nonlinearity through activation functions like ReLU, deep neural networks can learn and approximate more complex decision boundaries, allowing them to solve problems like the XOR dataset effectively. The power of deep neural networks lies in their ability to learn hierarchical representations and extract intricate patterns from data, enabling them to address tasks that were previously considered challenging or even impossible for traditional shallow networks. This has been a significant driver behind the success of deep learning in various real-world applications,

making it a powerful tool in the field of artificial intelligence and machine learning.

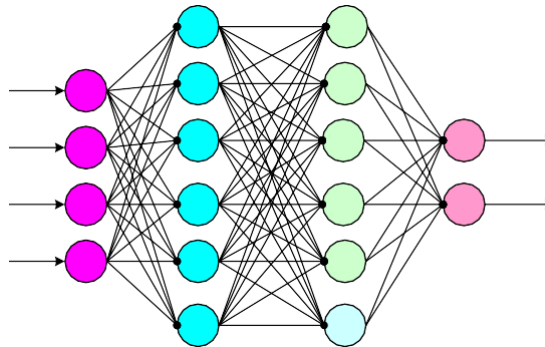


Figure 3.6: Above is Deep Neural Network with two hidden layers [Vignon,Colin et.al. (2023)]

One of the fundamental challenges in the development of deeper neural networks was the requirement for significant computational resources, which were not widely available until more recent times. Traditional CPUs were limited in their ability to efficiently handle the extensive computations required for training large deep neural networks. The advent of powerful (GPUs) played a crucial role in overcoming this computational bottleneck. GPUs are highly parallel processing units designed to handle large-scale computations, particularly those used in graphics rendering. However, researchers and practitioners soon recognized the potential of GPUs in accelerating various types of numerical computations, including those involved in training deep neural networks. GPUs offer significant advantages over traditional CPUs for deep learning tasks. They can perform numerous mathematical operations simultaneously, allowing for massive parallelism in the computations involved in neural network training. This parallelism significantly reduces the training times for large networks, often by several orders of magnitude, when compared to running the same computations on CPUs.

The tests result showed, training times for a given network can be dramatically reduced when using a powerful GPU. In some cases, training that would take hours or even days on a CPU can be completed in just minutes or seconds on a GPU, depending on the complexity of the network and the size of the dataset. The availability of powerful GPUs

has been a game-changer for the field of deep learning, enabling researchers and practitioners to train more extensive and complex models efficiently. This has accelerated progress in various deep learning applications and has played a crucial role in driving the widespread adoption of deep learning in numerous industries and domains. As technology continues to advance, we can expect further innovations that will enhance the performance and capabilities of deep neural networks even further.

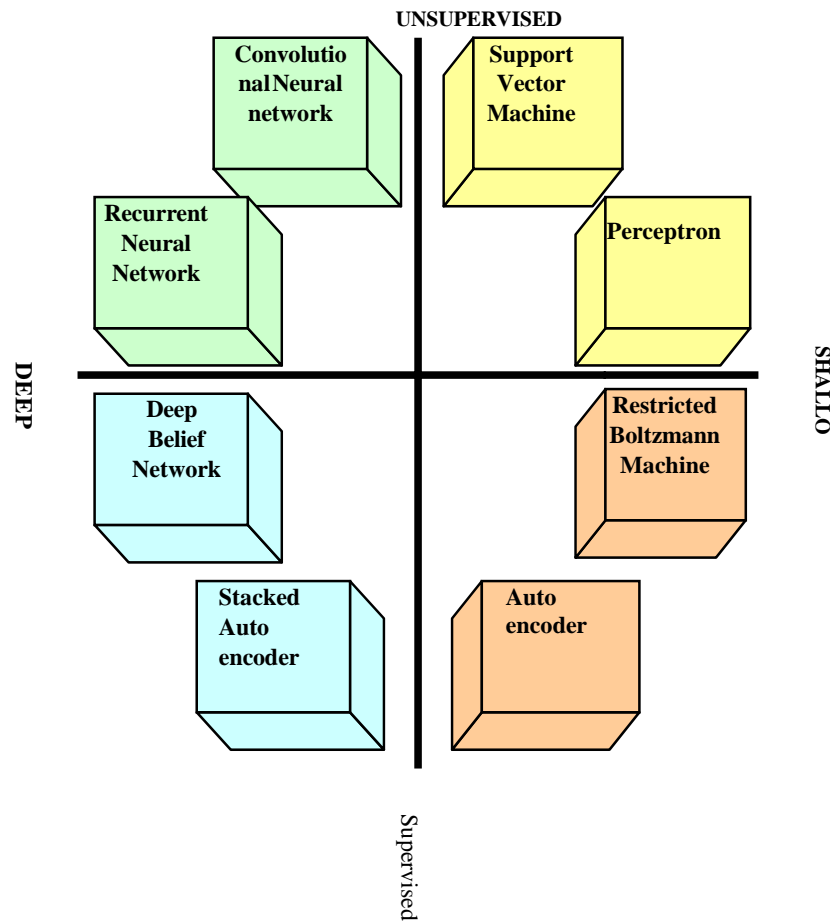


Figure 3.7: Types of Machine Learning Models, Neural Networks and their properties [Shiyong Zheng et.al. (2023)]

3.5 Deep Network Architectures

Figure 3.7 in the section presents a range of network classes based on training and distance properties, along with other network architectures. It likely illustrates various types of deep neural network architectures, each with its own unique characteristics and applications. One of the architectures mentioned in the section is the autoencoder.

Autoencoders are a type of artificial neural network used for unsupervised learning, and they aim to learn a compressed and distributed representation of a specific set of inputs. The primary goal of an autoencoder is to reconstruct the input data as accurately as possible. Encoder and decoder are the two fundamental components of an autoencoder. The decoder attempts to recreate the original input data from the compressed representation after the encoder compresses the input data into a lower-dimensional representation. The encoder and decoder are usually symmetric in structure. Figure 3.8 depicts a stacked autoencoder, which is a variation of the basic autoencoder. In a stacked autoencoder, multiple layers of encoding and decoding are stacked together. This stacking of multiple layers allows the autoencoder to learn more complex and hierarchical representations of the input data. In the training process of an autoencoder, the network tries to minimize the dissimilarity factor or reconstruction error between the original data and the reconstructed data using inverse weights. By minimizing this error, the autoencoder learns to capture essential features and patterns in the input data, leading to an effective compressed representation. Autoencoders are used for various tasks, including dimensionality reduction, data compression, denoising, and feature learning. They have found applications in areas such as Digital Image Processing, computer vision, and natural language processing.

Overall, autoencoders are valuable tools for unsupervised learning, allowing neural networks to learn efficient representations of data without the need for explicit labels or supervision. Stacked autoencoders, in particular, have demonstrated their effectiveness in capturing hierarchical features and have been a significant contribution to the field of deep learning.

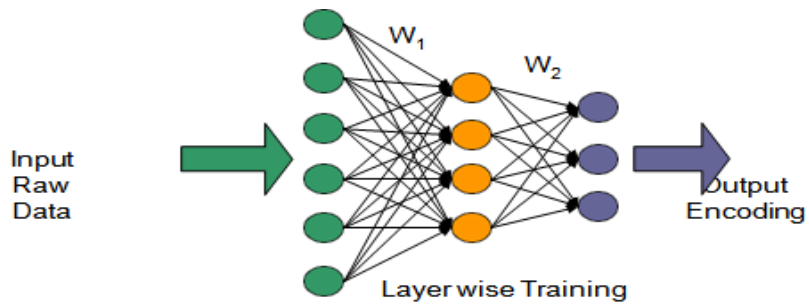


Figure 3.8: Deep neural network architectures [Zhang, Minhao, et.al. (2022)]

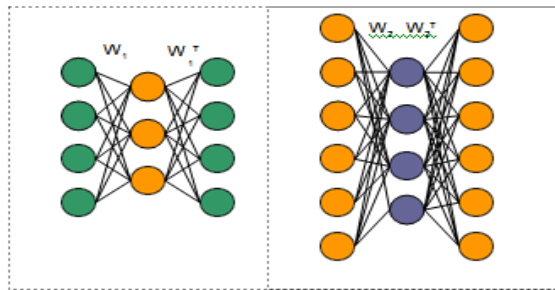


Figure 3.9: Stacked Auto encoder [Truong, D. et. Al. (2019)].

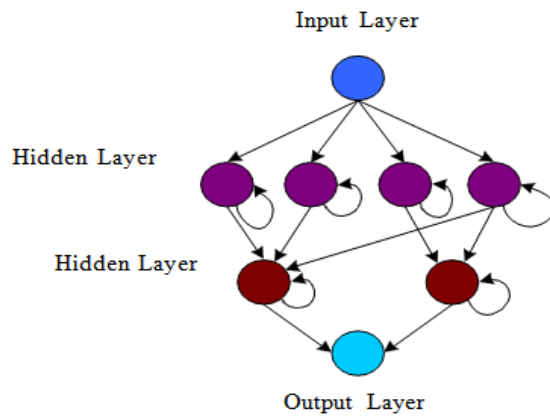


Figure 3.10: Recurrent Neural Network [Bengio et al., 2007]

One of the most valuable benefits of stacked automatic encoders: ease of use layer by layer (Bengio et al., 2007), which enables them to learn from unchecked input encoding.

3.6 Recurrent Neural Networks (RNN)

Current neural networks often incorporate time-based encoding information through architectures RNNs (Hochreiter & Schmidhuber, 1997), as shown in Figure 3.10. RNNs are designed to process sequential data, such as time series or natural language, where each input is associated with a specific time step. The activation characteristics of neurons in RNNs are influenced not only by the current input but also by the recent input history, allowing them to remember past information and maintain short-term memory. In RNNs, the weights of the connections among neurons can be interpreted as a form of long-term memory. These weights are learned and adapted based on the network inputs and the temporal relationships in the data. Over time, the network gradually changes these weights as it processes data sequentially. However, RNNs have limitations in capturing long-term dependencies, as they can suffer from the vanishing gradient problem. This problem arises when the gradients become too small as they are back-propagated through time, making it difficult to learn dependencies that span long sequences. To address this issue, variants like Long Short-Term Memory (LSTM) and Gated Recurrent Unit (GRU) were introduced, which have gating mechanisms that allow them to better capture long-term dependencies and mitigate the vanishing gradient problem.

Figure 3.11 illustrates a feature map generated by a convolutional layer in a CNN. CNNs are designed to recognize patterns and features in spatial data, such as images. The feature map is a visualization of the response of a specific filter (or kernel) to different regions of the input data. Each color in the feature map corresponds to the strength of the filter's response at a particular location. The blue-colored neurons represent the basis of activation, indicating the neurons that are activated and contribute to the specific features detected in the input data. CNNs use convolutional filters to scan the input data and learn relevant patterns, which are then represented in the feature map. Both RNNs and CNNs are powerful tools in the field of deep learning, and they have enabled significant advancements in various applications, including sequence-to-sequence tasks, image recognition, natural language processing, and more.

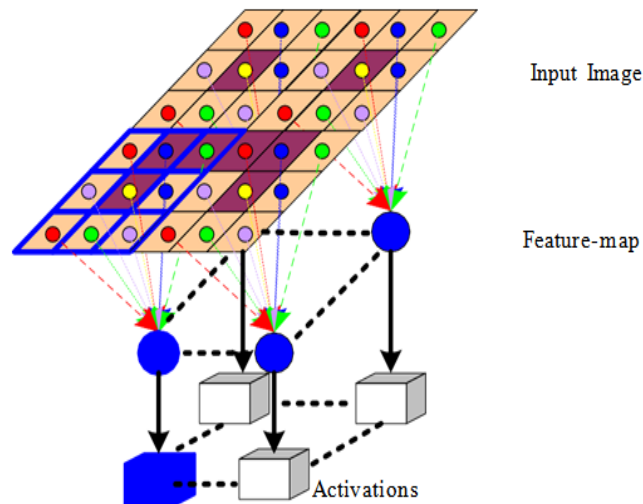


Figure 3.11: Feature map through a convolution layer [BN. Chandrasekhar et.al. (2020)]

3.7 Convolutional Neural Networks

- Use different network designs as Convolutional Neural Networks or (LSTM) Long Short-Term Memory Networks.
- You are doing deep learning if the network gaining depth is less than 2.

The statement discusses the concept of deep networks, implying that networks with a depth greater than 10 can be considered "deep" networks. If a network has a depth of over 10, it suggests a more complex architecture with multiple layers, indicating a deep learning model. The statement also highlights the historical development of deep learning over the past sixty years, emphasizing that profound training has been a subject of research across various educational institutions. Different researchers and think tanks have focused on understanding the function and structure of artificial neural networks, drawing inspiration from the workings of the human brain. Machine learning involves the utilization of artificial neural networks regardless of their size, width, or advanced architecture. However, some types of problems, particularly those involving visually detailed data, may not be well addressed by standard network architectures. The statement points out that the proliferation of weights in deep layers can lead to weak gradients, which can be a challenge in training deep networks.

One major downside of standard network architectures is their limited consideration of spatial input structures, such as images. The statement proposes the use of network structural design to leverage the spatial properties of the data and reduce the training constraints. This can be achieved by employing convolutional layers with shared filters that apply to spatially organized inputs, leading to output maps with similar spatial structures. Figure 3.12 illustrates the concept of Local Contrast Normalization (LCN) with a kernel size of 2x2 over a 4x4 serial input. LCN is a technique used to enhance the contrast of features in an image or input, helping the neural network focus on important details and patterns. The output matrix boxes represent the outputs generated by the LCN kernels over the inputs displayed in the same colored boxes.

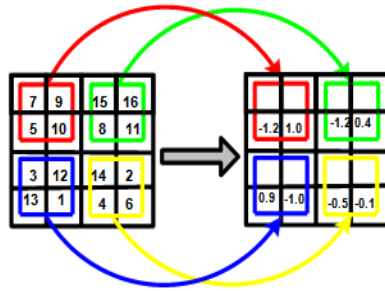


Figure 3.12: The operation of Local Contrast normalization [Patrik Kamencay et.al. (2017)]

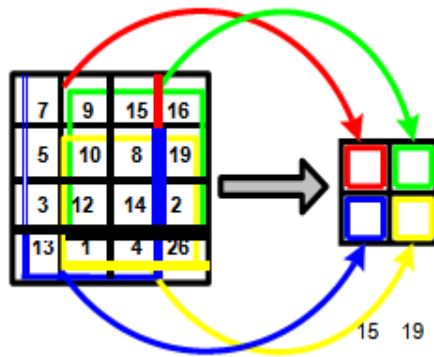


Figure 3.13: The max-pooling operation [Patrik Kamencay et.al. (2017)]

Figure 3.13 illustrates the max pooling operation with a kernel size of 3x3 and a stride of 1 applied to a 4x4 input. The colored boxes on the left side represent max-pooling kernels, and the corresponding colored boxes on the right side display the maximum pooling outputs. The process involves using the filter at different positions of the input

matrix and selecting the maximum value within each filter's receptive field. When dealing with network inputs in a two-dimensional matrix structure, such as images, the weight layer between a 2D input patch and a single neuron output is represented as a filter or kernel.

These filters are repeatedly applied at multiple positions (they can overlap) across the input to generate outputs with a 2D activation matrix. By using the max pooling operation, the network gains an understanding of the spatial arrangement of the input data. Max pooling helps reduce the spatial dimensions of the data while retaining the most relevant features, enhancing the network's ability to recognize patterns and spatial relationships in the input data. Overall, Figure 3.12 demonstrates how max pooling, with appropriately chosen kernel size and stride plays a significant role in spatial data processing and contributes to the network's spatial awareness and ability to capture important patterns in the data. Assume that a matrix which is 2-D in size $I \times J$ and the size of $\hat{I} \times \hat{J}$ for Convolutional layer translate into a two-dimensional input room, with a

stride \hat{I} & \hat{J} . This layer brings into being the size of the output $\frac{I-\hat{I}}{\hat{I}} \times \frac{J-\hat{J}}{\hat{J}}$. The neurons layers calculate their Activations based on equation 3.1

$$\left(y_{i,j} = f \sum_{j=0}^{\hat{J}-1} \sum_{i=0}^{\hat{I}-1} K_{\hat{I}, \hat{J}} x_{i+\hat{I}, j+\hat{J}} \right) \forall i \in \left[1, \frac{I-\hat{I}}{\hat{I}} \right), \hat{J} \in \left[1, \frac{J-\hat{J}}{\hat{J}} \right) \quad (3.2)$$

Where the i^{th} row and j^{th} column in the input and output space are denoted by $x_{i,j}$, and $y_{i,j}$, the primary feature of convolutionary layers is the combination of the filter weights at different points throughout the input.

3.8 Max-Pooling

The construction of a convolutional layer in a neural network involves applying a function that captures patterns defined in the input space at specific locations. If this function is shifted to a different location in the input, the activation pattern of the layer will still be similar, but proportionally transformed. The goal of this process is to create a degree of invariance to small input irregularities and provide robustness to the filters. The convolutional layer typically operates by reading a 2-D input patch (also called a receptive field) and computing a single output value based on the features present in the

input patch. This process is repeated across the entire input data, preserving the spatial information of the data region.

Pooling is an essential operation in CNNs, and it involves subsampling the output of the previous layer to reduce its spatial dimensions. The pooling operation does not involve any weights; it acts as a downsampling step. One common type of pooling is max pooling, where the output value is determined by selecting the maximum value from the input patch. For example, in max pooling, the output value is the maximum value calculated from a given 2-D input patch X . This process helps to reduce the spatial dimensions of the data while retaining important features and creating a degree of translation invariance in the network. Max pooling has been a widely used technique in CNNs for handling spatial information in image recognition tasks and achieving higher accuracy and robustness.

$$y = \max (X) \quad (3.3)$$

It cannot be regarded as a place on the input room but rather as a function in the field of the input area. The overlapping kernel activity is displayed in Figure 3.13.

3.9 Understanding Transfer Learning

Transfer learning is a concept that is dedicated to deep learning. As compared to traditional learning in which the system is designed and dedicated to a particular task, transfer learning is the process in which anyone can leverage weights, features, etc. from a model that is pre-trained and can be used to train a new model which is even having lesser number of datasets.

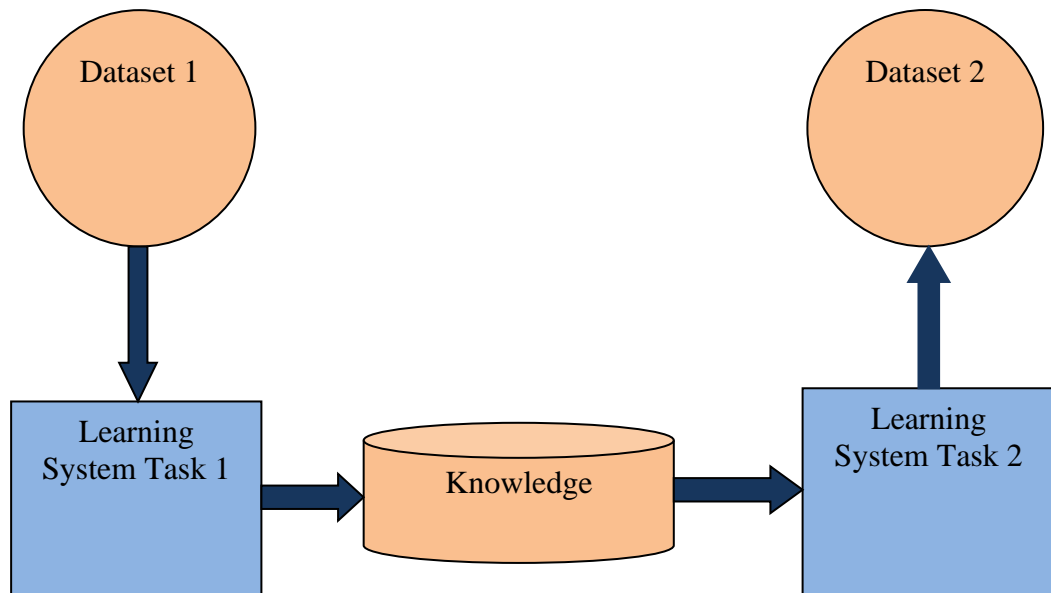


Figure 3.14: Transfer Learning [Priyanka Gupta et.al. (2021)]

3.10 Transfer Learning for Deep Learning

Many misconceptions are popular in context with deep learning. The most popular one is that deep learning cannot be done until and unless anyone is not having millions of labeled examples for any problem. The truth is that the unlabeled data can also be trained, and the training can be done on the nearby surrogate objective and for those, the labels can be easily generated. The learned representation can also be transferred from any related task, as shown in Figure 3.14.

3.11 Shelf Pre-trained Models as Feature Extractors

Deep learning is the process in which different layers present in a network used for learning different features. These layers finally connected to the last layer from which the final output is achieved. So basically, we can utilize this layered architecture to extract the features without utilizing its final fully connected layer. The main question that arises here is that if these networks perform well in actual practice. The literature has proved that such networks are strong enough to perform well in different tasks.

3.12 Pre-trained Models

One of the standard requirements of transfer learning is the models that can handle the task in hand. Fortunately, the world of deep learning believes in sharing. There are plenty of deep learning architectures that are available for people and research community by the developers and team of those networks, and those networks are state of the art networks. In deep learning, the most common and popular fields are computer vision and Natural language Processing. The models that pre-trained and available are huge in count in terms of weight and parameters that model achieves while training. All these pre-trained models are available in different forms, and the most popular deep learning Python library is Keras, via which the most popular models can be downloaded. Not only that, but one can also download various web sources, and most of them are open-sourced.

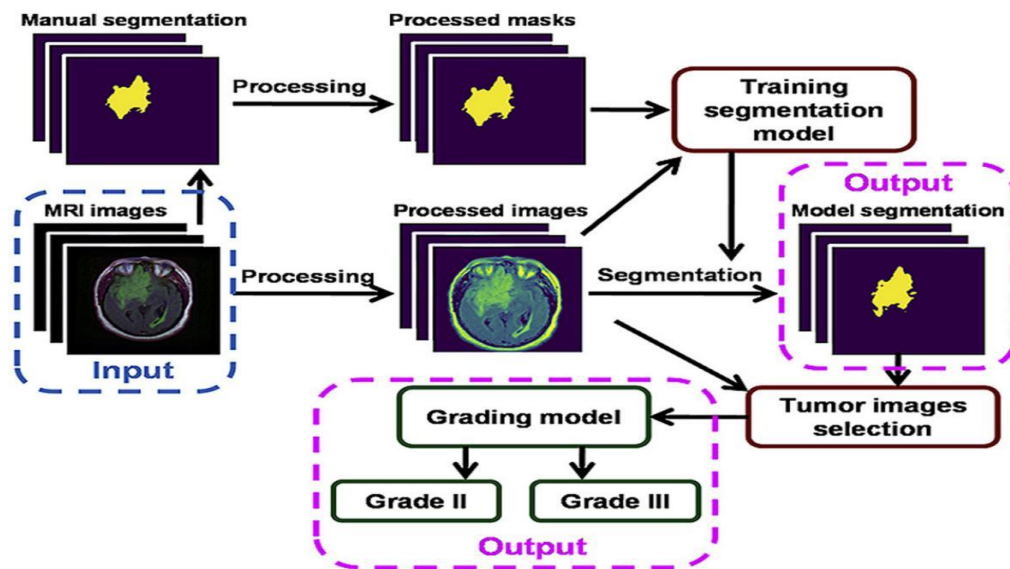


Figure 3.15: Representation of Deep neural networks learn hierarchal feature representations [Taye, M.M et.al. (2023)]

Some popular models for computer vision are:

- VGG-16
- VGG-19
- Inception-V3
- RestNet50

CHAPTER 4

Segmentation of Tumor Regions in Magnetic Resonance Images with Tailored Convolutional Neural Networks

4.1 INTRODUCTION

In today's era, brain tumors pose a significant health challenge in various countries due to factors like global warming, genetic predisposition, and occupational influences. Gliomas, the most aggressive type of brain tumor, result in a shortened lifespan with high severity. The chapter highlights that early detection of brain tumors is crucial for successful treatment outcomes. By identifying tumors in their initial stages, patients can benefit from more effective therapies and better prognosis.

While MRI can easily pinpoint the location of tumors, the substantial amount of MRI-generated data makes manual segmentation time-consuming. This in turn limits the practical use of dependable quantitative methods in clinical settings. The demand for an automated and dependable solution for accurate tumor segmentation is evident. Concurrently, cancer, amplified by the aging population, has evolved into a worldwide health concern. As indicated by the latest data from the World Cancer Research Fund, cancer stands as the most fatal global ailment. Annually, approximately 12.7 million individuals receive a cancer diagnosis, with 7.6 million losing their lives to it. The annual mortality rate due to cancer continues to climb, underscoring the urgency of the issue.

Extensive information on most cancer sub types is a challenge due to their abundance. Following stomach, uterine, breast, and esophageal cancer, brain cancer stands as the fifth most prevalent in terms of both occurrence and fatality. The WHO reports an excess of 120 diverse brain tumor types. Classification relies on factors such as location, tissue type, presence of non-cancerous or cancerous cells (benign or malignant), origin (primary or secondary), and other key attributes. Precise determination of the proportional volume of brain tumor sub components holds significant importance for purposes like monitoring progression, planning radiation treatments, assessing outcomes, and conducting follow-up examinations.

Brain tumors encompass growths that emerge from brain tissue or its immediate

surroundings. Primary tumors are categorized based on factors like benign or malignant nature, composition of glial cells or non-glial elements, and their origin within brain structures, encompassing nerves, blood vessels, and glands. Tumors can be either glial or non-glial. Additionally, metastatic tumors, which stem from other body parts such as the lungs or breasts and spread to the brain, often via the bloodstream, are typically malignant and cancerous. The manual segmentation of tissues presents significant hurdles for human experts due to the diverse appearances that tumors can assume and the necessity to analyze multiple images derived from various MRI sequences for accurate tissue classification. This intricate process is prone to human inaccuracies and time-consuming efforts, leading to substantial levels of variability among different raters and even within the same rater.

Manual segmentation proves to be a time-intensive and challenging endeavor in the context of MRI scans due to their complex multi-modality and the voluminous nature of the 3D images. Moreover, the subjective experiences of the raters can introduce errors into the manual segmentation process. Consequently, there is a considerable demand for fully automated and precise methodologies for brain tumor segmentation in practical applications. Nonetheless, crafting an accurate brain tumor segmentation system remains a formidable undertaking, primarily due to several factors. Firstly, tumors exhibit diverse shapes and internal structures. Secondly, the variable positions of tumors and the influence of the "tumor bulk effect" lead to a wide spectrum of appearances in the surrounding normal tissues. Thirdly, the boundaries between normal and malignant tissues frequently lack clarity, posing challenges in their differentiation. To develop MRI classifiers, it is essential to label training data with tissue types. However, expert labelling is subjective and often focuses on specific areas with high confidence in labeling accuracy. Incorporating model uncertainties can improve the segmentation process as it enables human experts to effectively address uncertain cases. A Bayesian deep learning approach, which not only predicts outcomes but also quantifies uncertainty for individual pixels, offers a means to estimate this uncertainty. This involves utilizing probability distributions for model weights rather than relying solely on deterministic weights of the model.

Medical images play a pivotal role in diagnosing, planning treatments, and monitoring cancer patients. Determining the size and location of tumors is often integral to treatment strategies. Clinicians face the task of manually delineating target volumes for radiation planning, which proves to be demanding and time-intensive. In the realm of brain cancer imaging, MR images offer invaluable insights. Different MR sequences, such as T2, T2-FLAIR, T1, and T1 with gadolinium, unveil distinct tumor subcomponents like edema, necrosis, and the contrast-enhancing core. Recent years have witnessed remarkable accomplishments by machine learning algorithms in various image recognition applications. CNNs are the backbone of most advanced segmentation techniques. However, directly extending segmentations derived from high-quality data to multi-channel images may result in diminished segmentation accuracy.

CNNs offer a noteworthy advantage by autonomously grasping essential features within images. This capability holds particular significance for tumor segmentation. CNN-driven techniques have remarkably excelled on the latest four iterations of the BRATS. Most machine learning-driven segmentation algorithms heavily rely on manually annotated images. The cost of such annotations is notably substantial in medical imaging due to the time-intensive nature and the necessity for profound medical expertise. In cases of MRI or CT scans, the image intensity of malignant tissues often resembles that of adjacent healthy or affected tissues, introducing complexity and subjectivity to precise tumor delineation. Therefore, approaches that can leverage images with less elaborate annotations are of special interest. Deep learning models, like deep neural networks, exhibit remarkable potency in this regard. This study introduces a new method for brain tumor segmentation utilizing a cascaded UNET architecture. Initially, the images are resized to dimensions of 128x128 pixels to ensure optimal computational efficiency. Moreover, an improved adaptive gamma correction technique is applied to enhance pixel quality in the input images. The training and validation process is conducted using selected image slices containing tumor regions. Previous research achieved notable results with an accuracy of 98.12% and a specificity of 97.43%. The presented model is validated using the BraTS 2020 dataset and yields an impressive accuracy of 99.78%. Notably, compared to existing methods, the suggested method performs better,

demonstrating significantly improved accuracy.

However, the approaches discussed earlier possess both advantages and drawbacks. Notably, the previous methods suffer from challenges related to computation time and accuracy. The primary objectives of this study include:

- a) To conduct tumor segmentation encompassing three distinct areas: the edematous, enhancing, and non-enhancing tumor regions.
- b) To enhance the algorithm's versatility in handling diverse MRI images produced by different imaging machines.
- c) To execute the prediction process using high-resolution MRI images while minimizing computational complexity.

4.2 Proposed Methodology

4.2.1 About UNET

U-Net is a convolutional neural network architecture designed primarily for biomedical image segmentation. Developed by Olaf Ronneberger and his colleagues in 2015, U-Net quickly became one of the most widely adopted models for segmentation tasks due to its simplicity and effectiveness. Unlike traditional image classification models, which focus on identifying objects in an image, U-Net excels at pixel-wise classification, making it ideal for tasks where the precise location and boundaries of objects are important, such as in medical imaging, satellite image analysis, and autonomous driving. Advantages of U-Net are High Accuracy, Efficiency and Flexibility.

The U-Net architecture is CNN architecture primarily for use in the field of biomedical image analysis when performing image segmentation jobs. A contracting path, also known as the encoder, and an expanded path, also known as the decoder, make up the characteristic U-shaped structure of the U-Net design. This layout enables the network to take pictures both contextual information and fine-grained details, making it highly effective for segmenting objects or regions of interest within images. Overall, U-Net's unique architectural design and its advantages make it a powerful tool for various image segmentation tasks, particularly in the context of biomedical image analysis.

4.3 Proposed Tumor Region Segmentation from MRI Images

Brain tumor segmentation from MRI data can be effectively achieved through the

application of UNET architecture. The proposed MRI image segmentation process is visually depicted in Figure 4.1. The procedure commences by reading and preprocessing input slices. Initially, slices are extracted from the image database, specifically focusing on those slices that exhibit tumor regions. These selected slices are then employed for both training and validation phases. The analysis of the slices is facilitated by referencing mask data present within the dataset. To streamline the network model's complexity and reduce memory consumption, a preliminary step involves downsizing the images to dimensions of 128×128 pixels before applying enhanced adaptive gamma correction. Subsequently, the UNET architecture is trained concurrently using distinct masks representing the enhancing tumor, non-enhancing tumor, and edema regions. The trained UNET model is subsequently harnessed to execute the testing phase during the final stage of the validation process.

4.4 Block Diagram

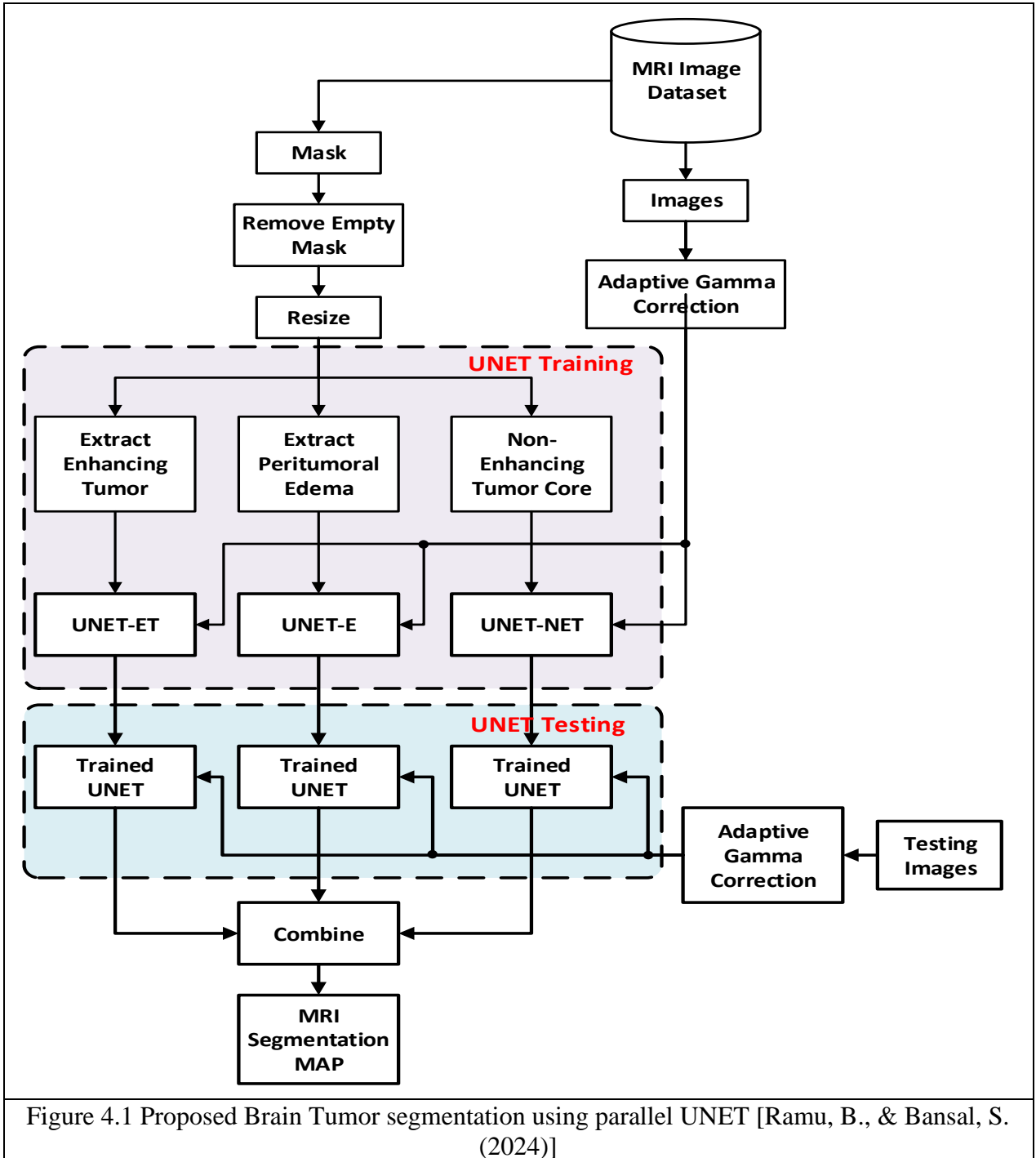


Figure 4.1 Proposed Brain Tumor segmentation using parallel UNET [Ramu, B., & Bansal, S. (2024)]

For the classification of the three distinct regions, a dedicated set of three UNETs is employed. These UNETs undergo individual training processes based on the edema mask, the non-enhancing tumor mask, and the enhancing tumor mask, respectively. These regions exhibit distinct attributes, including pixel density, intensity fluctuations, and textural patterns. This information is harnessed to educate the UNETs, enabling them to effectively discern and categorize the three diverse tumor regions. In the initial training phase, various mask images sourced from the database, each labeled differently, are utilized. Prior to training, a down sampling procedure is implemented to optimize computational efficiency during the convolutional process. The choice of an optimal image size strikes a balance between performance and computational speed. It is important to note that reducing the image size may potentially impact training performance, which could subsequently lead to a reduction in classification accuracy. The testing phase involves loading individual images into the respective UNETs following image enhancement and resizing procedures. This process yields segmentation maps for each tumor region through their corresponding trained UNET architectures. These segmented tumor regions are then consolidated to identify the distinctive attributes of each region. The segmentation results are independently generated by the three previously mentioned UNET models. To mitigate model discrepancies and amplify segmentation performance, a weighted voting technique is employed for producing a fused segmentation outcome. This approach effectively decreases model variation and contributes to an improved overall segmentation performance.

The proposed MRI image classification procedure utilizes Algorithm 1. The process initiates with the reading of a training image from the dataset IdB. Sequentially, each k^{th} image I_k and its corresponding Mask M_{ik} are processed through preprocessing and resizing steps. Subsequently, the Mask M_{ik} is resized to dimensions of 128x128, aimed at reducing computational complexity. The arrangement of images for the training phase is based on information contained within the mask data. For images with non-empty masks, the masks are accumulated for the training process. The images are then categorized based on the labels present in the masks, resulting in the creation of Enhancing Tumor Mask M_{kET} , Non-Enhancing Tumor Mask M_{kNET} , and Edema Mask M_{kER} . The

training process ensures using input images alongside the generated mask data. The process culminates with the execution of both training and validation stages to comprehensively assess the performance of the algorithm.

Algorithm: 1. Algorithm for Proposed MRI Image Classification

Input: Training Image Dataset I_{dB}
Output: Trained $UNET_{ET}$, $UNET_{NET}$, $UNET_{ER}$
: Segmentation Map I_{SG}

1	Get Number of Images N from Database
2	For k=0 to N-1
3	Read Image I_k , and Mask M_{ik}
4	M_{ik} = Resize (M_{ik})
5	Perform Improved adaptive gamma correction on I_k , using threshold $t = \frac{m_i - T_i}{T_i}$
6	If (\sim Empty (M_k))
	Extract
7	a) Enhancing Tumor Mask M_{kET}
	b) Non-Enhancing Tumor Mask M_{kNET}
	c) Edema Mask M_{kER}
8	Collect All Mask in a variable for training $M_{k,m,nET}$, $M_{k,m,nNET}$, $M_{k,m,nER}$
9	Collect All Mask in a variable for training $I_{k,m,n}$
	Perform Training UNET using $I_{k,m,n}$, $M_{k,m,nET}$,
	$I_{k,m,n}$, $M_{k,m,nNET}$,
10	$I_{k,m,n}$, $M_{k,m,nER}$
	Using Loss function $LOSS_b^x = -\sum_{i=1}^{k+m} \sum_{x,y} w_{x,y}^i \log [p_{i,(x,y)}^l(\theta)]$
11	Generate Trained $UNET_{ET}$, $UNET_{NET}$, $UNET_{ER}$
12	Perform Testing on Trained $UNET_{ET}$, $UNET_{NET}$, $UNET_{ER}$
13	Generate I_{SG}

4.5 Improved Adaptive Gamma Correction

Improved Adaptive Gamma Correction (IAGC) is a technique used in Digital Image Processing to enhance the visual quality of images by adjusting the gamma correction parameter in a more intelligent and adaptive manner. Gamma correction is a non-linear operation applied to images to account for the non-linear behavior of display devices such as monitors and screens. It helps ensure that the perceived brightness levels of an image match the actual intensity levels. Traditional gamma correction involves applying a fixed gamma value to the entire image, which might not always provide the best results. Improved Adaptive Gamma Correction, on the other hand, takes into consideration the local characteristics of an image and adjusts the gamma correction parameter

accordingly. This can lead to better contrast, improved visibility of details, and overall enhanced visual quality. The process of Improved Adaptive Gamma Correction typically involves the following steps:

- Image Analysis
- Local Gamma Calculation
- Gamma Adjustment
- Image Enhancement
- Smooth Transition

Improved Adaptive Gamma Correction can be particularly useful in scenarios where images have varying lighting conditions, complex lighting environments, or areas with extreme contrast. It can be applied to various fields such as photography, medical imaging, computer graphics, and more, to provide images that are more visually pleasing and informative. It is important to note that specific implementations of Improved Adaptive Gamma Correction can vary, and there might be different algorithms or approaches that fall under this concept. The precision of the analysis and the caliber of the local gamma correction computations determine how well the procedure performs. The techniques may not effectively enhance the quality of images captured under normal lighting conditions, as these conditions are considered unsuitable for augmentation based on AGC. To strike a balance between improved quality and technical feasibility, the value of 't' is established through experimental evaluation. For contrast enhancement and brightness restoration, an Adaptive Gamma Correction (AGC) approach is employed. Specifically, the negative image-based AGC technique is utilized for bright images, while the Cumulative Distribution Function (CDF) truncation method is applied for dimmed images. This combination of approaches ensures effective enhancement of both bright and dimmed image types while accommodating the intricacies of their respective lighting conditions.

$$t = \frac{m_i - T_i}{T_i} \quad (4.1)$$

As the anticipated average brightness for typical natural photographs, the constant T_i is established. Evidence obtained from numerous standard images databases suggests that T_i is best set around 128 for 8-bit images, or about half of the maximum pixel intensity.

When analyzing a source image, if the threshold 't' falls below $-T_t$, the image is classified as dimmed; conversely, if 't' surpasses T_t , the image is considered bright. It is important to note that images with normal illuminance are not amenable to AGC-based augmentation and are therefore excluded from our methods. The selection of 't' is made through empirical analysis, carefully balancing the quest for enhanced quality with the practical feasibility of the approach. For images falling into the bright and dimmed categories, the AGC technique based on negative images and the CDF truncation method are employed to respectively achieve contrast enhancement and brightness restoration. This approach effectively tailors the enhancement strategies to address the specific characteristics of bright and dimmed images, providing comprehensive image improvement.

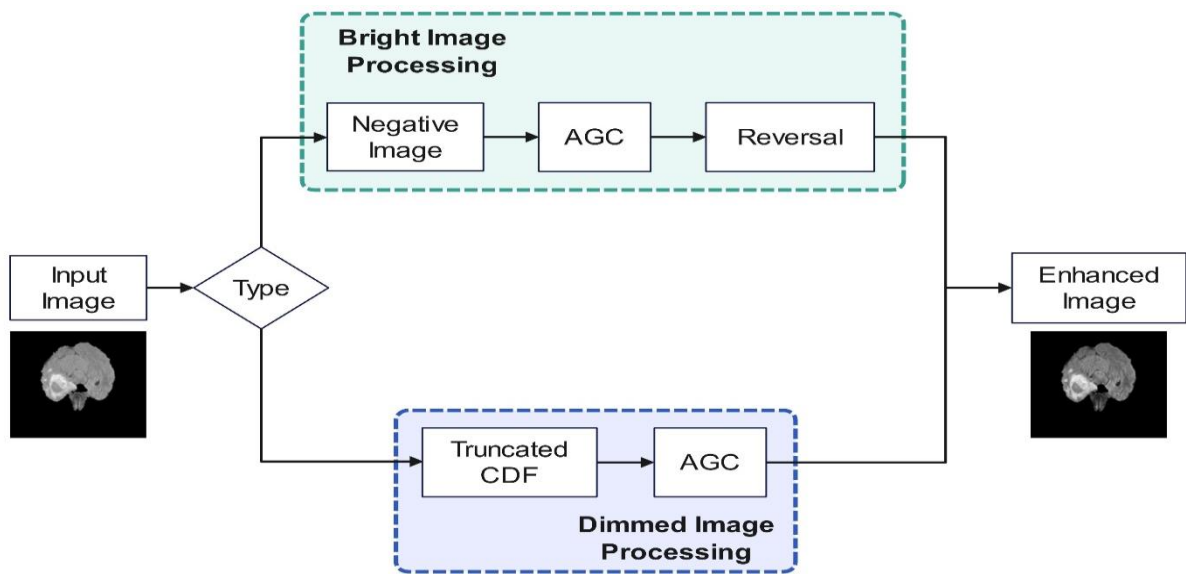


Figure 4.2 Block diagram for Improved Adaptive Gamma Correction [Ramu, B., & Bansal, S. (2024)]

Figure 4.2 illustrates the block diagram outlining the process of enhanced adaptive gamma correction. The Digital Image Processing is contingent on the classification of the image type. In the case of a bright image, the process involves applying a negative image transformation, followed by adaptive gamma correction. Here's a breakdown of the process based on the image:

The block diagram represents a process for enhancing images based on their brightness. It begins with an input image, which undergoes a classification based on its brightness level

into one of two categories: bright image processing or dimmed image processing. This categorization occurs at the decision point labeled "Type."

For bright images, the process starts with the creation of a negative image, which inverts the colors of the original input. Following this, an automatic gain control (AGC) step is applied. AGC adjusts the contrast of the image to optimize the brightness and detail. After the AGC step, the image is reversed, restoring it to its original orientation but now enhanced in terms of contrast and brightness. The result is a visually improved image with more detail and balance in the bright areas.

For dimmed images, a different path is followed. First, a truncated cumulative distribution function (CDF) is applied. The truncated CDF adjusts the image's histogram, limiting extreme values in order to enhance details in darker areas while preventing overexposure. Following this, AGC is also applied to further optimize contrast, adjusting the dim areas to reveal more details. The outcome is an enhanced image with improved visibility in darker regions. Both the bright and dimmed image processing paths lead to a final "Enhanced Image" output, which presents improved contrast, clarity, and visibility. This system, combining negative image inversion, histogram adjustments (CDF), and AGC, works dynamically based on the initial brightness of the input image, ensuring appropriate enhancement is applied for both bright and dimmed images. This method is especially useful in medical imaging, where clarity in both bright and dark areas is essential for accurate diagnosis.

4.6 Convolutional Neural network UNET

U-Net stands as a convolutional neural network initially devised for segmenting biological images within the medical domain. The core principle revolves around enhancing a standard contracting network by appending consecutive layers. These newly added layers replace pooling operations with upsampling operators, thereby yielding performance enhancements. Consequently, this sequence of layers contributes to an enhanced resolution of the output. Subsequently, a following convolutional layer has the capacity to acquire insights from the preceding layer's information and generate a refined output, thus contributing to the network's accurate segmentation capabilities. The architecture of the network comprises two distinct paths: a contracting route and an

expanding path, culminating in a U-shaped network design. The contracting route mirrors a conventional convolutional network structure, involving the repeated application of convolutions, each followed by a rectified linear unit (ReLU) activation and a subsequent max-pooling operation. This sequence is iterated to achieve spatial contraction while simultaneously amplifying feature information. In contrast, the expansive route focuses on combining feature and spatial information from the contracting path with high-resolution data. This is achieved through a series of up-convolutions and concatenations, which effectively integrate the acquired information. The amalgamation of these two routes results in the distinctive U-shaped network architecture, enabling the network to effectively capture and refine features across different scales while maintaining spatial information.

$$Loss_b^x = - \sum_{i=1}^{k+m} \sum_{x,y} w_{x,y}^i \log [p_{i,(x,y)}^l(\theta)] \quad (4.2)$$

Where $p_{i,(x,y)}^l$ is the arrangement notch is agreed by the organization to the ground truth for pixel (x,y) of the i^{th} image of the consignment and $w_{x,y}^i$ is the assumed heaviness to the pixel. Since cancer pixels just make up a little level of the image, the loads are utilized to lessen the impact of class unevenness.

4.7 Training

During the network's training process, The Caffe stochastic gradient descent implementation is paired with input images and the appropriate segmentation maps. This integration generates segmentation maps. To maintain a consistent border width between the output image and the input image, unpadded convolutions are employed on the input image. Notably, large input tiles are distributed across a sizable batch size. This approach reduces the batch size to a single image, there by conserving computational overhead and optimizing GPU RAM utilization. In our optimization stage, a high momentum value of 0.99 is utilized to ensure that a substantial number of previously processed training samples contribute to the update process. The energy function is computed by applying softmax over the final feature map and subsequently combining the outcome with the cross-entropy loss function. The softmax function is defined as part of this process. This comprehensive approach during the training phase aids in effectively enhancing the network's performance and segmentation capabilities.

$$p_k(x) = \exp(a_k(x)) / \sum_{k=1}^K \exp(a_k(x)) \quad (4.3)$$

In the given context, the notation $a_k(x)$ represents the activation in the feature channel denoted by 'k' at the pixel position 'x', where 'x' belongs to the set Ω contained within Z^2 . The value 'K' signifies the total number of classes, and $p_k(x)$ represents an approximation of the maximum function. Specifically, $p_k(x)$ is approximately equal to 1 for the class 'k' that possesses the highest activation $a_k(x)$, while it approximates to 0 for all other classes 'k'. Consequently, the cross-entropy mechanism functions by penalizing deviations from the ideal value of 1 at each pixel position, as defined by $p(x)(x)$. This deviation assessment is a crucial element for optimizing the network's performance and aligning the segmentation outcomes more accurately with the desired results.

$$E = \sum_{x \in \Omega} \omega(x) \log(p_{l(x)}(x)) \quad (4.4)$$

In the given context, the notation $\Omega \rightarrow \{1 \dots K\}$ denotes the true label assigned to each pixel, while $w: \Omega \rightarrow \mathbb{R}$ represents a weight map that has been introduced to assign varying degrees of importance to different pixels during training. The inclusion of this weight map is essential for several reasons: firstly, it compensates for the varying frequencies of pixels belonging to specific classes within the training dataset; and secondly, it encourages the network to effectively learn and distinguish the finer borders separating adjacent cells, which are introduced in the dataset. To accurately capture these separation borders, morphological operations are executed on the data, culminating in the calculation of the weight map. This weight map is subsequently derived using the following methodology:

$$\omega(x) = \omega_c(x) + \omega_0 \cdot \exp\left(-\frac{(d_1(x) + d_2(x))^2}{2\sigma^2}\right) \quad (4.5)$$

In the given expression, $w_c: \Omega \rightarrow \mathbb{R}$ corresponds to the weight map introduced for the purpose of balancing class frequencies. Additionally, $d_1: \Omega \rightarrow \mathbb{R}$ represents the distance from each pixel to the border of the nearest cell, while $d_2: \Omega \rightarrow \mathbb{R}$ signifies the distance to the border of the second nearest cell. In our experimental setup, we set the values of w_0 to be 10 and σ to be approximately 5 pixels. In the context of deep networks characterized by multiple convolutional layers and diverse pathways, the proper initialization of weights holds significant importance. Improper initialization can lead to certain sections of the network displaying excessive activations, while other portions

remain relatively dormant. To address this concern, it is crucial to modify the initial weights in such a way that each feature map within the network attains approximately unit variance. This strategy aids in achieving a more balanced and effective flow of information throughout the network, thereby enhancing its overall performance

In the case of our designed network, which incorporates alternating convolution and ReLU layers, the appropriate weight initialization is possible by selecting initial weights from a Gaussian distribution with a standard deviation of $\frac{2}{N}$. Here, 'N' corresponds to the number of input nodes for a specific neuron. This method is particularly suited to our design where convolution and ReLU layers are interchanged. To elaborate, the goal is to ensure that the starting weights of each feature map within the network exhibit roughly unit variance. This is realized by sampling weights from a Gaussian distribution with a standard deviation of $\frac{2}{N}$, where N is determined by the number of input nodes for a given neuron. For example, if we consider a scenario involving a 3x3 convolution and 64 feature channels in the preceding layer, the value of N would be calculated as $9 \times 64 = 576$. This weight initialization strategy contributes to a balanced and effective information flow throughout the network, optimizing its overall performance.

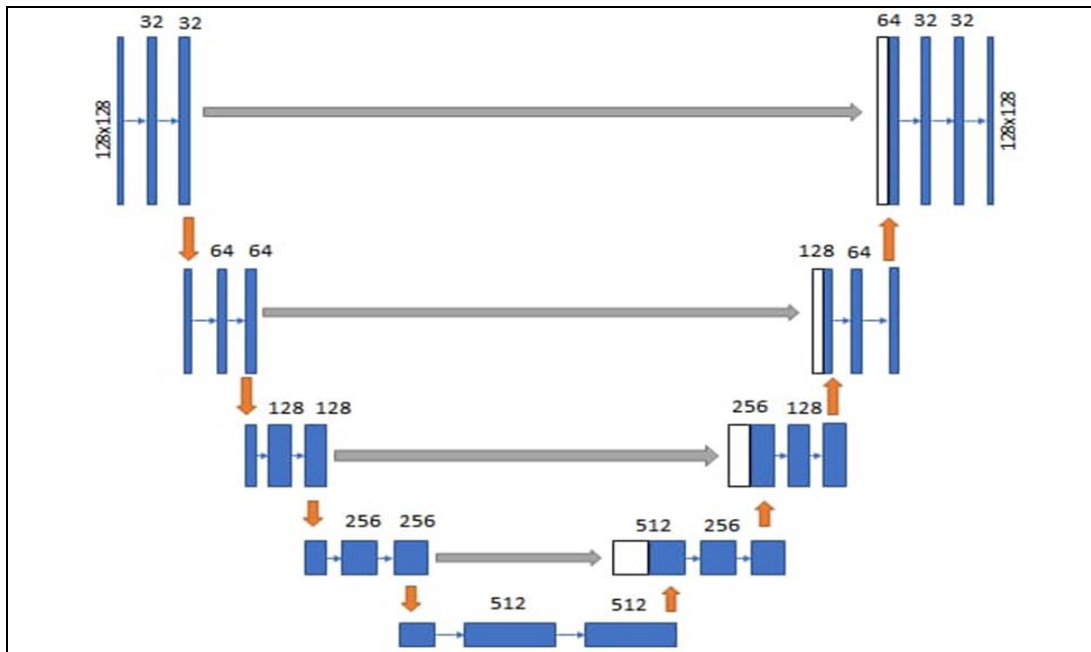


Figure 4.3 UNET Architecture used for MRI segmentation[Ramu, B., & Bansal, S. (2024)]

Figure 4.3 depicts the UNET Architecture employed for MRI segmentation. The input image undergoes resizing to dimensions of 128x128, which serves as the input layer size for the UNET. The UNET architecture, tailored for MRI image segmentation, is structured with a total of 9 layers, each fulfilling distinct roles as visualized in Figure 4.3. The culmination of this architecture is marked by the final layer, which is pivotal for the decision-making process. This layer incorporates the sigmoid activation function, a mathematical operation that facilitates the decision-making process by determining the probability of the presence of certain features or attributes within the segmented image. This activation function enhances the network's ability to make accurate and meaningful segmentation decisions based on the input data.

4.8 Result and Discussion

The envisioned MRI segmentation approach is realized through Python programming within the Kaggle environment. Direct access to the BraTS 2020 database is facilitated using Python commands, enabling efficient data retrieval. Specifically chosen slices from the database are employed for both the training and validation phases of the process. The implementation of the proposed UNET architecture is coded utilizing the Tensor Flow and sklearn libraries, harnessing their capabilities to create the required architecture and facilitate efficient training and validation processes. It is important to note that comprehensive details about the BraTS 2020 dataset are provided in the subsequent section, shedding light on the dataset's composition, characteristics, and relevance to the segmentation task. This thorough description offers valuable insights into the dataset's significance within the context of the proposed MRI segmentation endeavor.

4.9 Dataset

The BraTS 2020 dataset utilized in this research to evaluate the performance of the suggested network. The dataset includes 369 multimodal brain MR studies for training, 125 for validation, and 169 for testing. These studies use fluid-attenuated inversion recovery (Flair) sequences, T1-weighted (T1), post-contrast (T1ce), T2-weighted (T2), and T2-weighted (T1) images. All MR images share a consistent size of $240 \times 240 \times 155$ pixels. Furthermore, experts have meticulously annotated key regions within each study, specifically the enhancing tumor (ET), peritumoral edema (ED), and the necrotic and

non-enhancing tumor core (NET). These annotations provide crucial ground truth data for training and validation purposes. Notably, the annotations for training studies have been made publicly available for online evaluation and as part of the final segmentation competition. However, the annotations corresponding to validation and test studies are deliberately withheld to ensure unbiased and rigorous evaluation of segmentation algorithms. This dataset's comprehensive composition and annotations offer a robust foundation for assessing the proposed network's segmentation performance in the context of brain tumor MR imaging.

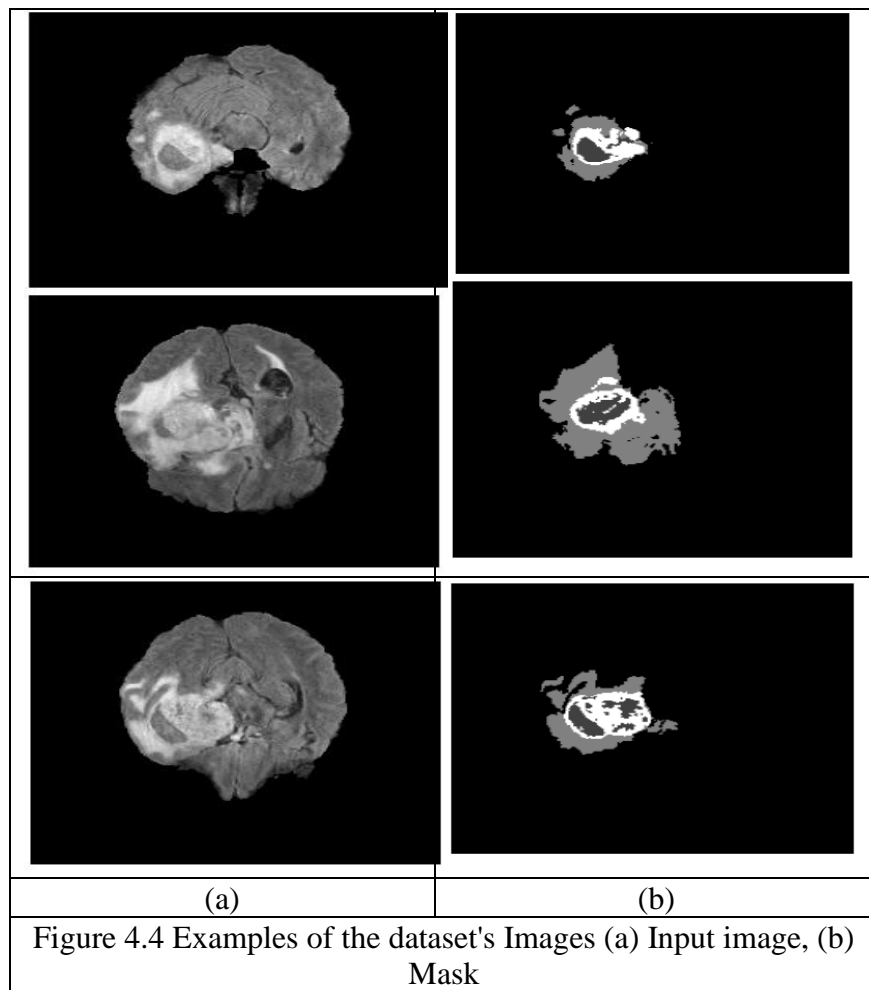


Figure 4.4 illustrates a set of sample images sourced from the BraTS 2020 dataset. In Figure 4.4 (a), the displayed image slices represent input images derived from the BraTS 2020 dataset (<https://www.kaggle.com/datasets/awsaf49/brats2020-training-data>). On the other hand, Figure 4.4 (b) showcases a mask image extracted from the same database.

The mask image delineates various regions within the MRI images. The black region within the mask corresponds to the background of the MRI image. The white region signifies the non-enhancing tumor area. Meanwhile, the gray region represents the enhancing tumor region, and the middle region of the mask depicts the edema present in the brain MRI. This visualization effectively provides insight into the different regions of interest that are annotated within the images, thereby facilitating a better understanding of the dataset's composition and the context in which the proposed segmentation is performed.

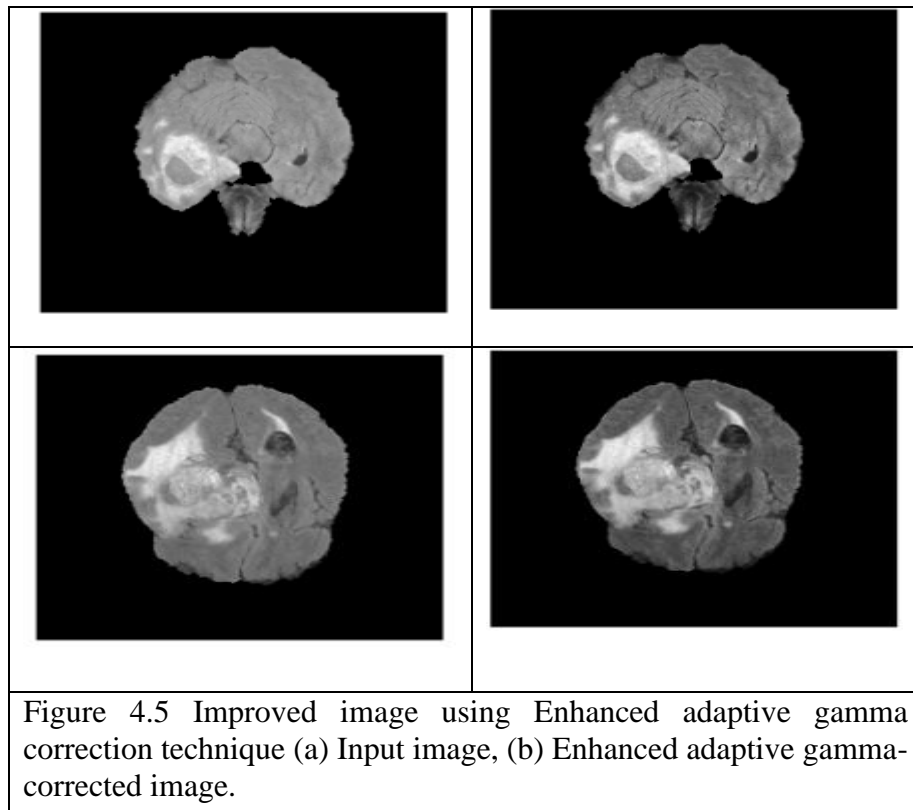


Figure 4.5 presents the outcome achieved through the utilization of the enhanced adaptive gamma correction technique. In Figure 4.5(a), the displayed image represents the input image under consideration. In Figure 4.5(b), the image depicts the output obtained after the application of the enhanced adaptive gamma correction process. It is evident from the comparison that the utilization of enhanced adaptive gamma correction yields improvements, particularly evident in the texture region of the tumor portion, as illustrated in Figure 4.5(b). This enhancement contributes to a clearer and more distinct representation of the specific features and characteristics present within the tumor area, underscoring the effectiveness of the applied technique in refining image quality and information.

4.10 Result Analysis

4.10.1 Accuracy

The accuracy of a system is quantified as the proportion of correct predictions in relation to the total number of predictions made. Notably, the proposed approach exhibits a notably higher accuracy compared to previous methods.

$$\text{Accuracy} = \frac{Tp+Tn}{(TP+TN+FP+FN)} \times 100\% \quad (4.6)$$

4.10.2 Sensitivity

The accuracy of a system is assessed by calculating the ratio of accurate predictions to the total number of predictions made. Importantly, it is worth noting that the proposed approach demonstrates a significantly superior level of accuracy when compared to previous methods.

$$\text{sensitivity} = \frac{Tp}{Tp+Fn} \times 100 \quad (4.7)$$

In this context, the terms are defined as follows:

TP (True Positives): Positive instances that are correctly classified as positive.

FP (False Positives): Negative instances that are incorrectly classified as positive.

TN (True Negatives): Negative instances that are correctly classified as negatives.

FN (False Negatives): Positive instances that are incorrectly classified as negatives.

These elements form the basis for evaluating the performance of a classification system by assessing the accuracy of its predictions.

4.10.3 *Specificity*

The ratio of true negative samples to all of the negative samples in the data set is what's meant by this term. It should be elevated. The calculation of the specificity is

$$specificity = \frac{T_n}{T_p + F_n} \times 100 \quad (4.8)$$

4.10.4 *Precision*

Precision defines how much was correctly classified as positive out of all positives. The formula for calculating precision is given below

$$precision = \frac{T_p}{T_p + F_p} \times 100 \quad (4.9)$$

4.10.5 *F1 Score*

The F1 Score is a metric that takes into account both precision and recall in a classification system. It is calculated as the harmonic mean (average) of precision and recall. The F1 Score is particularly useful when there is a need to strike a balance between precision and recall within the system. The F1 score can be computed using the following formula this formula encapsulates the combined influence of both precision and recall, providing a comprehensive assessment of the classification system's performance.

$$F1Score = \frac{T_p}{T_p + 0.5(F_p + F_n)} \times 100 \quad (4.10)$$

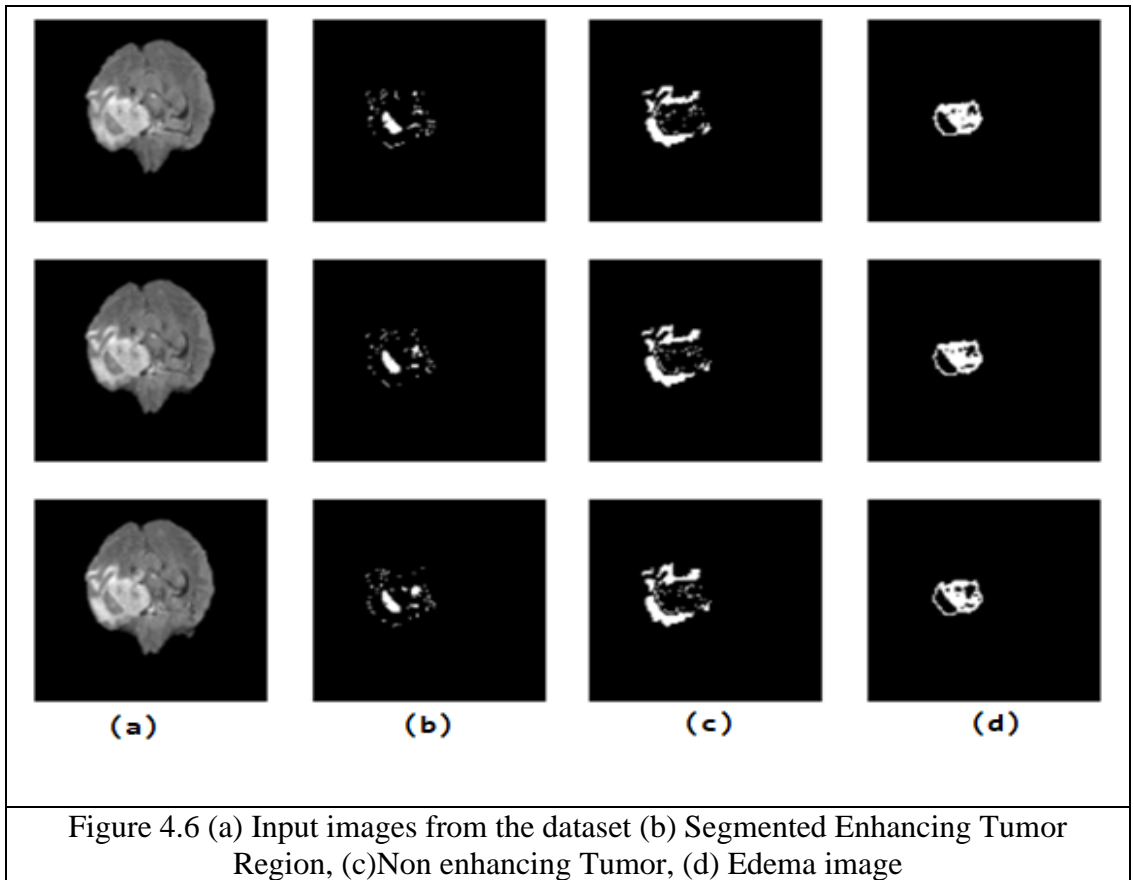


Figure 4.6 visually presents the input images and the corresponding generated segmentation maps. Specifically: In Figure 4.6 (a), a sequence of three successive input slices derived from the MRI of individual 1 is depicted. Figure 4.6 (b) displays the segmentation map produced through the application of the UNET trained to identify the enhancing tumor region. Figure 4.6 (c) illustrates the segmentation map generated using the UNET trained to identify non-enhancing tumor regions. Finally, Figure 4.6 (d) showcases the segmentation map derived via the utilization of the UNET model trained to detect the edema region. This visualization effectively demonstrates the segmentation outcomes achieved by each specialized UNET model for distinct regions of interest within the input images. It provides a clear insight into the network's ability to accurately delineate and identify specific tumor and edema regions, showcasing its potential in the field of medical image analysis.

Table 4.1 provides a comprehensive overview of the suggested approach's performance based on the number of iterations conducted. The accuracy scores for different tumor

regions are as follows: For the enhancing tumor region, after 50 iterations, the accuracy stands at 90.56%, while with 100 iterations, it improves to 99.62%. In the case of the edema tumor region, the accuracy is 91.23% after 50 iterations, and it increases to 98.62% after 100 iterations. Regarding non-enhancing tumors, the accuracy reaches 91.63% after 50 iterations and further improves to 98.99% after 100 iterations. This table effectively showcases the incremental improvements in accuracy achieved through a higher number of iterations, highlighting the method's ability to refine segmentation performance with increasing computational steps.

Table 4.1 Assessment of the Proposed Approach's Performance through Iteration

Iteration	Metrics	50	60	70	80	90	100
Enhancing Tumor	Accuracy %	90.56	93.82	93.82	98.42	98.91	99.62
	Sensitivity %	97.36	96.84	86.49	98.13	98.23	98.93
	Specificity %	98.36	97.18	93.25	98.76	98.81	98.99
Edema	Accuracy %	91.23	91.66	92.12	96.23	97.91	98.62
	Sensitivity %	91.44	92.15	92.52	96.32	96.89	99.23
	Specificity %	91.32	92.56	92.63	96.85	96.83	99.12
non-Enhancing Tumor Core	Accuracy %	91.63	93.82	93.82	98.42	98.91	99.62
	Sensitivity %	91.65	96.84	86.49	98.13	98.23	98.93
	Specificity %	91.85	97.18	93.25	98.76	98.81	98.99

Table 4.2 Evaluating the Proposed Method's Performance across Epochs

No of Epochs	Training loss	Training Accuracy	Validation loss	Validation Accuracy
25	0.5217	96.5	0.5112	96.251
30	0.4631	97.1	0.4421	97.058
35	0.4123	97.5	0.3912	97.563

40	0.3621	98.6	0.3325	98.321
45	0.2516	99.1	0.2351	99.101
50	0.1475	99.6	0.1523	99.261

Table 4.2 presents an overview of the suggested approach performance based on the number of epochs employed. The recorded metrics are as follows: For 20 epochs, the accuracy is 96.5%, the validation loss is 0.5112, and the validation accuracy is 96.251%. With 30 epochs, the accuracy increases to 97.1%, while the validation loss decreases to 0.44. The validation accuracy is noted as 97.058%. After 50 epochs, the accuracy reaches 99.6%, accompanied by a significantly reduced validation loss of 0.15. The validation accuracy notably improves to 99.261%. This table provides valuable insights into the method's performance trajectory as the number of epoch's increases, highlighting the positive impact of additional training iterations on accuracy, loss, and validation metrics.

Table 4.3 Assessing the Performance of the Proposed Method Using Testing-to-Training Ratio

Testing	Training	Accuracy %	Specificity %	Sensitivity %	F1-Score
75	25	72.89	66.94	70.43	81.658
50	50	86.43	82.61	88.31	90.125
25	75	99.71	98.99	98.46	98.92

Table 4.3 provides a comprehensive overview of the proposed method's performance as influenced by the ratio of testing to training images. Notably: When using a ratio of 75% testing images and 25% training images, the performance exhibits lower outcomes. Conversely, with a ratio of 25% testing images and 75% training images, a significant improvement is observed. Specifically, the accuracy achieves a high value of 99.71%, accompanied by an impressive specificity score of 98.99% and a sensitivity score of 98.46%. This table underscores the substantial impact that the distribution of testing and training images can have on the overall performance of the suggested approach, with the

higher training image ratio yielding notably enhanced results across multiple performance metrics.

Table 4.4 Performance of Proposed Method Concerning Conventional Techniques

Methods	Accuracy	Specificity	Sensitivity	Precision
CNN [28]	79.53	88.21	91.52	94.86
OWT [29]	88.53	90.53	90.17	97.83
WAE [30]	92.46	94.82	93.43	92.83
GA [31]	89.39	92.49	94.82	93.49
UNET [32]	96.43	89.43	93.46	96.44
Watershed [41]	92.0	93.46	90.14	97.3
CNN [42]	97.4	98.6	96.0	98.4
This work	99.56	99.71	96.43	98.49

Table 4.4 presents a comprehensive performance comparison between the proposed method and conventional techniques. The results are as follows: CNN (Wang Guotai, et.al) method yields an accuracy of 79.53%, specificity of 88.21%, sensitivity of 91.52%, and precision of 94.86%. (Arif M, et.al) method achieves an accuracy of 88.53%, specificity of 90.53%, sensitivity of 90.17%, and precision of 97.83%. WAE (Abdelkadev I, et.al) method returns an accuracy of 92.46%, specificity of 94.82%, sensitivity of 93.43%, and precision of 92.83%. GA (Aswathy, et.al) method attains an accuracy of 89.39%, specificity of 92.49%, sensitivity of 94.82%, and precision of 93.49%. UNET (Huang C, et.al) method demonstrates an accuracy of 96.43%, specificity of 89.43%, sensitivity of 93.46%, and precision of 96.44%. The proposed method in this work showcases superior performance, achieving an accuracy of 99.56%, specificity of 99.71%, sensitivity of 96.43%, and precision of 93.49%. Table 4.4 provides a comprehensive comparative analysis that underscores the remarkable performance of the suggested approach when compared to existing techniques, solidifying its position as a high-performing approach within the field.

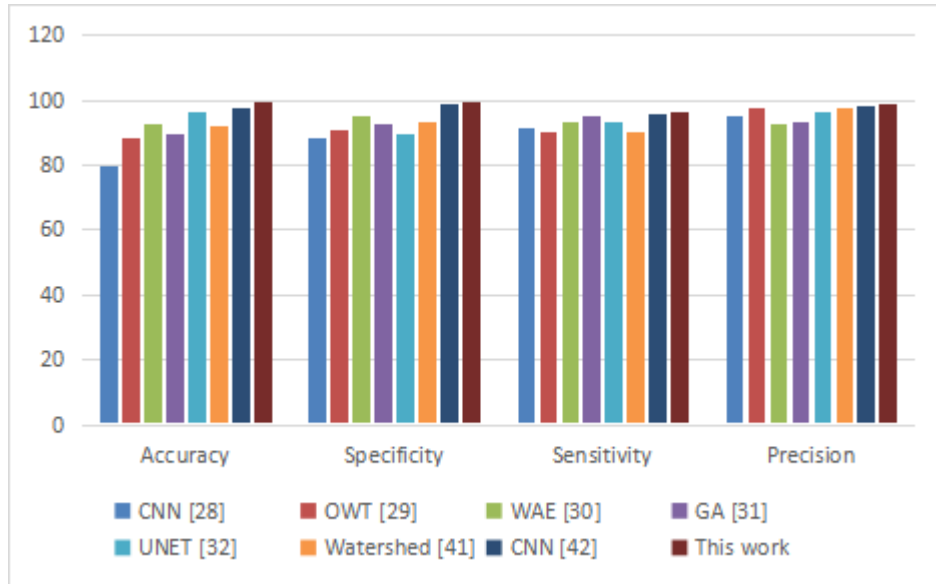


Figure 4.7 Shows the Comparison of the Proposed Technique with Previous Works

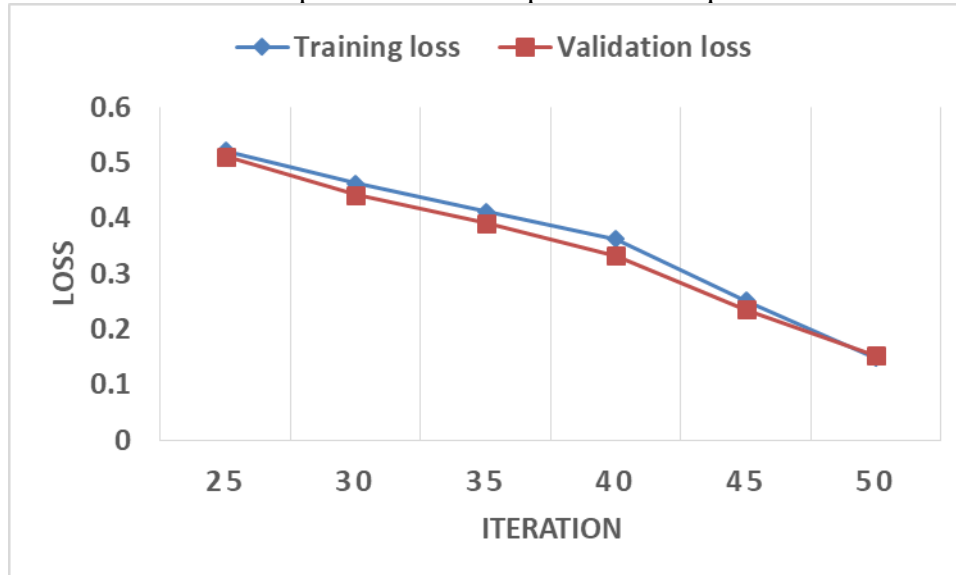


Figure 4.8 Shows the Validation and Training Loss Regarding the Quantity of Iterations

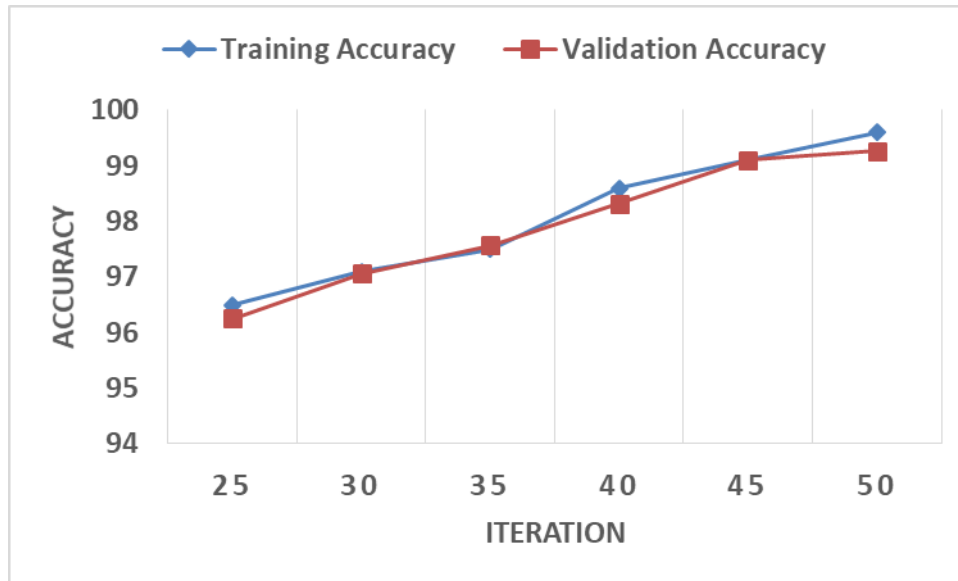


Figure 4.9 Depicts Validation and Training Accuracy Regarding the Quantity of Iterations

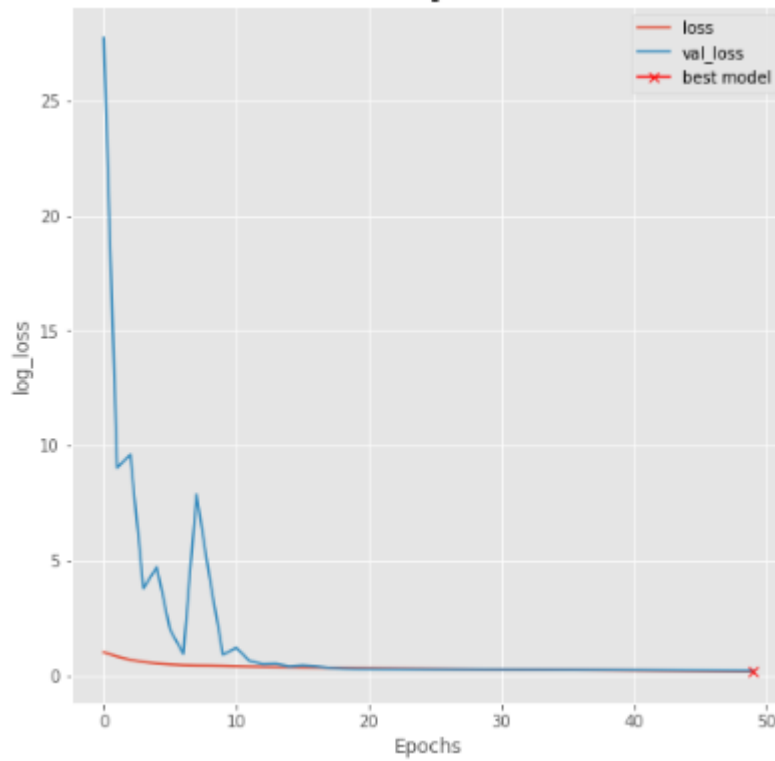


Figure 4.10 Indicates Training and Validation Loss for Non-Enhancing Tumor UNET Training Process

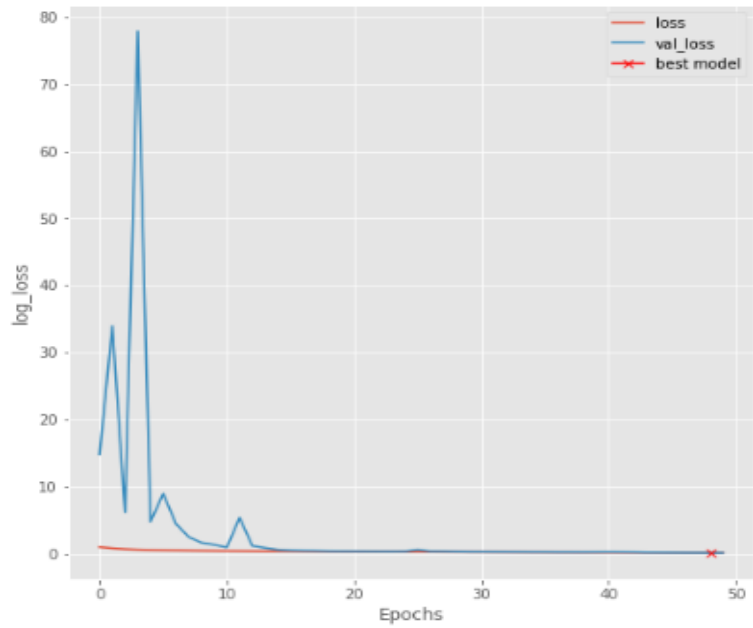


Figure 4.11 Indicates the Training and Validation Loss for Enhancing Tumor UNET Training Process.

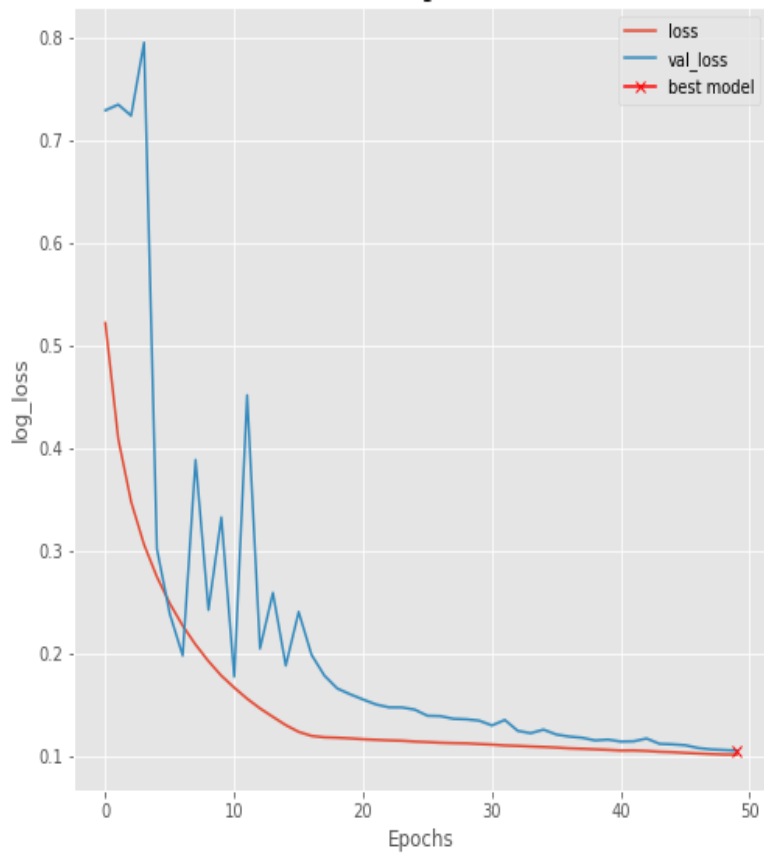


Figure 4.12 Indicates the Training and Validation Loss for Edema UNET Training Process

Table 4.5 UNET Specifications

1	Input Size	128x128
2	Output Size	128x128
3	Output Labels	4
4	Number of Filters	16
5	Minimum Learning Rate	0.00001
6	Batch Size	32
7	Minimum Epoch	50
8	Loss Function	Binary Cross Entropy
9	Training Algorithm	Adam
10	Dropout	0.05
11	Training Testing Ratio	75:25
12	Number of Layers	9

Table 4.5 outlines the UNET specifications employed in the proposed work to generate the segmentation map. The specifications are as follows: Input Size: The UNET input size is established as 128x128 pixels, chosen to enhance performance. Output Size: The output size is aligned with the input, set at 128x128 pixels. Layer Configuration: The UNET architecture is structured with a total of 9 layers, facilitating the segmentation process. Training Algorithm: The Adam training algorithm is utilized for optimizing weights during the training process. Validation Ratio: A training-to-testing ratio of 75:25 is adopted for the validation process. These UNET specifications collectively contribute to the design and operational characteristics of the segmentation process within the proposed approach, promoting efficient and accurate segmentation of the input images.

Table 4.6 Confusion Matrix

	Non-Enhancing Tumor	Enhancing Tumor	Edema
Non-Enhancing Tumor	15423	251	12
Enhancing Tumor	123	15236	2
Edema	102	120	5326

Table 4.6 provides the confusion matrix obtained from the proposed work's results. This matrix is established through pixel classification, utilizing ground truth images to

compare with predicted outcomes. The matrix categorizes predictions into different classes, specifically Non-Enhancing Tumor, Enhancing Tumor, and Edema. The entries in the matrix reflect the number of pixels falling into various categories based on the classification. In Table 4.6, the following observations are made: Non-Enhancing Tumor: A total of 15,423 pixels are accurately predicted as Non-Enhancing Tumors. Enhancing Tumor: 123 pixels are classified as Enhancing Tumor, while they actually belong to other classes. Edema: Similarly, 102 pixels are falsely classified as Edema. The matrix also reflects the misclassification of pixels across the different true classes. This confusion matrix provides valuable insights into the model's performance, shedding light on the areas of accurate classification and instances of misclassification.

4.11 Conclusion

Due to the substantial class imbalance present in MRI scans, segmenting brain tumors from those images is a difficult task. The objective is to accurately predict tumor regions by meticulously segmenting the entire MRI images, a task that benefits from the application of advanced artificial intelligence techniques. In response, we have introduced a novel framework, a modified U-NET, which has demonstrated superior performance in glioma tumor segmentation compared to existing frameworks. Our proposed approach has surpassed previous methods in terms of outcomes. Furthermore, we have conducted a comprehensive examination of available datasets, considering their unique challenges and contributions. Specifically, we have delved into the BraTS 2020 dataset challenge, highlighting its significance in the field. Within this context, it is noteworthy that among various methodologies, machine learning methods have been employed, with deep learning techniques consistently delivering better results. Despite their efficacy, it is crucial to acknowledge that deep learning methods can sometimes be associated with longer processing times and time constraints. Overall, our work emphasizes the importance of adopting innovative AI solutions, particularly deep learning approaches, to discuss the challenging process of segmenting brain tumors from MRI scans, contributing to enhanced accuracy and understanding within the medical imaging domain.

CHAPTER 5

DETECTING AND CLASSIFYING BRAIN TUMORS WITH U-NET AND EXTREME LEARNING MACHINE

5.1. INTRODUCTION

The brain governs the central nervous system and regulates all human actions. While brain tumors can be life-threatening, early detection can greatly enhance survival rates. These tumors arise from abnormal growth of brain cells, and their high prevalence in society presents a significant concern. Gliomas are the most prevalent types of malignant brain tumors, and MRI is frequently used as a non-invasive diagnostic tool for detecting and treating them, including both high-grade and low-grade variants. According to the 2020 GLOBOCAN Cancer Statistics, brain cancer ranks as the second leading cause of death among females, with breast cancer being the primary cause. In males aged 10-39, brain cancer is responsible for 3,700 deaths, as reported by the 2020 Statistics for Adolescents and Young Adults. The same statistics predicted 19.3 million cancer deaths and new cases in 2020, with 300,000 new cases and 250,000 deaths specifically related to brain and nervous system cancers. There are four commonly used MRI techniques for imaging the brain, which include Contrast-enhanced T1, T1, T2, and Recovery after Fluid-Attenuated Inversion (FLAIR).

Manual segmentation relies on the expertise of medical professionals to assess brain tumors, which can vary significantly in morphology and location. Consequently, factors such as fatigue, memory lapses, and lack of experience can contribute to inaccuracies in diagnostic outcomes. The convergence of computer science and medicine has given rise to Medical Imaging and Computer-Aided Diagnostics (MICAD). Leveraging MICAD technology in tandem with computer vision to present MRI image segmentation results to clinicians has the potential to expedite and enhance diagnostic processes.

Brain tumors have the capacity to adversely affect an individual's quality of life as well as that of their family. The presence of visible tumors amplifies the risk of mortality. However, the knowledge that early tumor detection can lead to effective treatment serves as a source of inspiration. In the realm of medical research, the most commonly employed imaging methods for tumor detection include MRI, CT, PET, x-ray, and

ultrasonic screening. X-rays, CT scans, and MRIs are instrumental in diagnosing diseases, with MRI being a prevalent technique for both identification and treatment of brain tumors within the medical field.

Recent advancements in neural network-based image segmentation techniques effectively address the limitations of traditional approaches. These modern methods excel in the segmentation of biological images. Present-day image segmentation technology leverages various image attributes such as color, monochrome, structure, and more to accurately delineate the main components within the image. Given that images typically contain a wealth of geometric data, the segmentation and extraction process represent fundamental applications. This technology finds widespread use in remote sensing, medical imaging, automated transportation, and fingerprint authentication. Regarding the segmentation of brain tumors, conventional methods have traditionally relied on Digital Image Processing techniques, with three widely employed approaches being image thresholding, edge detection, and region-based growth

Manual multimodal brain tumor segmentation is a time-consuming and costly process compared to automated segmentation. An experienced radiologist typically dedicates three hours to meticulously segment a pixel-level image, achieving a Dice Similarity Coefficient (DSC) score ranging from 74% to 85% in manual segmentation. The precise delineation of tumors is crucial for clinical diagnosis and treatment planning.

In recent times, CNNs have gained widespread popularity. They have demonstrated exceptional performance in various tasks such as object recognition, semantic segmentation, depth estimation, object spotting, and more. CNNs employ convolutional layers to autonomously extract meaningful features from input images, enabling them to tackle perceptual tasks without human intervention. CNN-based systems excel in feature extraction and are well-suited for processing biological segmentation tasks like lung and brain tumor segmentation, making them a popular choice in this domain

Increasing the depth of deep learning models has demonstrated improvements across various network segmentation techniques, including CNN, FCN, GNN, RNN, GAN, and more. The development of stronger neural network models is critical for improving brain tumor segmentation. Deep learning has gained significant attention in the context of brain

tumor segmentation. In 3D medical imaging, particularly for brain tumors, the U-shaped model known as U-Net has proven to be highly effective. U-Net consists of four encoder and decoder layers and leverages features from both deep and peripheral neural units, making it a straightforward yet powerful segmentation network. The presence of abnormal cells in the brain can lead to the formation of brain tumors. Among these tumors, gliomas are particularly dangerous due to their low survival rates and the difficulty in physically detecting them, given their irregular shape and intricate boundaries. Gliomas are the most dangerous kind of brain tumor because of this. The most used imaging technique for this purpose is MRI. MRI employs radio waves and a magnet to enable radiologists to peer inside the brain, providing valuable insights into its structure and any potential abnormalities such as tumors.

Identifying the tumor area manually is a laborious and challenging task, which is why there is a pressing need for an accurate and automated solution. To achieve precise segmentation and prediction of brain tumors, a dependable and efficient method is essential. Therefore, the objective of this study is to propose a method that employs U-Net for brain tumor segmentation and an ensemble learning model for predicting patient survival probabilities. In this study, both U-Net and Extreme Learning Machine (ELM) are utilized. Statistical and shape characteristics are extracted using Local Binary Patterns (LBP). The study utilizes the BraTS 2020 dataset, which involves the use of data or images for both training and testing a model. The images undergo segmentation through U-Net, and the classification of brain tumors is accomplished using ELM. The results of this work demonstrate an impressive performance, achieving approximately 99.87% accuracy, 98.96% specificity, 99.58% sensitivity, and 98.75% precision.

This work's main goals:

- By extracting statistical and textural information from the preprocessed image, the process of categorizing the image becomes simpler.
- Reducing the dimensionality of features can lead to faster training and improved classification performance.
- The U-Net algorithms can accurately predict whether an image represents a healthy brain or one affected by a tumor.

- Using an UNET-based segmentation technique, tumor -affected regions can be accurately cropped from abnormal images.

5.2. Materials and Methods

5.2.1 Block Diagram.

The proposed approach to treating brain tumor classification using ELM and segmentation using U-Net is elaborated in Figure 5.1, providing a more in-depth view of the process. The initial stage involves image preprocessing, which includes two key steps: image smoothing and Adaptive Histogram Equalization (AHE). Additionally, the images undergo refinement through Wiener smoothing. Following the preprocessing steps, the U-Net approach is applied for image segmentation. Subsequently, further feature extraction is conducted to capture a diverse range of characteristics, encompassing statistical, shape, and texture information. To perform the classification task, an additional layer of ELM is utilized. This comprehensive approach ensures a thorough analysis of brain tumor images, ultimately enhancing the accuracy and reliability of the classification process.

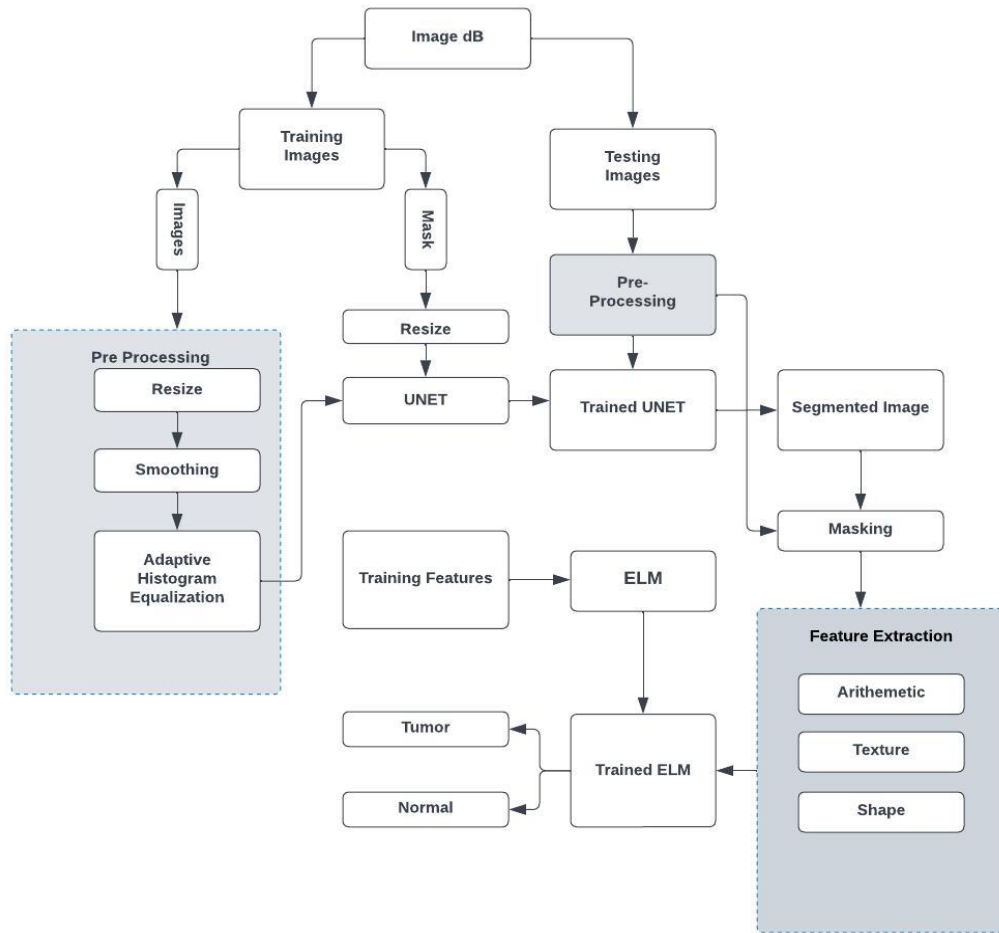


Figure 5.1 Proposed Method Block Diagram

5.2.2. Preprocessing

MR images may have noise from a number of different sources. It is possible that the noise was brought either by image compression or transmission errors. To reduce the noise in this inquiry, nonlocal approaches and local smoothing methods, respectively, were applied.

5.2.3. Image smoothing.

In this study, the Wiener filter is employed to eliminate noise from the normalized image. The Wiener filter effectively reduces noise while preserving image details and softening sharp edges, gradually decreasing corruption step by step. It acts as a concealment and smoothing tool, effectively addressing noise-related issues. The Wiener filter is

particularly proficient at handling mean square error, making it a robust choice for noise reduction. It is important to note that the Wiener filter method is inherently stochastic, meaning it incorporates elements of randomness or probability in its processing.

$$w_x = \frac{w_y - w_n}{|H|^2} \quad (5.1)$$

The power spectrum w_y can be estimated directly from the observation using the periodogram estimate. H is the blurring filter.

5.2.4. Adaptive Histogram Equalization.

The Adaptive Histogram Equalization (AHE) algorithm excels at enhancing an image's contrast because it adapts to the local distribution of pixel intensities, which is more effective than methods that rely solely on global information from the entire input image. This adaptability enables the algorithm to deliver more precise and improved results. However, it is important to note that AHE tends to produce excessive contrast enhancement, especially in regions of the image that are already somewhat homogenous. This is because the adaptive technique boosts contrast locally, in contrast to the standard histogram equalization method, which is one of the key distinctions between the two approaches.

5.2.5. UNET.

Image segmentation is the process of partitioning an image into distinct regions or categories based on the similarities among pixels, with each pixel being assigned to a specific category. In the realm of medical image segmentation, state-of-the-art techniques often involve the use of CNNs, such as the U-Net architecture. The fundamental U-Net architecture comprises two main pathways: the contracting path (also known as the encoder) and the expansive path (or decoder). In the encoder, CNNs consist of input, convolutional, pooling, and fully connected layers. This encoder path progressively reduces the spatial dimensions of the input image while increasing the extracted features. Each pooling operation effectively down samples the image, resulting in a doubling of the features extracted from the image. On the other hand, the decoder path in U-Net involves transposed convolutions, which help localize the features and recover spatial information. The feature map is upsampled in the decoder, effectively halving the number of feature channels at each step. This decoder path is essential for reconstructing a

segmented image with detailed information. In summary, U-Net and similar CNN-based architectures have proven to be highly effective in medical image segmentation, allowing for accurate and precise delineation of regions of interest within the images. In the U-Net architecture, the final step involves a convolutional layer that maps the channels to specific classes after concatenating the feature maps from both the encoder and decoder paths. These feature maps capture essential information for classifying different regions or categories within the segmented image. Both the encoder and decoder in the U-Net architecture are composed of various layers, including convolutional layers, pooling layers, and dense layers. Each convolutional layer applies filters to process the input data, extracting relevant features. These layers play a crucial role in learning and representing important characteristics of the image. The encoder network in the U-Net architecture is responsible for gathering features from data-augmented images, enabling it to learn abstract representations and patterns. This abstract learning is vital for the subsequent steps in image segmentation, where the model must accurately classify pixels into different categories or regions.

The Rectified Linear Unit (ReLU) activation function is employed to address negative outputs at the Convolutional layer outputs in the encoder part of the U-Net architecture. ReLU replaces negative values with zero while leaving positive values unchanged, promoting the learning of more meaningful features. The U-Net decoder replicates the architecture and performs reverse operations compared to the encoder. Specifically, while the encoder utilizes down-sampling operations to reduce spatial dimensions and increase the number of features, the decoder employs up-sampling operations to recover spatial information and reduce the number of feature channels, ultimately aiding in the reconstruction of the segmented image. The proposed U-Net architecture consists of an encoder and decoder, with each internal layer output employing down-sampling and up-sampling, respectively. These operations are crucial for the successful segmentation of the image, capturing and preserving essential information throughout the process; table 5.1 shows the U-Net training settings.

Table 5.1 Training parameters of UNET

Parameters	UNET
Convolutional blocks	4,5,6
Regularization	L1, dropout, L2
Deconvolutional blocks	4,5,6
Batch size	32
Epochs	40
Learning rate	1xe-4

5.3. Statistical Feature Extraction

Brain tumor detection using medical imaging, such as MRI or CT scans, often relies on statistical feature extraction to identify abnormal regions and distinguish tumors from healthy brain tissue. Statistical features summarize important information about the intensity, texture, and structure of the brain tissues in the images, which are then used by machine learning or deep learning models to detect and classify brain tumors. Below is an explanation of how statistical features are extracted from brain scans and how they are used for tumor detection.

5.3.1 Energy

Energy is the probability (normalized histogram) of colour intensity at the point and N is the grey level. The variable "N" represents the number of grey levels or discrete color values that can be observed in the image. In many cases, N is used to represent the range of color or intensity values that are possible in a given image, often expressed as the number of levels or shades of grey in a gray scale image or the number of discrete color values in a color image

$$EG = \sum_i^{NG} \sum_j^{NG} \{p(i,j)\}^2 \quad (5.2)$$

5.3.2 Entropy (EN)

The lowest EN value measures unpredictability. This coefficient's equation is below.

$$EN = - \sum_i^{NG} \sum_j^{NG} p(i,j) \log(p(i,j)) \quad (5.3)$$

5.3.3 Inertia (IN)

The IN, also known as the Contrast feature, measures visual contrast or local variations to show texture quality.

$$IN = - \sum_i^{NG} \sum_j^{NG} (i - j)^2 p(i, j) \quad (5.4)$$

5.3.4 Correlation (CO)

Correlation (CO) describes the linear connection between the co-occurrence matrix's rows and columns. The equation defines this parameter.

$$CO = \frac{\sum_i^{NG} \sum_j^{NG} (i - \mu_x)(j - \mu_y) p(i, j)}{\sigma_x \sigma_y} \quad (5.5)$$

Where $\mu_x, \mu_y, \sigma_x,$ and σ_y are the means and standard deviations of $p_x p_y$

5.3.5 Inverse Difference Moment (IDM)

Homogeneity, also known as inverse difference moment, gauges the density of the co-occurrence matrix and diagonal elements.

$$IDM = \sum_i^{NG} \sum_j^{NG} \frac{1}{1 + (i - j)^2} p(i, j) \quad (5.6)$$

5.3.6 Difference Entropy (DE)

Digital Image Processing discrete entropy measures the amount of bits needed to encode visual data.

$$DE = - \sum_{k=0}^{NG-1} P_{x-y}(k) \log_2 P_{x-y}(k) \quad (5.7)$$

5.3.7 LBP

The local texture information is encoded by the LBP features, which may be used for a variety of tasks including classification, detection, and identification. The image is thresholded with the value of the center pixel, which results in the production of a binary code for each pixel in the image. A histogram is constructed by basing its construction on the many patterns that this binary number presents. LBP stands for pattern number and refers to a gray scale texture operator. It is this operator's job to describe the spatial structure of a local image, and the formula for doing so is as follows:

$$L(x_c, y_c) = \sum_{n=0}^7 2^n g(I_n - I(x_c, y_c)) \quad (5.8)$$

$L(x_c, y_c)$ Is an LBP value at the center pixel (x_c, y_c) and $I(x_c, y_c)$ are the values of the neighbor pixel and center pixel respectively. The function $g(x)$ can be zero if $x < 0$ and $g(x) = 1$ if $x \geq 0$.

5.3.8 Shape Feature

Applying parametric curve concepts to the level sets of the image is the key to defining the curvature of images. These level sets are not explicitly parameterized, but we can specify an implicit parameterization. By equating the contour normal to the image gradient.

$$\hat{N}(x, y) = \frac{1}{(f_x^2 + f_y^2)^{1/2}} \begin{pmatrix} f_x \\ f_y \end{pmatrix} \quad (5.9)$$

5.3.9 ELM

Extreme Learning Machine offers significant advantages in terms of speed, simplicity, and generalization, making it a suitable choice for classification and detection tasks, particularly when computational efficiency is a priority. Its ability to avoid local minima and quickly train without iterative optimization gives it an edge in real-time or large-scale applications. However, its performance depends on the number of hidden neurons and can be sensitive to initialization, In comparison to other classifiers like deep neural networks or SVMs, ELM is much faster to train and easier to implement. ELM is especially useful when the goal is to achieve a balance between speed and accuracy the advantages of ELM are Fast Training Speed and Scalability.

After the identification of the relevant features, an ELM classification approach is used in order to determine whether the MRI brain image in question is healthy or affected by tumor . The ELM is a single hidden layered feed forward neural network. The output weights of this network are obtained analytically, while the input weights are decided on a case-by-case basis. Because of the model that is learnt by output hidden weights, the training procedure may be completed very quickly. In this model, the training samples $\{(H_i, [\text{tar}]_j)\}_{j=1}^N$ is considered with x classes, N number of samples, hidden nodes g , and activation function $\rho(h)$. It is mathematically represented by using the following equation:

$$\sum_{i=1}^g \omega_i \rho_i(h_j) = \sum_{i=1}^g \omega_i \rho(\tau_i \times h_j \times \beta_i) = OP_j \quad (5.10)$$

Where, $j = 1, 2 \dots N$, $h_j = [h_{j1}, h_{j2}, h_{j3}, \dots, h_{jn}]^s$, $tar_j = [tar_{j1}, tar_{j2}, tar_{j3}, \dots, tar_{jn}]^s$, weight value $\tau_i = [\tau_{i1}, \tau_{i2}, \tau_{i3}, \dots, \tau_{in}]^s$, β_i indicates the bias value, and OP_j denotes the output value. ELM transmits several discriminations to regression output functions via One against all coding. The actual output index sample is determined before applying predicted labels. The regularized least-squares approach finds the optimum solution for statistically unstable pseudo-inverses. Based on the regularization parameter, the identity matrix predicts the categorized label. This technique improves training speed, time efficiency, classification accuracy, and implementation. Table 5.2 shows the training parameters of ELM.

Table 5.2 Training Parameters of ELM

Parameters	ELM
Optimization method	SGDM
Shuffle	Every epoch
Momentum	0.90
Batch size	128
Epochs	10
Learning rate	0.01
Frequency Validation	30

5.4. Result and Discussion

Utilizing MATLAB 2019a, the suggested method was put into practice. On a computer with an Intel Core i5 6300 processor and 8 GB of RAM, the testing was carried out. The dataset was divided randomly into two separate sets: During the training process, a training set containing 70% of the data is used to train the network. The remaining 30% of the dataset is used as a validation set to evaluate the performance of the learned model in an unbiased manner.

5.4.1. Dataset

The 3D MRI dataset for the Brain Tumor Segmentation Competition (BraTS) 2020 we are using this dataset. 166 test examples and 369 training instances are available; the sample count is the sole element. The dataset includes both high-grade gliomas (HGG) and low-grade gliomas (LGG), providing a wide variety of cases that exhibit different growth patterns and aggressiveness. This ensures that models trained on the dataset can generalize across a range of tumor types, from slower-growing low-grade tumors to highly aggressive high-grade tumors; Table 5.3 shows the description of dataset.

Table 5.3 Description of Dataset

BraTS 2020	
No of training images	369
No of testing images	166
volume	Each MRI image represented by $240 \times 240 \times 155$ voxels (Width \times Height \times Depth).
Labels	3: Enhancing Tumor (ET), Tumor Core (TC), Whole Tumor (WT)
Tumor Types	Tumor or Normal

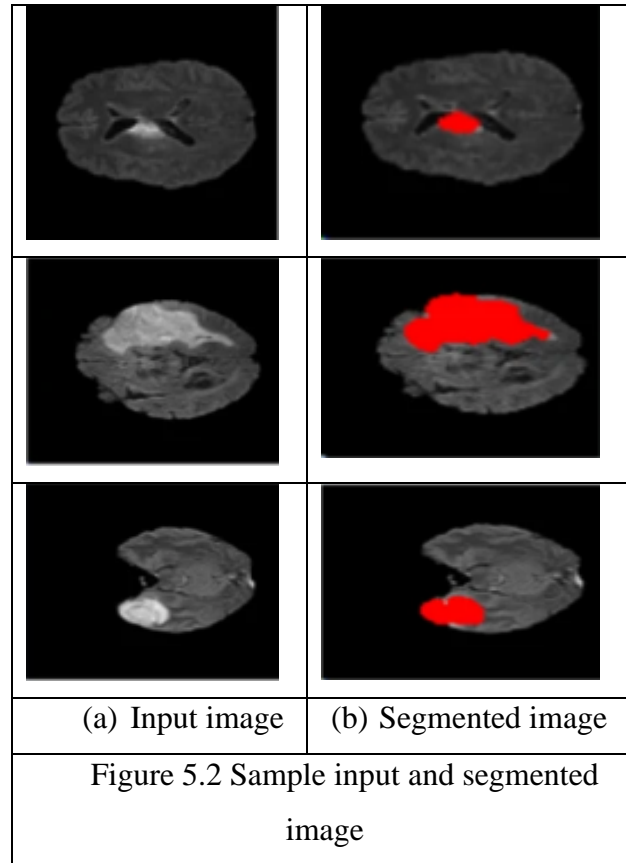
5.4.2 Performance Matrices

Accuracy: The use of accuracy is required for calculating the rate of correctly classifying malignancies.

$$\text{Accuracy} = \frac{(TP + TN)}{(TP + TN) + (FP + FN)} \times 100 \quad (5.11)$$

Sensitivity: A method's sensitivity is measured using sensitivity, as well as the rate at which tumor is discovered.

$$\text{Sensitivity} = \frac{(TP)}{(TP + FN)} \times 100 \quad (5.12)$$



Specificity: The ratio of true negatives (TN) to true positives (TP) is known as specificity.

$$Specificity = \frac{(TN)}{(TN + FP)} \times 100 \quad (5.13)$$

Precision: The term "precision" refers to the number of digits that are used to signify a certain value.

$$Precision = \frac{(TP)}{(TP + FP)} \times 100 \quad (5.14)$$

Figures 5.2 to 5.3 depict the results and comparative performance of the proposed method. Figure 5.2 presents the sample input (a) and the segmented input image (b), while Table 5.4 summarizes the comparative performance of the proposed method. Additionally, Figure 5.3 displays the comparative accuracy, Figure 5.4 presents the comparative precision.

Table 5.4 Performance Evaluation of the Proposed Method

Performance	CNN [3]	SVM [4]	KELM [11]	RESNET-18 [12]	This work
Accuracy	98.04 %	95.81 %	93.68 %	98.0 %	99.87 %
Sensitivity	96.89 %	91.93 %	-	-	99.58 %
Specificity	98.55 %	96.13 %	-	-	98.96 %
Precision	95.27 %	93.5 %	94.5 %	98.3 %	98.75 %

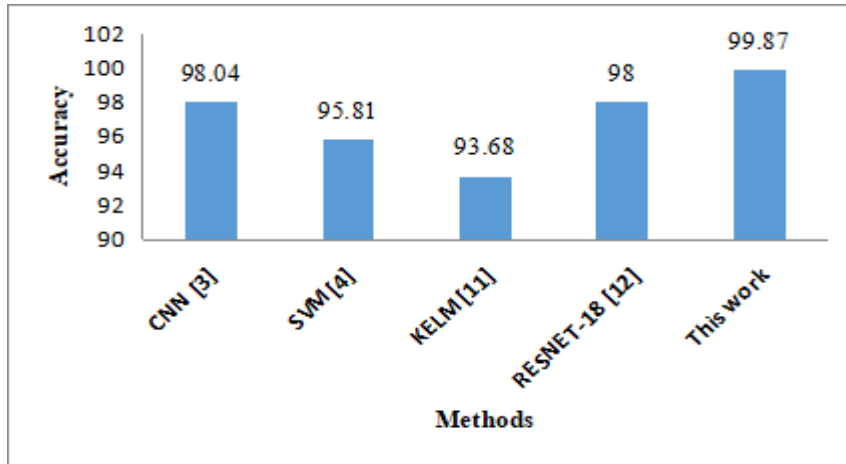


Figure 5.3. Comparative accuracy of proposed method

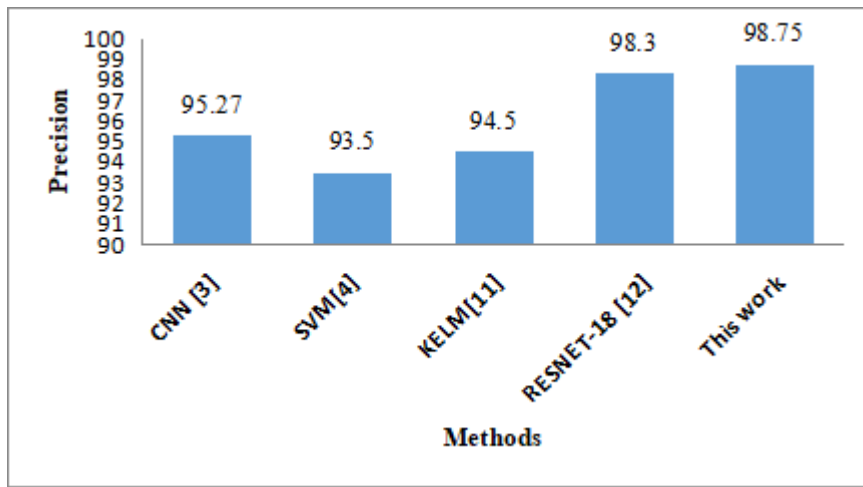


Figure 5. 4. Comparative precision of proposed method

5.5. Conclusion

The primary objective of this study is to provide a method for the classification of brain tumor that is both accurate and effective, despite its relatively simple nature. In the traditional method of brain tumor classification, U-Net based segmentation, ELM-based extraction of texture and shape features and ELM-based classification are all carried out. The classifications findings are shown as either normal brain images or tumor images. ELM is a deep learning approach that involves a series of feed forward layers. The Image BraTS 2020 database is used in order to classify images. During implementation of our pre-trained models, only the top layer undergoes training. This model got the accuracy is 99.87%, sensitivity is 99.58%, specificity is 98.96, and precision is 98.75.

CHAPTER 6

TUMOR CLASSIFICATION via GOOGLNET and EXTREME LEARNING MACHINE (ELM) UTILIZING MULTIPLE FEATURES

6.1 INTRODUCTION

Brain tumors are currently the most dangerous illness in the world. Tumors can damage healthy brain tissue or elevate intracranial pressure, affecting the brain. So, a tumor cell's fast development might result in death. Thus, early brain tumor diagnosis is more important since it might spare the patient from negative consequences. A common imaging method for evaluating these cancers is Magnetic Resonance Imaging (MRI). A brain tumor is sometimes called intracranial cancer when abnormal cell development occurs in the brain tissues. In the United States (US), there were anticipated to be 23,820 new instances of brain tumors and 17,760 expected fatalities from the disease. Twenty-four thousand five hundred thirty incidences of brain tumors have been anticipated in the US, including 13,840 males and 10,690 women, according to 2021 cancer data. Primary and secondary (metastatic) brain tumors are the two types of brain cancers. A primary tumor has not metastasized to other organs. Malignant brain tumors, even if they are not situated in critical brain regions, still pose a grave threat due to their rapid development, atypical characteristics, and potential to metastasize to other parts of the brain. The utilization of MRI proves highly advantageous in the detection of brain cancer. The contrast-enhanced core is observable across multiple MRI sequences, including T2, T2-Fluid Attenuated Inversion Recovery (FLAIR), and T1, T1 + gadolinium. These sequences unveil distinct tumor components like edema, necrosis, and the contrast-enhanced core. Brain tumors are typically diagnosed through imaging techniques such as Positron Emission Tomography (PET), Computed Tomography (CT), and MRI. CT imaging relies on the distinct radiation properties of different tissues, employing radioactive rays to penetrate the human body. On the other hand, PET involves the injection of radioactive agents into the body, which circulate through the bloodstream, reaching all cells, tissues, and organs.

Manual segmentation of MRIs is a laborious and challenging task, primarily due to the multi-modality and voluminous nature of 3D images. Additionally, the subjective

experiences of the individuals performing manual segmentation can introduce errors into the process. Consequently, there is a significant demand for automated and precise methods to segment brain tumors. These automated techniques are sought after for several reasons. Firstly, brain tumors come in diverse shapes and internal structures. Secondly, the wide array of appearances in surrounding normal tissues, attributable to the varying positions of tumors and the associated tumor bulk effects, adds complexity. Thirdly, the boundaries between normal and malignant tissues often lack clarity, posing a challenge in their differentiation.

Brain MRI images are favored for applications relying on the depiction of soft brain tissues due to their superior contrast compared to Computed Tomography (CT) images, which are less suitable for this purpose. Computer-Aided Design (CAD) systems frequently incorporate machine learning methods to detect and classify brain tumors. Various approaches for feature extraction have been put forth in this context. Subsequently, brain tumors are identified and categorized by employing structured form models and the collected data. Nevertheless, these systems often make an assumption of independence among the essential components of MRI images, a simplification aimed at managing the computational complexity of the task.

CNNs offer a significant advantage by autonomously learning essential image characteristics. This capability proves particularly invaluable in tumor segmentation tasks. In the latest iterations of the multimodal BRATS competition, CNN-based techniques consistently outperformed other methods in all four rounds. Many machine learning-based segmentation approaches predominantly rely on images that have undergone manual segmentation. Manual segmentation, especially in the context of medical imaging, is both time-consuming and demanding in terms of the required medical expertise. Given that the imaging intensity of malignant tissues often closely resembles that of surrounding healthy or diseased tissues in magnetic resonance imaging or computed tomography scans, achieving precise tumor delineation becomes a challenging and subjectivity-prone endeavor. This study introduces an innovative approach for brain tumor segmentation utilizing a single GoogLeNet model. Initially, the process involves tumor image classification, which employs multiple-feature extraction

in conjunction with an ELM classifier. Subsequently, the segmentation task separates the image into three distinct regions: the core, enhancing tumor, and non-enhancing tumor regions. The primary advantage of this approach lies in its ability to employ a single GoogLeNet model to segment three different regions within a classified image. The performance of both the classification and segmentation processes is assessed using sensitivity evaluation techniques. To determine whether the suggested method is effective, the BRATS2020 dataset serves as the reference dataset.

This study introduces an advanced approach for precise tumor classification through the utilization of Extreme Learning Machine (ELM), coupled with region segmentation in classified images using GoogLeNet. Initially, the image classification phase employs an ELM classifier, allowing for the classification of images into three distinct groups: 1. Core, 2. Enhancing Tumor, and 3. Non-Enhancing Tumor. Subsequently, GoogLeNet is leveraged to segment tumor images, specifically identifying core, enhancing, and non-enhancing regions. Notably, this technique demonstrates the capacity to decrease computational time while enhancing accuracy in comparison to traditional methods. The effectiveness of the approach is quantified through accuracy, sensitivity, and specificity calculations across various image sizes. Remarkably, this endeavor achieved an impressive average accuracy of 99.5%, a notable improvement over conventional classification and segmentation methods.

The main objectives of this work are as follows:

- To progress the detection performance of accuracy by using more training with multiple higher priority features with optimized training parameters
- To perform multiple tumor regions of classified images with high accuracy.
- To reduce the computational complexity of the classifier by choosing optimized training parameters.

6.2 PROPOSED METHOD

6.2.1 Block diagram

Figure 6.1 depicts the comprehensive framework outlining the suggested approach for brain tumor classification through ELM and subsequent segmentation utilizing

GoogLeNet. The process initiates with image preprocessing, encompassing operations such as image normalization, smoothing, and contrast enhancement. Image normalization is grounded in the range of minimum and maximum pixel values. Notably, the normalization process employs the mean value derived from the image matrix for its execution. Following the normalization step, the images undergo smoothing through Wiener smoothing. Subsequently, the preprocessing advances to the application of the Fuzzy C Means (FCM) technique on the smoothed image to execute the segmentation process. Moving forward, the process involves feature extraction to capture a range of features encompassing statistical, shape, texture, and Gray-Level Co-Occurrence Matrix (GLCM) attributes. This feature-rich data is then subjected to classification using the Extreme Learning Machine (ELM), allowing differentiation between normal, malignant, and benign types. Subsequent to the classification, the classified images are subjected to training using GoogLeNet to discern and analyze core, enhancing, and non-enhancing tumor regions.

6.2.2 Normalization

The data within all four columns of the datasets cover a wide range from significantly positive to significantly negative values. In this study, Minmax normalization is employed to confine these values within the range of 0 to 1. This normalization technique preserves the linear relationship of the features. The formula depicting Minmax normalization is as follows.

$$N = \frac{n_j - \text{mini}}{\text{maxi} - \text{mini}} \quad (6.1)$$

Here, mini signifies the smallest value of the attribute, and maxi denotes its maximum value

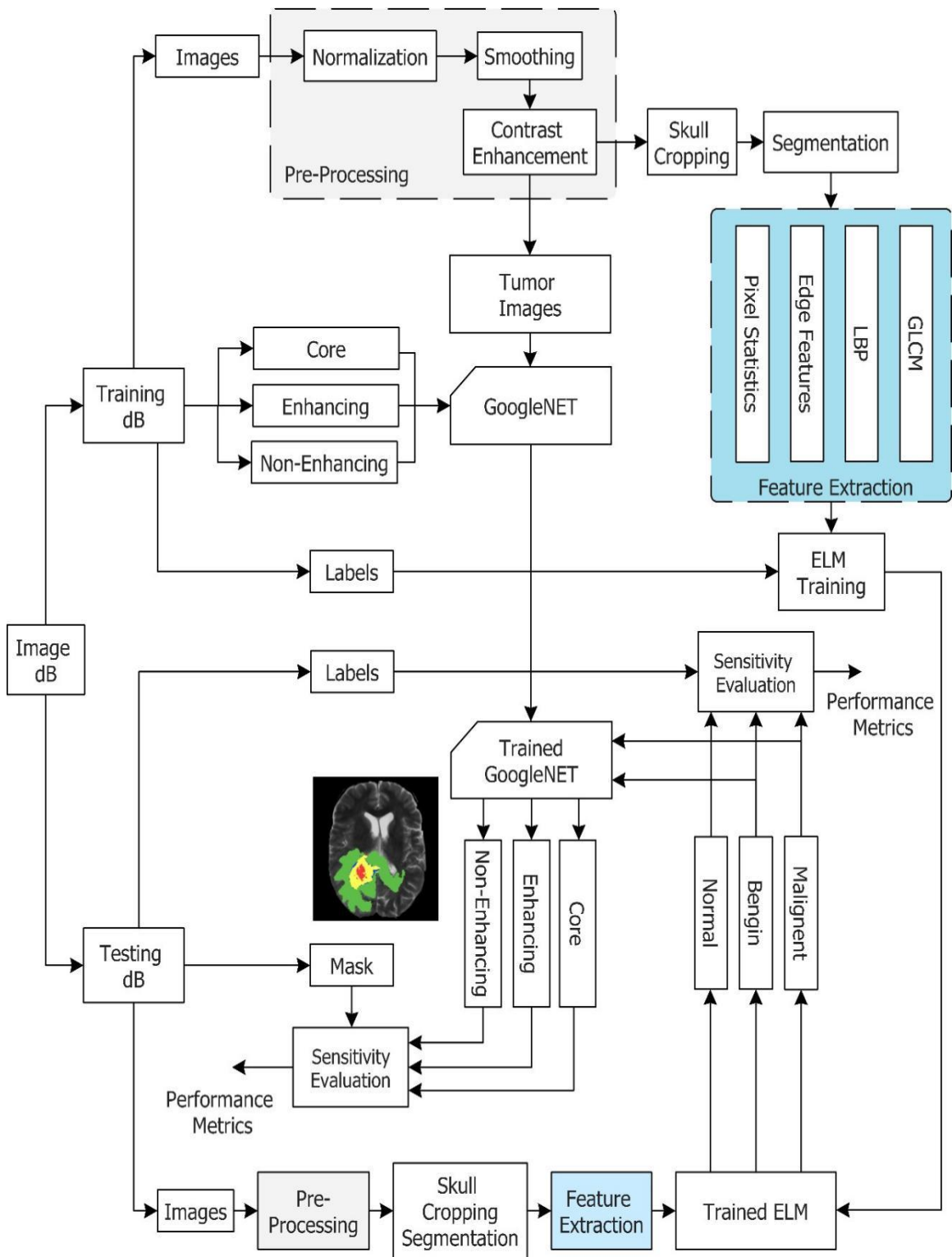


Figure 6.1 Block diagram of the proposed method of brain tumor classification and segmentation techniques

6.2.3 Image smoothing

In this study, the Wiener filter is employed to eliminate noise from the normalized images. The Wiener filter is known for its ability to reduce noise while retaining the essential interior features of an image, albeit at the cost of slightly softening its sharp edges. To achieve this, a reconstruction computation is created for each type of corruption, addressing them one at a time, and then these reconstructions are combined. The Wiener filter strikes a favorable balance between noise reduction and preservation of the underlying structure. It achieves this by simultaneously adjusting the filtering and reducing the additional signal amplitude. In essence, the Wiener filter is particularly effective in managing mean square error and operates on a stochastic foundation.

$$w_x = \frac{w_y - w_n}{|H|^2} \quad (6.2)$$

The power spectrum w_y can be estimated directly from the observation using the periodogram estimate. H is the blurring filter.

6.2.4 Contrast Enhancement

The Contrast Limited Adaptive Histogram Equalization (CLAHE) stands as a frequently employed algorithm for enhancing low-contrast medical images, significantly advancing the quality of medical imagery. Upon segmenting the MRI image into $N \times N$ sub-blocks, the histogram of each image block is computed. Subsequently, a clipping limit is defined as a threshold for the sub-blocks. By adjusting the clipping limit setting, the contrast of local image sub-blocks can be intensified. However, this adjustment is constrained to ensure that the histogram alteration does not surpass the specified clipping limit. This process aligns with a mathematical representation of a uniform distribution.

$$x = [x_{max} - x_{min}] * p(f) + x_{min} \quad (6.3)$$

6.2.5 Edge Sharpening

Most of the image's essential structural information is concentrated within its edges. Enhancing an image sharpness and clarity can be achieved by identifying these edges within the image and then utilizing this information to enhance the regions of the image that contain these edges. This study introduces an adapted Sobel edge detection technique that focuses on sharp edges. Before detecting the image's edges, it is important to

eliminate any extraneous pixels from the data. Additionally, reducing noise in the image can be achieved by applying a Gaussian filter. Subsequently, a suitable mask is chosen and convolved with the image to perform edge detection.

6.2.6 GLCM

GLCM, which stands for Gray-Level Co-Occurrence Matrix, is an alternate term used to describe the gray-level spatial dependency matrix. Among its numerous applications, texture analysis is a notable one, with a strong track record in the domain of medical image analysis. This technique mandates the quantization of image data. In this context, each sample is interpreted as a pixel within an image, and its value corresponds to the intensity of that pixel. The process involves constructing the GLCM itself, followed by the selection of a specific feature of interest. The computed value of this chosen feature then replaces the sample's within the resulting virtual variable. When presented with a grayscale image I , the co-occurrence matrix determines the frequency with which a pair of pixels with a certain value and offset appears in the image. It is parameterized by an offset $(\Delta a, \Delta b)$ as:

$$C_{\Delta a, \Delta b}(i, j) = \sum_{a=1}^p \sum_{b=1}^q \begin{cases} 1, & \text{if } I(a, b) = i \text{ and } I(a + \Delta a, b, \Delta b) = j \\ 0, & \text{otherwise} \end{cases} \quad (6.4)$$

Where x and y are the image's spatial coordinates and I and j are the pixel values; the offsets, $(\Delta a, \Delta b)$ define the spatial relation for which this matrix is calculated; and I indicates the pixel value at pixel (a, b) .

6.2.7 Features of GLCM

Contrast

Contrast is indeed determined by the discrepancy between the highest and lowest intensity values present in an image. However, the formula mentioned earlier, $\sum_{(i,j=0)}^{(\text{level}-1)} P(i,j)(i-j)^2$ is utilized to compute the variance of contrast as a texture characteristic derived from the Gray-Level Co-Occurrence Matrix (GLCM) For computing the average contrast of an image, the following formula is typically employed

$$\text{Average Contrast} = \frac{\text{Max Intensity} + \text{Min Intensity}}{\text{Max Intensity} - \text{Min Intensity}}$$

In this equation:

- Max Intensity represents the highest intensity value detected within the image.
- Min Intensity corresponds to the lowest intensity value found in the image.

This formula yields a standardized measurement of contrast, considering both the scope of intensity values and their distribution throughout the image. The outcome typically falls within the range of -1 to 1, where elevated values indicate more pronounced contrast.

Dissimilarity

The average dissimilarity of an image refers to the absolute difference between consecutive pixels. This value can be computed using the following formula.

$$\sum_{i,j=0}^{\text{level}-1} P_{i,j} |i - j| \quad (6.5)$$

Homogeneity

An image is considered homogeneous when all the pixels within it have the same color. Conversely, if there are noticeable contrasts present within the image, it is categorized as inhomogeneous. In the most basic scenario, the standard deviation of each pixel from the mean gray value can be determined using the following equations.

$$\sum_{i,j=0}^{\text{level}-1} \frac{P_{i,j}}{1+(i-j)^2} \quad (6.6)$$

ASM (Angular Second Moment)

Angular Second Moment (ASM) is a measure that signifies the uniformity of the gray level distribution within an image. The calculation of ASM involves the following formula.

$$\sum_{i,j=0}^{\text{level}-1} P_{i,j}^2 \quad (6.7)$$

Energy

Energy is derived from the square root of ASM. The provided formula pertains to the probability, which is essentially the normalized histogram of color intensity at a specific position. Here, N represents the gray level, often corresponding to 256 in standard grayscale images.

$$\sqrt{\text{ASM}} \quad (6.8)$$

Correlation

Correlation is a mathematical method used to assess the degree of relationship between two entities. In the context of Digital Image Processing, it is employed to calculate the output of a mask applied to an image. The process involves sliding a mask over a matrix from left to right, shifting by one unit with each step.

$$\sum_{i,j=0}^{\text{level}-1} P_{i,j} \left[\frac{(i-\mu_i)(j-\mu_j)}{\sqrt{(\sigma_i^2)(\sigma_j^2)}} \right] \quad (6.9)$$

6.2.8 Statistical Feature Extraction

Standard Deviation (SD)

The standard deviation, denoted as σ , quantifies the extent to which data points are spread out from the mean. A smaller standard deviation suggests that the data is closely concentrated around the mean, while a larger standard deviation indicates that the data is more widely distributed

$$s = \sqrt{\frac{1}{N-1} \sum_{i=1}^N (x_i - \bar{x})^2} \quad (6.10)$$

Mean

The mean value is obtained by dividing the sum of pixel values by the total number of pixels. A way to gauge the relative intensity of an image is by considering its brightness, which is represented by the mean pixel intensity. This comparison can help assess how bright the image appears in relation to another image

$$\bar{x} = \frac{1}{n} (\sum_{i=1}^n x_i) = \frac{x_1 + x_2 + \dots + x_n}{n} \quad (6.11)$$

Kurtosis

Kurtosis is a metric used to determine if the data distribution has heavy tails or light tails compared to a normal distribution. High kurtosis values indicate the presence of heavy tails or outliers in the dataset. Conversely, low kurtosis values suggest light tails or a scarcity of outliers in the data.

$$\text{Kurtosis}[X] = E \left[\left(\frac{X-\mu}{\sigma} \right)^4 \right] = \frac{E[(X-\mu)^4]}{(E[(X-\mu)^2])^2} = \frac{\mu_4}{\sigma^4} \quad (6.12)$$

Skewness

Skewness is a numerical measure that quantifies the degree of asymmetry in a distribution. When the left and right sides of a distribution are not symmetrical, the distribution is said to be skewed. Skewness can take three forms: right (positive), left (negative), or zero, indicating the absence of skewness.

$$\tilde{\mu}_3 = E \left[\left(\frac{X-\mu}{\sigma} \right)^3 \right] = \frac{\mu_3}{\sigma^3} = \frac{E[(X-\mu)^3]}{(E[(X-\mu)^2])^{3/2}} = \frac{k_3}{k_2^{3/2}} \quad (6.13)$$

Moment

The moment invariant is a method employed for feature extraction, specifically to derive global features for shape recognition and identification analysis. Over time, various types of moment invariant techniques have been developed and applied for this purpose.

$$\mu_n = \int_{-\infty}^{\infty} (x - c)^n f(x) dx \quad (6.14)$$

Energy

Energy represents the square root of Angular Second Moment (ASM). The equation mentioned pertains to the probability of normalized histogram values for color intensity at a specific position. The parameter "N" signifies the gray level, such as 256 in the case of typical grayscale images.

$$EG = \sum_i^{N_G} \sum_j^{N_G} \{p(i,j)\}^2 \quad (6.15)$$

Entropy (EN)

For a GLCM matrix with irregular patterns, the Entropy (EN), a metric of unpredictability, takes on its lowest value. The coefficient EN is defined by the following equation:

$$EN = - \sum_i^{N_G} \sum_j^{N_G} p(i,j) \log(p(i,j)) \quad (6.16)$$

Inertia (IN)

The Intensity Variance (IN), also referred to as the Contrast feature, quantifies the image's contrast or the presence of local fluctuations within the image, providing insight into the texture quality. The following equation defines this parameter:

$$IN = - \sum_i^{N_G} \sum_j^{N_G} (i - j)^2 p(i, j) \quad (6.17)$$

Correlation (CO)

The term correlation (CO) metric evaluates the linear correlation between elements in the GLCM or indicates the interdependencies between the rows and columns of the co-occurrence matrix. The mathematical expression defining this parameter is as follows:

$$CO = \frac{\sum_i^{N_G} \sum_j^{N_G} (i - \mu_x)(j - \mu_y) p(i, j)}{\sigma_x \sigma_y} \quad (6.18)$$

Where μ_x , μ_y , σ_x , and σ_y are the means and standers deviations of $p_x p_y$

Inverse Difference Moment (IDM)

Homogeneity, alternatively referred to as inverse difference moment, quantifies the compactness of the distribution of elements within the co-occurrence matrix and its diagonal elements. The calculation of homogeneity is expressed as follows: (20.4). Moreover, correlation serves as an indicator of linear relationships present within the image.

$$\text{IDM is written as:} \quad \text{idm} = \sum_i^{N_G} \sum_j^{N_G} \frac{1}{1+(i-j)^2} p(i, j) \quad (6.19)$$

Difference Entropy (DE)

Difference entropy is particularly useful in applications like texture analysis in images or feature extraction from audio signals, where understanding the variations or transitions between adjacent elements is important.

$$DE = - \sum_{k=0}^{N_G-1} P_{x-y}(k) \log_2 P_{x-y}(k) \quad (6.20)$$

Local Binary Patterns (LBP)

LBP, or Local Binary Pattern, is a visual descriptor commonly utilized in computer vision to characterize objects. Typically applied in grayscale images, the LBP operator processes each pixel with a specific code. In the proposed system, the LBP operator is adapted for color images, implying that the individual R, G, and B components of the image are extracted, organized into a matrix, and then subjected to the LBP operator independently. This texture operator represents a local region by forming a binary pattern through thresholding the differences between the center pixel and its neighboring pixels.

However, in the proposed approach, color images introduce new challenges. As the LBPs are aggregated into a single histogram, the spatial relationships between them are often disregarded. To address this limitation, enhancements have been made to the LBP histogram feature, integrating information about the co-occurrence among the LBPs. This augmentation enables a more comprehensive analysis of the spatial correlations present among the LBPs within the image.

$$L(x_c, y_c) = \sum_{n=0}^7 2^n g(I_n - I(x_c, y_c)) \quad (6.21)$$

In the LBP computation, (x_c, y_c) denotes the LBP value at the center pixel coordinates (x_c, y_c) , while $I(x_c, y_c)$ represent the intensity value of the center pixel. Additionally, the function $g(x)$ is defined as zero if $x < 0$, and $g(x) = 1$ if $x \geq 0$. For instance, consider selecting 54 as the threshold value for the center pixel. When the neighboring pixel values are below this threshold, they are set to 0. Conversely, if the neighboring pixel values are greater than or equal to the threshold, they are assigned a value of 1. The LBP value is determined through scalar multiplication of these two values. The weight and binary matrices are then combined to calculate the LBP value.

6.2.9 Google Net

The research paper titled "Going Deeper with Convolutions," published in 2014, introduced the Google Net architecture, also known as Inception V1. This endeavor was a collaborative venture involving Google researchers and several universities. The architecture gained prominence by securing the top position in the 2014 image classification competition. In the Inception V1 design, innovative strategies were employed, including the utilization of global average pooling and 1x1 convolutions. Central to the architecture is the Inception module, a pivotal element situated in the middle of the overall structure. This module employs various techniques to create a more intricate and efficient architecture. Notably, it incorporates methods such as global average pooling and 1x1 convolutions. The architecture's layout and key constituents are depicted in Figure 6.2, providing an overview of the Google Net's design. This section provides an in-depth exploration of several of these architectural techniques that contribute to the model's robust and high-performing nature.

1x1 convolution:

The concept of employing 1x1 convolutions is a unique and defining aspect of the inception architecture. The integration of these convolutions serves the specific purpose of reducing the total number of parameters within the architecture. Through the strategic use of 1x1 convolutions, the inception architecture achieves an increased depth while concurrently minimizing the overall parameter count. This deliberate incorporation of 1x1 convolutions significantly enhances the architecture's depth and its ability to handle intricate tasks, all while ensuring computational efficiency and optimized performance.

Global Average Pooling:

A notable fraction of parameters within different architectures, often responsible for driving up computational costs, is concentrated in these fully connected layers. As the network approaches its final stages, the GoogLeNet design introduces a technique called global average pooling. This layer functions by computing the average of a seven-by-seven feature map, resulting in a compressed one-by-one size representation. By employing global average pooling in this manner, the architecture achieves dual benefits: it reduces the dimensions of the data while still preserving critical information. This strategic implementation of global average pooling serves to optimize the architecture's efficiency by curbing complexity and mitigating computational demands during the latter phases of processing.

Inception Module:

The inception module distinguishes itself as a novel and distinct feature in contrast to preceding network architectures. This system employs a predetermined convolution size for each layer. Within the inception module, the outcomes of the 1x1, 3x3, and 5x5 convolutions, as well as the 3x3 max pooling operations, are concurrently processed. This parallel processing approach facilitates the extraction of features across various scales and dimensions. By harnessing this innovative method of parallel processing within the inception module, the architecture adeptly captures a wide spectrum of features and patterns from the input data. This capability enhances the network's capacity to comprehend and represent intricate relationships inherent in the data.

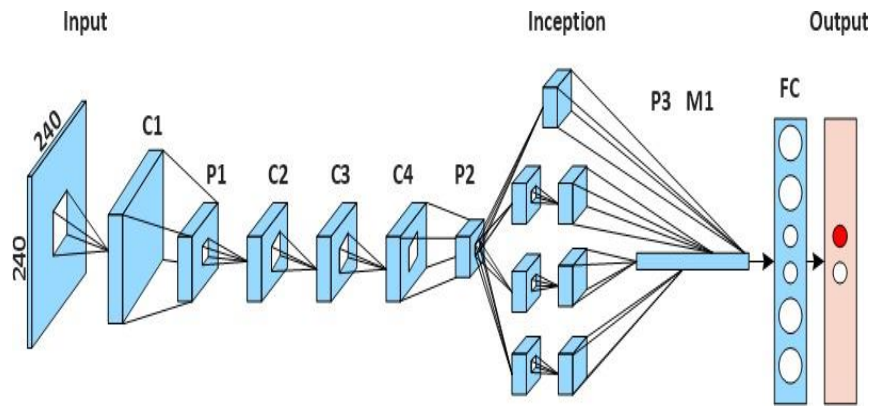


Figure 6.2 Architecture of GoogLeNet [Zhiling Guo et.al. (2017)]

6.3 Extreme Learning Machine

ELM offers several advantages, including rapid and efficient learning, strong generalization capabilities, a swift convergence rate, and straightforward implementation. Its variants are commonly applied in sequential, batch, and incremental learning scenarios. Unlike conventional learning algorithms, ELM's primary objective is to enhance generalization performance by achieving minimal output weight norms and minimizing training errors.

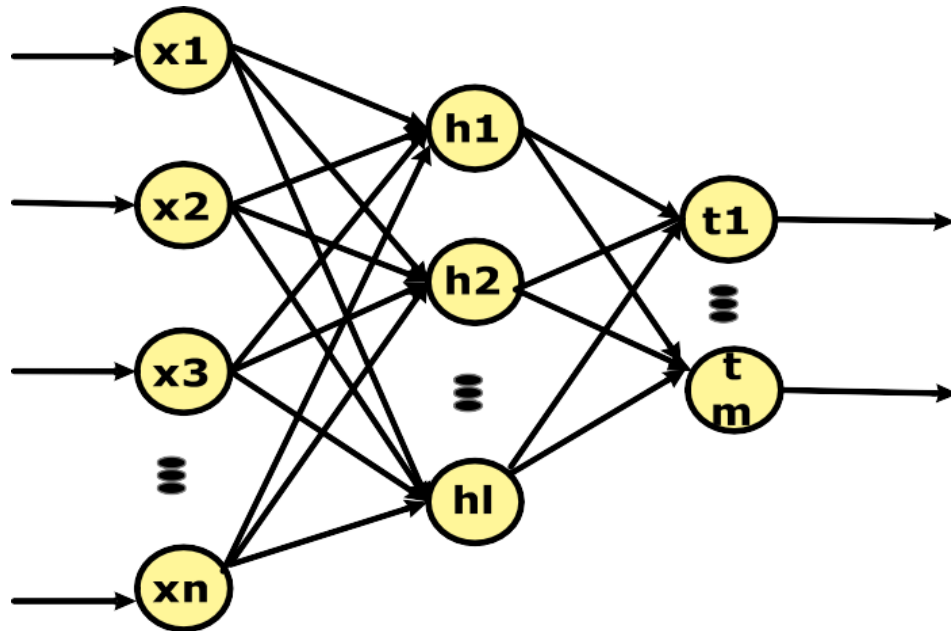


Figure 6.3 Architecture of ELM [Fan Zhang et.al. (2019)]

Prior to computing the output layer's weights, ELM employs a random adjustment of biases and weights within the input layer. This technique not only yields improved performance but also accelerates the learning process compared to conventional neural network algorithms. The architecture of ELM is depicted in Figure 6.3.

$$f_L(x) = \sum_{i=1}^L \beta_i h_i(x) = h(x)\beta \quad (6.22)$$

$$\text{Sigmoid Function: } G(a, b, x) = \frac{1}{1 + \exp(-(a \cdot x + b))} \quad (6.23)$$

Here, since the input layer to the hidden layer, x is an input sample, a is the value of the weight and b is the bias value. Minimized: $\|H\beta - T\|^2$ and $\|\beta\|$ where H is the hidden layer output matrix;

$$\begin{bmatrix} h_1(x_1) & \dots & h_L(x_1) \\ \vdots & \ddots & \vdots \\ h_1(x_N) & \dots & h_L(x_N) \end{bmatrix} \quad (6.24)$$

$$\beta = H^\dagger T$$

In this scenario, T represents the tag matrix, and H^\dagger stands for the inverse of the Moore-Penrose generalized hidden layer output matrix. The matrix H is formed by concatenating the transposed hidden layer outputs for the training samples, denoted as $H = [h^T(x_1), \dots, h^T(x_N)]^T$, where N is the total number of training samples. To enhance the robustness and generalization capacity of the ELM, the optimization process incorporates a regularization coefficient denoted as C . Consequently, when K kernels are involved, the weight set is determined as follows:

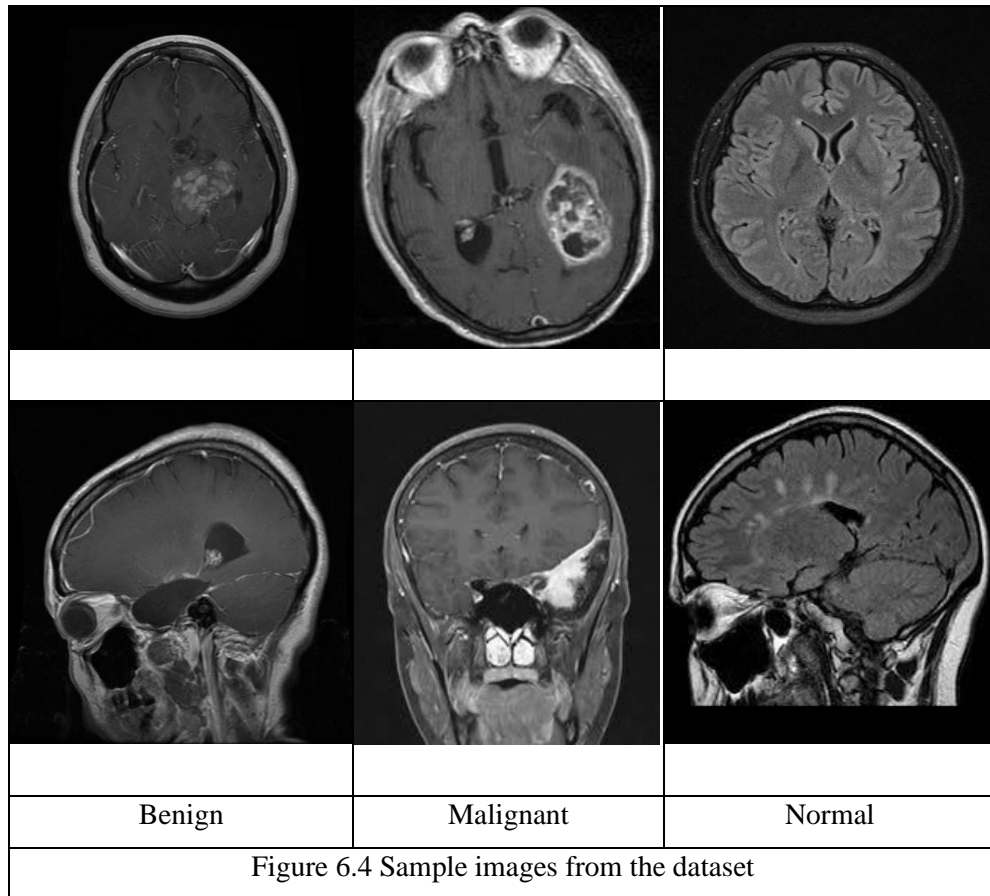
$$\beta = \left(\frac{I}{C} + K\right)^{-1} T \quad (6.25)$$

The system was modeled using kernels incorporating linear, polynomial, and radial basis functions. After careful evaluation, it was established that the radial basis function (RBF) kernel yielded the most favorable outcomes. Hence, the study employed the RBF kernel. Moving on to the final phase of our endeavor, which is classification, a tenfold cross-validation approach was employed in the classification process.

6.4 RESULTS AND DISCUSSIONS

6.4.1 Dataset

The brain tumor dataset comprises a total of 1426 slices of glioma, 708 slices of meningioma, and 3064 slices of pituitary tumors, collectively amounting to 233 patients with distinct brain tumor types. The dataset encompasses 930 slices, covering the three tumor forms. Additionally, the dataset offers 5-fold cross-validation indices for assessment purposes. Figure 6.4 provides a visual representation of sample images extracted from the dataset.



6.4.2 Performance Metrics

In accordance with the previously stated definition, accuracy represents a composite measure encompassing various forms of observational errors. Thus, achieving a heightened accuracy necessitates a concurrent emphasis on both precision and trueness.

The formula for calculating accuracy is as follows:

$$Accuracy = \frac{TP + TN}{TP + TN + FP + FN} \quad (6.26)$$

Where TP = True positive; FP = False positive; TN = True negative; FN = False negative

The ability of a test to accurately distinguish between individuals with and without the condition is denoted as its sensitivity (Se). It is often colloquially known as the True Positive Rate (TPR). This can be mathematically expressed as:

$$Sensitivity = \frac{TP}{TP + FN} \quad (6.27)$$

Where TP = True Positives, FN = Number of False Negatives

Specificity refers to the ability of a test to accurately classify individuals who do not have the specific condition. It quantifies the probability that a patient is indeed without the disorder (Sp). At times, it is also referred to as the True Negative Rate (TNR).

$$Specificity = \frac{TN}{TN + FP} \quad (6.28)$$

The Precision (Pr) is calculated as:

$$Precision = \frac{TP}{TP + FP} \quad (6.29)$$

Where, TP=True Positive; FP=False Positive.

6.5 Results Analysis

The parallel and vertical histogram is shown in Figure 6.5. Histogram of the images of the brain tumor's horizontal and vertical axes. Since the kurtosis for the Gaussian distribution is 3, the wavelet transform coefficients are strongly non-Gaussian.

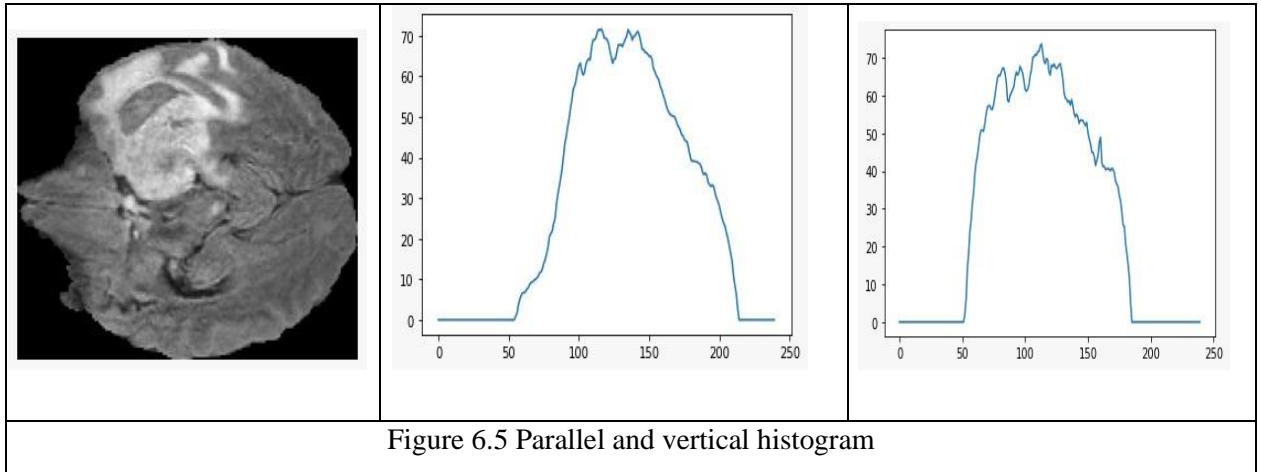


Table 6.1 Performance of Proposed Method with existing methods

Performance	Benign	Malignant	Normal
Accuracy %	0.97	0.99	0.96
Sensitivity %	0.98	0.98	0.97
Specificity %	0.98	0.97	0.97
Precision %	0.99	0.93	0.99

Table 6.1 illustrates the performance outcomes of the proposed method. For the classification of benign tumors, an accuracy of 0.97, sensitivity of 0.98, specificity of 0.98, and precision of 0.99 were achieved. In the case of malignant tumors, the accuracy reached 0.99, sensitivity was 0.98, specificity reached 0.97, and precision achieved 0.99. Lastly, normal tumors achieved an accuracy of 0.96, sensitivity of 0.97, specificity of 0.97, and precision of 0.99.

Table 6.2 Performance of Proposed Method with existing methods

Method	Accuracy %			Specificity %			Precision %		
	NET	Core	ET	NET	Core	ET	NET	Core	ET
VGG16 [82]	0.92	0.93	0.85	0.94	0.92	0.96	0.92	0.91	0.97
U-Net [83]	0.97	0.97	0.79	0.93	0.86	0.98	0.96	0.96	0.75
CNN-M-SVM	0.86	0.75	0.71	0.96	0.96	0.95	0.95	0.86	0.79

[84]									
Deep CNN [85]	0.79	0.73	0.83	0.87	0.93	0.93	0.75	0.94	0.87
This work	0.99	0.94	0.88	0.98	0.98	0.95	0.97	0.97	0.99

Table 6.2 presents a comparison between the performance of the suggested method and existing methods. The accuracy performance in comparison to the current approaches is depicted in Figure 6.6 the comparison of specificity's performance with previous techniques can be observed in Figure 6.7 Furthermore; Figure 6.8 illustrates the comparison of precision performance with those of existing techniques. To provide insight into the suggested technique's outcomes, the confusion matrix is presented in Figure 6.9.

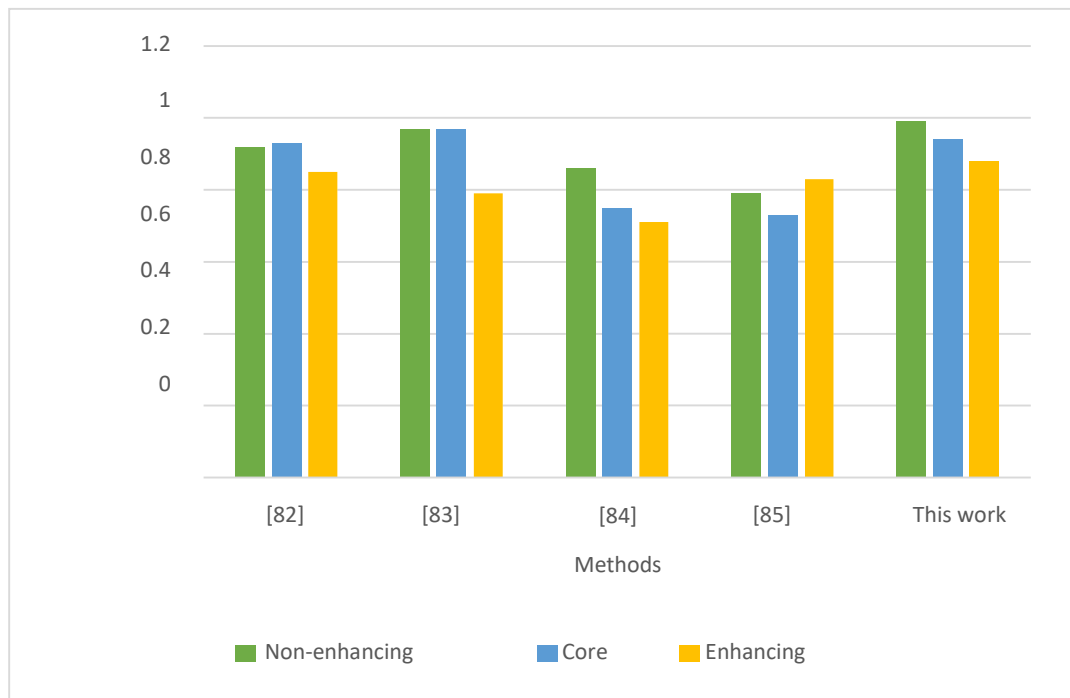


Figure 6.6 Comparative performance of accuracy with existing methods

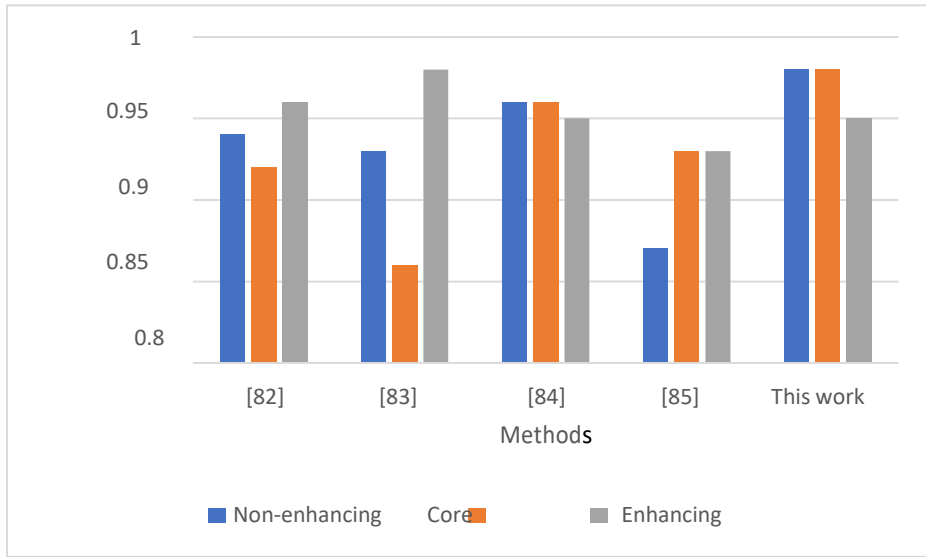


Figure 6.7 Comparative performance of specificity with existing methods

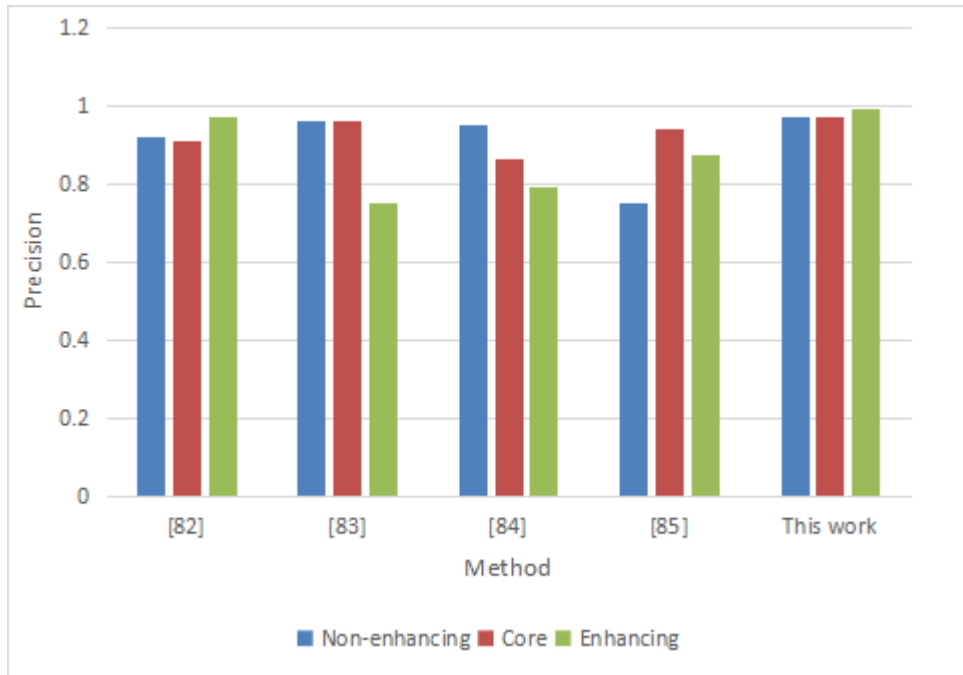


Figure 6.8 Comparative performance of precision with existing methods

	Normal	Benign	Malignant
Normal	35200	300	965
Benign	1520	28500	1002
Malignant	153	135	35050

Figure 6.9 Confusion Matrix for the Proposed Method

6.6 CONCLUSIONS

In this research introduces a novel methodology for brain tumor classification coupled with region segmentation. The approach involves the utilization of Google Net for brain tumor detection, where an ELM classifier performs image classification, and Google Net handles region segmentation. The process initiates with image normalization, followed by wiener smoothing to filter the images. Additionally, contrast enhancement is employed to enhance the image quality. The dataset is divided into three categories: benign, malignant, and normal, paving the way for subsequent tumor segmentation through the FCM technique. Feature extraction is executed, encompassing edge features, LBP, and pixel statistics. The trained Google Net is then employed to extract distinct regions: core, enhancing tumor, and non-enhancing tumor. The outcomes are promising, boasting an accuracy of 0.97, sensitivity of 0.98, specificity of 0.98, and precision of 0.99 for the benign stage. Likewise, the malignant stage demonstrates an accuracy of 0.99, sensitivity of 0.98, specificity of 0.97, and precision of 0.93. Finally, the normal stage showcases an accuracy of 0.96, sensitivity of 0.97, specificity of 0.97, and precision of 0.99.

CHAPTER 7

CONCLUSION AND FUTURE SCOPE

7.1 Conclusion

Brain tumor is one of the deadliest diseases and causes millions of new cases each year. There is an urgency to classify or resolve brain cancer in the early stage. The early diagnosis will increase the survival rate of the patient. With this motivation, the presented research work concentrates more on developing an automated brain tumor identification and detection module. Initially, the detailed literature review is carried out to get the knowledge of brain tumor and its detection framework modules. It was observed that most of the researchers suggested improving the current detection framework to make diagnosing automatic and to perform rapid operations. The important objective of this research work is to develop an efficient framework to diagnose the brain tumor using various filtering, segmentation, classification techniques. This work presents a robust approach to brain tumor region segmentation through the development and training of three distinct U-Net models, each targeting specific tumor regions. By integrating an improved adaptive gamma correction technique and utilizing the BraTS 2020 dataset for rigorous testing and validation, the proposed method achieves significant enhancements in training and testing accuracy. The segmentation process is further refined through sensitivity analysis and the use of an ELM classifier in conjunction with GoogLeNet for effective classification.

The systematic image processing steps, including normalization, filtering, and contrast enhancement, contribute to the overall success of the method, resulting in an impressive accuracy rate of 99.5%. This study not only advances the field of brain tumor detection but also lays the groundwork for future research in medical image analysis, emphasizing the importance of innovative techniques in improving diagnostic capabilities.

Using three U-Net models for different tumor regions adds complexity to the training process. Time is taking the process of training multiple models and requires significant computational resources. The technology majorly depends on BraTS2020 datasets for validation, which may limit its generalizability to other datasets. The performances on various MRI datasets with changing characteristics persist uncertain.

7.2 Future Scope

The UNET model's classification accuracy can be further improved by exploring various weight optimization techniques. This includes experimenting with different optimizers, learning rate schedules, and advanced techniques like automated hyper parameter tuning. Extending the work to incorporate a 3D active contour model could lead to significant improvements in segmenting complex structures like tumors in volumetric scans. Active contours in 3D can better capture the shape and boundaries of tumors by leveraging information from neighboring slices.

In future work could also apply the proposed segmentation method to other organ tumor regions, such as lung cancer in CT scans or liver tumors in MRIs. Each organ presents unique segmentation challenges, and the model could be fine-tuned or adapted to better handle these variations.

List of Publications

1. Ramu, B., Bansal, S. Highly accurate tumor region segmentation from magnetic resonance images using customized Convolutional neural networks. *Multimed Tools Appl* (2023). <https://doi.org/10.1007/s11042-023-15480-0> (Published in: SCI).
2. B. Ramu and S. Bansal, "A Novel Deep Learning Scheme for Brain Tumor Detection in Medical Images," 2023 4th International Conference on Smart Electronics and Communication (ICOSEC), Trichy, India, 2023, pp. 1616-1623, doi: 10.1109/ICOSEC58147.2023.10275827. (Published in: IEEE).
3. Dr. Navjot Rathour, B. Ramu (2021). A Study of Deep Learning-Based Brain Tumor Segmentation Strategies for MRI Image. *Annals of the Romanian Society for Cell Biology*, 25(6), 15460-15476 (Published in: Scopus).
4. Ramu, B., & Bansal, S., has given oral presentation on Accurate Brain Tumor Detection and Classification Using UNET and Extreme Learning Machine in the 4th International Conference on "Recent Advances in Fundamental and Applied Sciences" (RAFAS 2023) held on March 24-25, 2023 at Lovely Professional University, Punjab, India.

List of Papers Accepted and under process

5. B. Ramu, Sandeep Bansal, Accurate Detection and Classification of Brain Tumors using U-Net, Submitted a paper in 5th International Conference on Smart Electronics and Communication(ICOSEC 2024),held on 18th -20 september 2024, Organised by Kongunadu College of Engineering and Technology Trichy, Tamil Nadu, India (Presented a Paper in Conference publication under process: Scopus).
6. Ramu, B., Bansal, S. Accurate Brain Tumor Classification Using GoogleNet and Extreme Learning Machine With Multiple Features. *Multimed Tools Appl* (2024). (Under Review: SCI).

References

1. Pereira, S, Pinto, A, Alves, V & Silva, CA 2016, „Brain Tumor Segmentation Using Convolutional Neural Networks in MRI Images“, in IEEE Transactions on Medical Imaging, vol. 35, no. 5, pp. 1240-1251, doi: 10.1109/TMI.2016.2538465.
2. Heba Mohsen, El-Sayed A.El-Dahshan, El-Sayed M.El-Horbaty & Abdel-Badeeh M Salem 2018, “Classification using deep learning neural networks for brain tumors”, Future Computing and Informatics Journal, vol. 3, no. 1, pp. 68-71.
3. Hemanth, DJ, Anitha, J, Naaji, A, Geman, O, Popescu, DE & Hoang Son, L 2019, „A Modified Deep Convolutional Neural Network for Abnormal Brain Image Classification“, IEEE Access, vol. 7, pp. 4275- 4283.
4. Sultan, HH, Salem, NM & Al-Atabany, W 2019, „Multi-Classification of Brain Tumor Images Using Deep Neural Network“, IEEE Access, vol. 7, pp. 69215-69225, doi: 10.1109/ACCESS.2019.2919122
5. Kumar Mallick, P, Ryu, SH, Satapathy, SK, Mishra, S, Nguyen, GN & Tiwari, P 2019, „Brain MRI Image Classification for Cancer Detection Using Deep Wavelet Autoencoder-Based Deep Neural Network“, IEEE Access, vol. 7, pp. 46278-46287, doi: 10.1109/ACCESS.2019.2902252
6. Zar Nawab Khan Swati, Qinghua Zhao & Jianfeng Lu 2019, „Brain tumor classification for MR images using transfer learning and finetuning“, Computerized Medical Imaging and Graphics, vol. 75, pp. 34-46.
7. Navid Ghassemi, Afshin Shoeibi & Modjtaba Rouhani 2019, „Deep neural network with generative adversarial networks pre-training for brain tumor classification based on MR images“, Biomedical Signal Processing and Control, vol. 57, Art. no. 101678.
8. Huang, Z 2020, „Convolutional Neural Network Based on Complex Networks for Brain Tumor Image Classification With a Modified Activation Function“, IEEE Access, vol. 8, pp. 89281-89290, doi: 10.1109/ACCESS.2020.2993618.
9. Kaur, T, Saini, BS & Gupta, S 2018, „A novel feature selection method for brain tumor MR image classification based on the Fisher criterion and parameter-free

- Bat optimization", *Neural Comput & Applic*, vol. 29, pp. 193–206, <https://doi.org/10.1007/s00521-017-2869-z>.
10. Sharif, M, Tanvir, U & Munir, EU 2018, „Brain tumor segmentation and classification by improved binomial thresholding and multi-features selection“, *J Ambient Intell Human Comput* <https://doi.org/10.1007/s12652-018-1075-x>.
 11. Jude Hemanth, D & Anitha, J 2019, „Modified Genetic Algorithm approaches for classification of abnormal Magnetic Resonance Brain tumor images“, *Applied Soft Computing*, vol. 75, pp. 21-28.
 12. Narmatha, C, Eljack, SM & Tuka, AARM 2020, 'A hybrid fuzzy brainstorm optimization algorithm for the classification of brain tumor MRI images“, *J Ambient Intell Human Comput*, <https://doi.org/10.1007/s12652-020-02470-5>.
 13. Alhassan, AM & Zainon, WMNW 2020, „BAT Algorithm With fuzzy C-Ordered Means (BAFCOM) Clustering Segmentation and Enhanced Capsule Networks (ECN) for Brain Cancer MRI Images Classification“, *IEEE Access*, vol. 8, pp. 201741-201751, doi: 10.1109/ACCESS.2020.3035803.
 14. Amin Kabir Anaraki, Moosa Ayati & Foad Kazemi 2018, „Magnetic resonance imaging-based brain tumor grades classification and grading via convolutional neural networks and genetic algorithms“, *Biocybernetics and Biomedical Engineering*, vol. 39, no. 1, pp. 63-74.
 15. Kaur, T, Saini, BS & Gupta, S 2019, „An adaptive fuzzy K-nearest neighbor approach for MR brain tumor image classification using parameter free bat optimization algorithm“, *Multimedia Tools Appl*, vol. 78, pp. 21853–21890, <https://doi.org/10.1007/s11042-019-7498-3>.
 16. Mishra, S, Sahu, P & Senapati, MR 2019, „MASCA–PSO based LLRBFNN model and improved fast and robust FCM algorithm for detection and classification of brain tumor from MR image“, *Evol. Intel.*, vol. 12, pp. 647–663, <https://doi.org/10.1007/s12065-019-00266-x>.
 17. Sathish, P & Elango, NM 2020, „Gaussian hybrid fuzzy clustering and radial basis neural network for automatic brain tumor classification in MRI images“, *Evol. Intel.*, <https://doi.org/10.1007/s12065-020-00433-5>.

18. Sharan Kumar & Dattatreya P Mankame 2020, „Optimization driven Deep Convolution Neural Network for brain tumor classification“, *Biocybernetics and Biomedical Engineering*, vol. 40, no. 3, pp. 1190-1204.
19. Whitney E Muhlestein, Dallin S Akagi & Lola B Chambless 2017, “The Impact of Race on Discharge Disposition and Length of Hospitalization After Craniotomy for Brain Tumor”, *World Neurosurgery*, vol. 104, pp. 24-38.
20. Siva Raja, PM & Antony Viswasarani 2020, „Brain tumor classification using a hybrid deep autoencoder with Bayesian fuzzy clustering-based segmentation approach“, *Biocybernetics and Biomedical Engineering*, vol. 40, no. 1, pp. 440-453.
21. Arokia Jesu Prabhu, L & Jayachandran, A 2018, „Mixture Model Segmentation System for Parasagittal Meningioma brain Tumor Classification based on Hybrid Feature Vector“, *J Med Syst* vol. 42, pp. 251, <https://doi.org/10.1007/s10916-018-1094-3>.
22. Varuna Shree, N & Kumar, TNR 2018, „Identification and classification of brain tumor MRI images with feature extraction using DWT and probabilistic neural network“, *Brain Informatics*, vol. 5, no. 1, pp. 23–30.
23. Shrot, S, Salhov, M & Dvorski, N 2019, „Application of MR morphologic, diffusion tensor, and perfusion imaging in the classification of brain tumors using machine learning scheme“, *Neuro radiology*, vol. 61, pp. 757–765, 2019. <https://doi.org/10.1007/s00234-019-02195-z>.
24. Kalpana, R & Chandrasekar, P 2019, „An optimized technique for brain tumor classification and detection with radiation dosage calculation in MR image“, *Microprocessors and Microsystems*, vol. 72, Art. no. 102903.
25. Krishna Kumar, S & Manivannan, K 2020, „Effective segmentation and classification of brain tumor using rough K means algorithm and multi kernel SVM in MR images“, *J Ambient Intell Human Comput*, <https://doi.org/10.1007/s12652-020-02300-8>.

26. Zaka Ur Rehman, Sultan Zia, M & Kaleem Arshid 2020, „Texture based localization of a brain tumor from MR-images by using a machine learning approach“, *Medical Hypotheses*, vol. 141, Art. no. 109705.
27. Gokulalakshmi, A, Karthik, S & Karthikeyan, N 2020, “ICM-BTD: improved classification model for brain tumor diagnosis using discrete wavelet transform-based feature extraction and SVM classified”, *Soft Computing* vol. 24, pp. 18599–18609, <https://doi.org/10.1007/s00500-020-05096-z>.
28. Wang Guotai, Wenqi Li, Sébastien Ourselin, Tom Vercauteren (2018) Automatic brain tumor segmentation using cascaded anisotropic convolutional neural networks. In *Brainlesion: Third International Workshop*, Springer International Publishing pp 178–190.
29. Arif M, Ajesh F, Shamsudheen S, Geman O, Izdrui D, Vicoveanu D (2022) Brain tumour detection and classification by MRI using biologically inspired orthogonal wavelet transform and deep learning techniques. *J Healthc Eng* 2022:1–18
30. Berkan Ural 2017, „A Computer-Based Brain Tumor Detection Approach with Advanced Image Processing and Probabilistic Neural Network Methods“, *Journal of Medical and Biological Engineering*, pp. 1–13.
31. Abd El Kader I, Xu G, Shuai Z, Saminu S, Javaid I, Ahmad IS, Kamhi S (2021) Brain tumour detection and classification on MR images by a deep wavelet auto-encoder model. *Diagnostics* 11(9):1589.
32. Aswathy SU, GlanDevadhas G, Kumar SS (2019) Brain tumour detection and segmentation using a wrapper-based genetic algorithm for the optimized feature set. *Clust Comput* 22(6):13369–13380.
33. Ma, C, Luo, G & Wang, K 2018, „Concatenated and Connected Random Forests With Multiscale Patch Driven Active Contour Model for Automated Brain Tumor Segmentation of MR Images“, *IEEE Transactions on Medical Imaging*, vol. 37, no. 8, pp. 1943-1954.
34. Zaka Ur Rehman, Syed S Naqvi, Tariq M Khan, Muhammad A Khan & Tariq Bashir 2019, „Fully automated multi-parametric brain tumor segmentation using

- super pixel based classification“, *Expert Systems with Applications*, vol. 118, pp. 598-613.
35. Shengcong Chen, Changxing Ding & Minfeng Liu 2019, „Dual-force convolutional neural networks for accurate brain tumor segmentation“, *Pattern Recognition*, vol. 88, pp. 90-100.
 36. Abhishek Bal, Minakshi Banerjee, Amlan Chakrabarti & Punit Sharma 2018, „MRI Brain Tumor Segmentation and Analysis using RoughFuzzy C-Means and Shape Based Properties“, *Journal of King Saud University - Computer and Information Sciences*.
 37. Adriano Pinto, Sérgio Pereira, Deolinda Rasteiro & Carlos A Silva 2018, „Hierarchical brain tumor segmentation using extremely randomized trees“, *Pattern Recognition*, vol. 82, pp. 105-117.
 38. Gumaei, A, Hassan, MM, Hassan, MR, Alelaiwi, A & Fortino, G 2019, „A Hybrid Feature Extraction Method With Regularized Extreme Learning Machine for Brain Tumor Classification“, *IEEE Access*, vol. 7, pp. 36266-36273, doi: 10.1109/ACCESS.2019.2904145.
 39. Siva Raja, PM & Antony Viswasa rani 2020, „Brain tumor classification using a hybrid deep autoencoder with Bayesian fuzzy clustering-based segmentation approach“, *Biocybernetics and Biomedical Engineering*, vol. 40, no. 1, pp. 440-453.
 40. Imtiaz, T, Rifat, S, Fattah, SA & Wahid, KA 2020, „Automated Brain Tumor Segmentation Based on Multi-Planar Superpixel Level Features Extracted From 3D MR Images“, *IEEE Access*, vol. 8, pp. 25335-25349, doi: 10.1109/ACCESS.2019.2961630.
 41. Mohamed T Bennai, Zahia Guessoum & Mohamed Mezghiche 2020, „A stochastic multi-agent approach for medical-image segmentation: Application to tumor segmentation in brain MR images“, *Artificial Intelligence in Medicine*, vol. 110, Art.no. 101980.

42. Iwata, R, Maruyama, M & Ito, T 2017, „Establishment of a tumor sphere cell line from a metastatic brain neuroendocrine tumor“, *Med Mol Morphol*, vol. 50, pp. 211–219, <https://doi.org/10.1007/s00795-017-0160-0>.
43. Neal S ParikhJaelyn, BurchBabak, E & Navi, B 2017, „Recurrent Thromboembolic Events after Ischemic Stroke in Patients with Primary Brain Tumors“, *Journal of Stroke and Cerebrovascular Diseases*, vol. 26, issue. 10, pp. 2396-2403.
44. Adela WuJon, D & Weingart Kaisorn L Chaichana 2017, „Risk Factors for Preoperative Seizures and Loss of Seizure Control in Patients Undergoing Surgery for Metastatic Brain Tumors“, *World Neurosurgery*, vol. 104, pp. 120-128.
45. Philipp Hendrix Elisa Hans Julia Karbach 2017, „Neurocognitive status in patients with newly-diagnosed brain tumors in good neurological condition: The impact of tumor type, volume, and location“, *Clinical Neurology and Neurosurgery*, vol. 156, pp. 55-62.
46. Oros-Peusquens, AK, Loução, R & Shah, NJ 2017, „Methods for molecular imaging of brain tumors in a hybrid MR-PET context: Water content, T2*, diffusion indices and FET-PET“, *Methods*, vol. 130, pp. 135-151.
47. Carla RuisIrene Huenges, Wajer Martine & van Zandvoort 2017, „Anxiety in the preoperative phase of awake brain tumor surgery“, *Clinical Neurology and Neurosurgery*, vol. 157, pp. 7-10.
48. Elisee Ilunga–MbuyambaJuan Gabriel Avina–CervantesClaire Chalopin 2017, “Automatic selection of localized region-based active contour models using image content analysis applied to brain tumor segmentation”, *Computers in Biology and Medicine*, vol. 91, pp. 69-79.
49. Markus Hoffer mann Lukas Bruckmann Gord von Campe 2017, “Preand postoperative neurocognitive deficits in brain tumor patients assessed by a computer based screening test”, *Journal of Clinical Neuroscience*, vol. 36, pp. 31-36.

50. Nidhi Gupta Pritee Khanna 2017, „A non-invasive and adaptive CAD system to detect brain tumor from T2-weighted MRIs using customized Otsu’s thresholding with prominent features and supervised learning“, *Signal Processing: Image Communication*, vol. 59, pp. 18-26.
51. Song, B, Wen, P, Ahfock, T & Li, Y 2016, „Numeric Investigation of Brain Tumor Influence on the Current Distributions During Transcranial Direct Current Stimulation“, in *IEEE Transactions on Biomedical Engineering*, vol. 63, no. 1, pp. 176-187, doi: 10.1109/TBME.2015.2468672.
52. Sallemi, L, Njeh, I & Lehericy, S 2015, “Towards a Computer Aided Prognosis for Brain Glioblastomas Tumor Growth Estimation”, in *IEEE Transactions on NanoBioscience*, vol. 14, no. 7, pp. 727-733, doi: 10.1109/TNB.2015.2450365.
53. Yang, G, Nawaz, T, Barrick, TR, Howe, FA & Slabaugh, G 2015, „Discrete Wavelet Transform-Based Whole-Spectral and Subspectral Analysis for Improved Brain Tumor Clustering Using Single Voxel MR Spectroscopy“, in *IEEE Transactions on Biomedical Engineering*, vol. 62, no. 12, pp. 2860-2866, doi: 10.1109/TBME.2015.2448232.
54. Huda, S, Yearwood, J, Jelinek, HF, Hassan, MM, Fortino, G & Buckland, M 2016, “A Hybrid Feature Selection With Ensemble Classification for Imbalanced Healthcare Data: A Case Study for Brain Tumor Diagnosis”, in *IEEE Access*, vol. 4, pp. 9145-9154, doi: 10.1109/ACCESS.2016.2647238.
55. Menze, BH 2015, „The Multimodal Brain Tumor Image Segmentation Benchmark (BRATS)“, in *IEEE Transactions on Medical Imaging*, vol. 34, no. 10, pp. 1993-2024, doi: 10.1109/TMI.2014.2377694.
56. Mendes, AC, Ribeiro, AS & Oros-Peusquens, AM 2015, „Brain connectivity study of brain tumor patients using MR-PET data: preliminary results“, *EJNMMI Phys*, vol. 2, <https://doi.org/10.1186/2197-7364-2-S1-A75>.
57. Yu, Z, Tao, L & Qian, Z 2016, “Altered brain anatomical networks and disturbed connection density in brain tumor patients revealed by diffusion tensor tractography” *Int J CARS*, vol. 11, pp. 2007–2019 <https://doi.org/10.1007/s11548-015-1330-y>.

58. Forster, MT, Heindl, N & Hattingen, E 2015, "Brain surface reformatted imaging (BSRI) for intraoperative neuronavigation in brain tumor surgery" *Acta Neurochir*, vol. 157, pp. 265–274, <https://doi.org/10.1007/s00701-014-2316-1>.
59. Arakeri, MP & Reddy, GRM 2015, "Computer-aided diagnosis system for tissue characterization of brain tumor on magnetic resonance images". *SIViP*, vol. 9, pp. 409–425, <https://doi.org/10.1007/s11760-013-0456-z>.
60. P. Saxena, A. Maheshwari, and S. Maheshwari, "Predictive modeling of brain tumor: a deep learning approach," in *Innovations in Computational Intelligence and Computer Vision*, Springer, 2021.
61. A. Sekhar, S. Biswas, R. Hazra, A. K. Sunaniya, A. Mukherjee, and L. Yang, "Brain tumor classification using fine-tuned GoogLeNet features and machine learning algorithms: IoMT enabled CAD system," *IEEE Journal of Biomedical and Health Informatics*, vol. 26, no. 3, pp. 983–991, 2022.
62. M. I. Sharif, M. A. Khan, M. Alhussein, K. Aurangzeb, and M. Raza, "A decision support system for multimodal brain tumor classification using deep learning," *Complex & Intelligent Systems*, vol. 2021, pp. 1–14, 2021.
63. P. Saxena, A. Maheshwari, and S. Maheshwari, "Predictive modeling of brain tumor: a deep learning approach," in *Innovations in Computational Intelligence and Computer Vision*, Springer, 2021.
64. Lee, H.H.; Novikov, D.S.; Fieremans, E. Removal of partial Fourier-induced Gibbs (RPG) ringing artifacts in MRI. *Magn. Reson. Med.* 2021.
65. S. Maqsood, R. Damasevicius, and F. M. Shah, "An efficient approach for the detection of brain tumor using fuzzy logic and U-NET CNN classification," in *Computational Science and Its Applications - ICCSA 2021*, pp. 105–118, Springer, New York, NY, USA, 2021.
66. Usman Zahid, Imran Ashraf, Muhammad Attique Khan, Majed Alhaisoni, Khawaja M. Yahya, Hany S. Hussein, Hammam Alshazly, "BrainNet: Optimal Deep Learning Feature Fusion for Brain Tumor Classification", *Computational Intelligence and Neuroscience*, vol. 2022, Article ID 1465173, 13 pages, 2022. <https://doi.org/10.1155/2022/1465173>.

67. Hornik, K., Stinchcombe, M., & White, H. (1989). Multilayer feedforward networks are universal approximators. *Neural Networks*, 2(5), 359-366.
68. Glorot, X., Bordes, A., & Bengio, Y. (2011). Deep sparse rectifier neural networks. Paper presented at the Proceedings of the fourteenth international conference on artificial intelligence and statistics.
69. Leshno, M., Lin, V. Y., Pinkus, A., & Schocken, S. (1993). Multilayer feedforward networks with a nonpolynomial activation function can approximate any function. *Neural Networks*, 6(6), 861- 867.
70. Hochreiter, S., & Schmidhuber, J. (1997). Long short-term memory. *Neural computation*, 9(8), 1735- 1780.
71. Bengio, Y., & LeCun, Y. (2007). Scaling learning algorithms towards AI. *Large-scale kernel machines*, 34(5), 1-41.
72. Zhang, L., & Zhang, B. (1999). A geometrical representation of McCulloch-Pitts neural model and its applications. *IEEE Transactions on Neural Networks*, 10(4), 925-929.
73. Rosenblatt, F. (1957). *The Perceptron-a Perceiving and Recognizing Automaton* (85-460-1). Ithica: Cornell Aeronautical Laboratory.
74. Minsky, M., & Papert, S. (1969). *An introduction to computational geometry*. Cambridge tiass, HIT.
75. Werbos, P. J. (1994). *The roots of backpropagation: from ordered derivatives to neural networks and political forecasting* (Vol. 1): John Wiley & Sons.
76. Abd El Kader I, Xu G, Shuai Z, Saminu S, Javaid I, Ahmad IS, Kamhi S (2021) Brain tumor detection and classification on MR images by a deep wavelet auto-encoder model. *Diagnostics* 11(9):1589.
77. Aswathy SU, GlanDevadhas G, Kumar SS (2019) Brain tumor detection and segmentation using a wrapper-based genetic algorithm for the optimized feature set. *Clust Comput* 22(6):13369–13380.
78. Gull S, Akbar S, Khan HU (2021) Automated detection of brain tumor through magnetic resonance images using convolutional neural network. *BioMed Res Int* 2021:1–4.

79. Huang C, Wan M (2022) Automated segmentation of brain tumor based on improved U-Net with residual units. *Multimedia Tools Appl* 81(9):12543–12566.
80. Huang C, Wan M (2022) Automated segmentation of brain tumor based on improved U-Net with residual units. *Multimedia Tools Appl* 81(9):12543–12566.
81. Ramya Manaswi, V., & Sankarababu, B. (2022). A Flexible Accession on Brain Tumor Detection and Classification Using VGG16 Model. In *Smart Intelligent Computing and Applications, Volume 1* (pp. 225-238). Springer, Singapore.
82. Dong, H., Yang, G., Liu, F., Mo, Y., & Guo, Y. (2017, July). Automatic brain tumor detection and segmentation using U-Net based fully convolutional networks. In *annual conference on medical image understanding and analysis* (pp. 506-517). Springer, Cham.
83. Thillaikkarasi, R., & Saravanan, S. (2019). An enhancement of deep learning algorithm for brain tumor segmentation using kernel based CNN with M-SVM. *Journal of medical systems*, 43(4), 1-7.
84. Thillaikkarasi, R., & Saravanan, S. (2019). An enhancement of deep learning algorithm for brain tumor segmentation using kernel based CNN with M-SVM. *Journal of medical systems*, 43(4), 1-7.
85. Ramya Manaswi, V., & Sankarababu, B. (2022). A Flexible Accession on Brain Tumor Detection and Classification Using VGG16 Model. In *Smart Intelligent Computing and Applications, Volume 1* (pp. 225-238). Springer, Singapore.
86. Dong, H., Yang, G., Liu, F., Mo, Y., & Guo, Y. (2017, July). Automatic brain tumor detection and segmentation using U-Net based fully convolutional networks. In *annual conference on medical image understanding and analysis* (pp. 506-517). Springer, Cham.
87. Thillaikkarasi, R., & Saravanan, S. (2019). An enhancement of deep learning algorithm for brain tumor segmentation using kernel based CNN with M-SVM. *Journal of medical systems*, 43(4), 1-7.
88. Thillaikkarasi, R., & Saravanan, S. (2019). An enhancement of deep learning algorithm for brain tumor segmentation using kernel based CNN with M-SVM. *Journal of medical systems*, 43(4), 1-7.

89. Debnath, S, Talukdar, F. A., & Islam, M. 1 (2022). Complete 3D brain tumor detection using a two-phase method along with confidence function evaluation. *Multimedia Tools and Applications*, 81(1), 437-458.
90. Sahu, S. P., Kumar, A., Gupta, A., & Sharmila, T. S. (2022). Brain Tumor Detection Using UNet Based Semantic Segmentation Scheme. In *International Conference on Computing in Engineering & Technology* (pp. 323-330). Springer, Singapore.
91. Zhao, X., Wu, Y., Song, G., Li, Z., Zhang, Y., & Fan, Y. (2018). A deep learning model integrating FCNNs and CRFs for brain tumor segmentation. *Medical image analysis*, 43, 98-111.
92. Chattopadhyay, A., & Maitra, M. (2022). MRI-based Brain Tumor Image Detection Using CNN based Deep Learning Method. *Neuroscience Informatics*, 100060.
93. Togacar, M., Ergen, B., & Cömert, Z. (2020). BrainMRNet: Brain tumor detection using magnetic resonance images with a novel convolutional neural network model. *Medical hypotheses*, 134, 109531.
94. Mlynarski, P., Delingette, H., Criminisi, A., & Ayache, N. (2019). Deep learning with mixed supervision for brain tumor segmentation. *Journal of Medical Imaging*, 6(3), 034002.
95. Kurmi, Y, and Vijayshri C.(2020). Classification of magnetic resonance images for brain tumor detection. *IET Image Processing* 14, no. 12 (2020): 2808-2818.
96. Wang, W., Chen, C., Ding, M., Yu, H., Zha, S., & Li, J. (2021, September). Transbts: Multimodal brain tumor segmentation using transformer. In *International Conference on Medical Image Computing and Computer-Assisted Intervention* (pp. 109-119). Springer, Cham.
97. Amin, J., Sharif, M., Yasmin, M., & Fernandes, S. L. (2020). A distinctive approach in brain tumor detection and classification using MRI. *Pattern Recognition Letters*, 139, 118- 127.
98. Rehman, A., Khan, M. A., Saba, T., Mehmood, Z., Tariq, U., & Ayesha, N. (2021). Microscopic brain tumor detection and classification using 3D CNN and

- feature selection architecture. *Microscopy Research and Technique*, 84(1), 133-149.
99. Mittal, M., Goyal, L. M., Kaur, S., Kaur, I., Verma, A., & Hemanth, D. J. (2019). Deep learning based enhanced tumor segmentation approach for MR brain images. *Applied Soft Computing*, 78, 346-354.
100. Iqbal, S., Ghani Khan, M. U., Saba, T., Mehmood, Z., Javaid, N., Rehman, A., & Abbasi, R. (2019). Deep learning model integrating features and novel classifiers fusion for brain tumor segmentation. *Microscopy research and technique*, 82(8), 1302-1315.
101. Bahadure, N. B., Ray, A. K., & Thethi, H. P. (2017). Image 1 analysis for MRI based brain tumor detection and feature extraction using biologically inspired BWT and SVM. *International journal of biomedical imaging*, 2017.
102. Gyórfi, Á, Szilágyi, L., & Kovács, L. (2021). A fully automatic procedure for brain tumor segmentation from multi-spectral MRI records using ensemble learning and atlas-based data enhancement. *Applied Sciences*, 11(2), 564.
103. Dehariya, A., & Shukla, P. (2020). Brain cancer prediction through segmentation of images using bio-geography based optimization. *Int J Adv Res Eng Technol (IJARET)*, 11(11).
104. Raj, M, Vikas, S, and Vikram, B. (2021).Brain Tumor Detection Using Fish Schooling Genetic Algorithm. In 2021 9th International Conference on Reliability, Infocom Technologies and Optimization (Trends and Future Directions) (ICRITO), pp. 1-6. IEEE, 2021.
105. Sasank, V. V. S., & Venkateswarlu, S. (2021). Brain tumor classification using modified kernel based softplus extreme learning machine. *Multimedia Tools and Applications*, 80(9), 13513-13534.
106. Padmaja, S., & Suseendran, G. (2017). MRI Geometric Distortion for Brain Tumor Detection and Segmentation. *Jour of Adv Research in Dynamical & Control Systems*, 9 (7).

107. Joshi, D., Nagwanshi, K. K., Choubey, N. S., & Rajput, N. S. (2022). Topological Optimized Convolutional Visual Recurrent Network for Brain Tumor Segmentation and Classification. arXiv preprint arXiv:2207.13021.
108. Kieran MW, Chi SN, Manley PE, et al. Tumors of the brain and spinal cord. In: Orkin SH, Fisher DE, Ginsburg D, Look AT, Lux SE, Nathan DG, eds. *Nathan and Oski's Hematology and Oncology of Infancy and Childhood*. 8th ed. Philadelphia, PA: Elsevier Saunders; 2015: chap 57.
109. Ullah, Zahid & Lee, Su-Hyun & An, Donghyeok. (2020). Histogram Equalization based Enhancement and MR Brain Image Skull Stripping using Mathematical Morphology. *International Journal of Advanced Computer Science and Applications*. 11. 10.14569/IJACSA.2020.0110372.
110. V. Vijaya Kishore and V. Kalpana, "ROI Segmentation and Detection of Neoplasm Based on Morphology Using Segmentation Operators," *Emerging Trends in Electrical, Communications, and Information Technologies*, pp. 501–509, Sep. 2019, doi: 10.1007/978-981-13-8942-9_41.
111. SMane, Mansa & Kulkarni, Nikita & Randive, Santosh. (2014). Review on Brain Tumor Detection and Segmentation Techniques. *International Journal of Computer Applications*. 95. 34-38. 10.5120/16593-6307.